UCRL 18793

SEMIANNUAL REPORT BIOLOGY AND MEDICINE

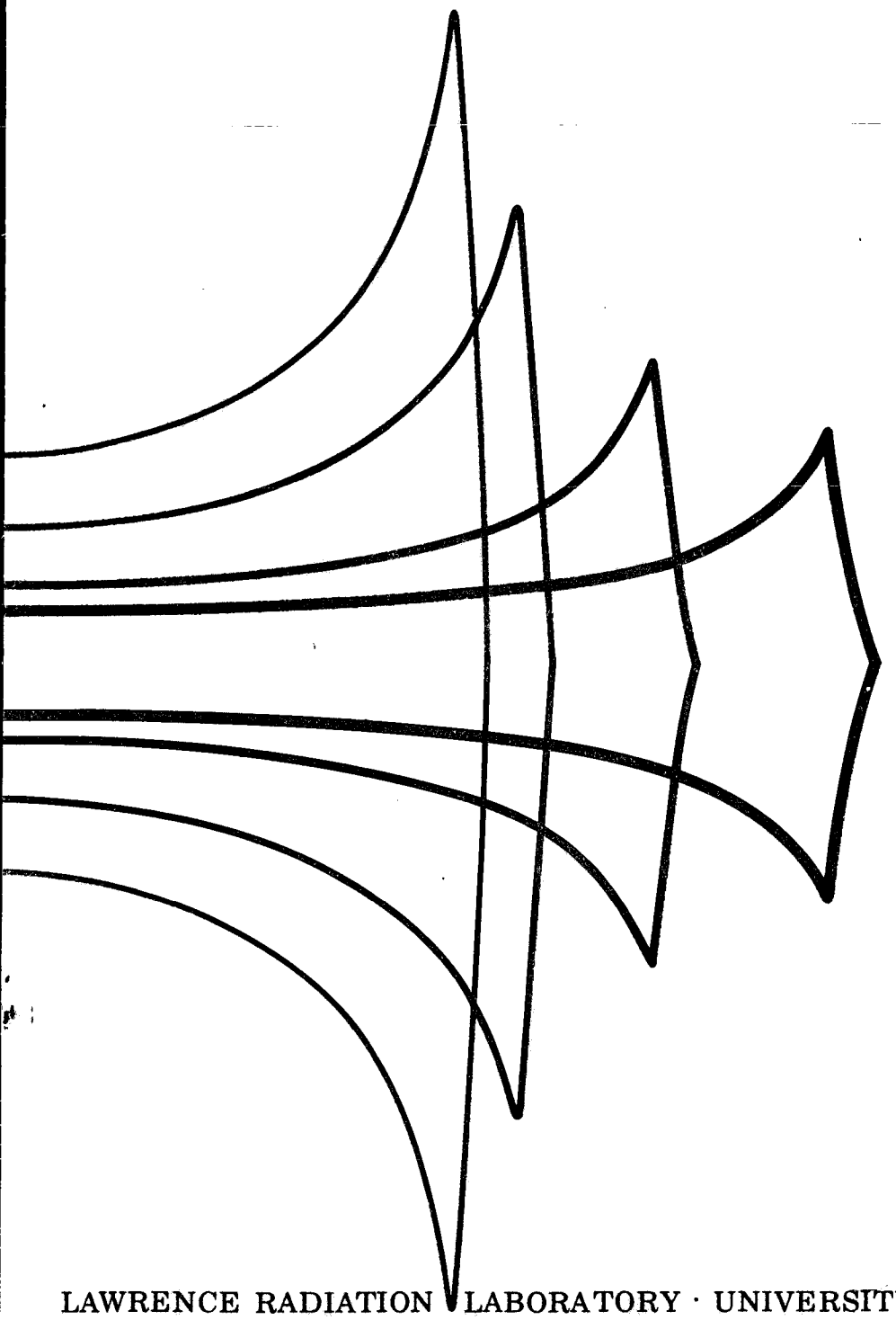

Donner Laboratory
and
Donner Pavilion

Fall 1968

LAWRENCE RADIATION LABORATORY · UNIVERSITY OF CALIFORNIA · BERKELEY

DISCLAIMER

UCRL-18793
UC-48 Biology and Medicine
TID-4500 (54th Ed.)

Fall 1968

SEMIANNUAL REPORT BIOLOGY AND MEDICINE

John H. Lawrence, M.D., Editor

DONNER LABORATORY AND DONNER PAVILION

LAWRENCE RADIATION LABORATORY UNIVERSITY OF CALIFORNIA
BERKELEY, CALIFORNIA

AEC Contract No. W-7405-eng-48

Table of Contents

Mammalian Nervous Tissue in Culture
ABDEL-MEGID MAMOON, WERNER T. SCHLAPFER AND CORNELIUS A. TOBIAS 1

Bioelectric Activity of Neurons in Tissue Culture: Synaptic Networks and Effects of Divalent Cations
WERNER T. SCHLAPFER, ABDEL-MEGID MAMOON, PAUL H. O' LAGUE AND CORNELIUS A. TOBIAS 9

Isolation of Disomics in Saccharomyces cerevisiae
PATRIC TAURO, UBALDO S. RODARTE-Y-RAMON, TOMMY J. McKEY AND ROBERT K. MORTIMER 19

Fluorescence of Serum High-Density Lipoprotein
NORMAN K. FREEMAN AND ALEX V. NICHOLS 25

Ultracentrifuge Data Acquisition from a Central Control System
ALFRED A. WINDSOR, LIN C. JENSEN, DAVID A. HOOPES AND FRANK T. LINDGREN 30

The Scanning Electron Microscope: A High-Information-Content Image of Biological Systems
THOMAS L. HAYES 35

Distribution of Spleen Colony Forming Units in Bone and Marrow
DONALD C. VAN DYKE 38

Clinically Applicable Fluoro-Kinetic Method for Bone Blood Flow Determination
DONALD C. VAN DYKE AND JEAN-PIERRE NAETS 43

Urinary Erythropoietin Assay in the Diagnosis of Hematologic Disease
DONALD C. VAN DYKE AND MARY LOU NOHR 52

Localization of ^{58}Co and ^{65}Zn Hematoporphyrin Complexes in Canine Lymph Nodes
RASHID A. FAWWAZ, H. SAUL WINCHELL, FREDERICK FRYE, WILLIAM P. HEMPHILL AND JOHN H. LAWRENCE 64

Evaluation of ^{111}Ag, ^{113}Sn, ^{90}Yt and ^{109}Pd Hematoporphyrin Complexes for Selective Lymphatic Irradiation
RASHID A. FAWWAZ, H. SAUL WINCHELL, MELDRUM B. WINSTEAD, GERY C. ARMALY, WILLIAM P. HEMPHILL AND JOHN H. LAWRENCE 73

The Synthesis of Sodium ^{11}C-Benzoate and Its Use in Renal Visualization
MELDRUM B. WINSTEAD, H. SAUL WINCHELL AND RASHID A. FAWWAZ 80

Synthesis of ^{11}C-Carboxylic Acids and Their Use in Organ Visualization
MELDRUM B. WINSTEAD, H. SAUL WINCHELL, RASHID A. FAWWAZ AND GERY C. ARMALY 86

Radiation Dosimetry Using Miniature Silicon Diodes
MUDUNDI R. RAJU 89

The Oxygen Effect of π^- Mesons in Vicia faba
MUDUNDI R. RAJU, NABIL M. AMER, MADVANATH GNANAPURANI AND CHAIM RICHMAN 92

A Method to Determine the Acute Radiation Response of Human Cells to π Mesons
H. JOHN BURKI, GERRIT W. BARENDSEN, MUDUNDI R. RAJU, NABIL M. AMER AND STANLEY B. CURTIS 100

The RBE of Negative Pions in 2-Day-Old Ascites Tumors
JOSE M. FEOLA, MUDUNDI R. RAJU, CHAIM RICHMAN AND JOHN H. LAWRENCE 105

The Determination of Testosterone and Epitestosterone in Urine Samples by Gas Liquid Chromatography
GERALD M. CONNELL AND JOHN A. LINFOOT 113

Whole-Body Marrow Distribution Studies in Polycythemia Vera
DONALD C. VAN DYKE, JOHN H. LAWRENCE AND HAL O. ANGER 118

Actinide Element Studies with a Si(Li) "Wound Counter"
HOWARD G. PARKER, STEPHEN R. WRIGHT AND ANNE de G. LOW-BEER 128

Heavy-Particle Therapy in Cushing's Disease: A Progress Report
JOHN A. LINFOOT, EDWARD MANOUGIAN, NORTON J. SNYDER, RICHARD A. CARLSON, CLAUDE Y. CHONG, JAMES L. BORN, CORNELIUS A. TOBIAS AND JOHN H. LAWRENCE 135

Staff Publications 140

Author Index 143

Personnel 144

Mammalian Nervous Tissue in Culture

Abdel-Megid Mamoon, Werner T. Schlapfer and Cornelius A. Tobias

In vitro cultures from nervous tissue can provide an experimental model for investigating a variety of anatomical, physiological, and pathological problems concerning this tissue. This model is used in an attempt to relate structure to function at the cellular level or at a level less complex than the whole organism. The cultures can be examined microscopically at all stages of growth, a definite advantage over the in vivo situation. Known physiological parameters such as pH, temperature, etc. can be maintained within narrow limits in the culture environment. Direct effects of various factors on neurons and glia can be studied at the structural or ultrastructural level and correlated with the observed biochemical or electrophysiological data (or both) without interference or indirect effects from the vascular bed and its humoral factors. The culture is, however, an approximation of the real in vivo situation, even though it is true that many of the structural and functional characteristics of this tissue are reproduced in vitro. Murray (1) reviewed the basic cytology and development of nervous tissue in vitro and its applications to different investigations. Lumsden (2) has provided a more recent survey of the new developments in this field.

A variety of methods for culturing nervous tissue are currently in use, e.g., the Maximow double cover slip method (3), the Rose chamber method (4), and the roller tube method (5). The nutrient medium favored by different investigators varies, but in all cases it has a high proportion of biological fluids, such as serum, serum ultrafiltrates, chicken embryo extract, etc. Completely synthetic media were found to be unable to support growth and differentiation of nerve tissue in vitro.

METHODS

We used a modification of the roller tube technique originally developed by Costero and Pomerat (5) and described by Hild and Tasaki (6). The cerebellum and midbrain of newborn rats were quickly dissected out under strictly sterile conditions and washed in several drops of Gey's balanced salt solution (BSS) to remove adhering blood and body fluids. The meninges and any visible blood capillaries were removed as much as possible. The tissue was cut into small pieces or explants about 1 to 1.5 mm in diameter and washed once again with BSS. One

to three explants were then deposited on a No. 1 12×50-mm glass cover slip coated with a film of heparinized chicken plasma to which one or two drops of 8-day chicken embryo extract was added and mixed quickly and left to clot. This process as well as the earlier dissection was done in sterile plastic petri dishes. After the clots had hardened, the cover slips carrying the cultures were placed in sterile plastic tissue culture test tubes and fed with 2 ml of nutrient medium. The tubes were then inserted into the holes of a rotating drum assembly tilted 5 deg with respect to the horizontal axis and rotating at about 10–12 revolutions per hour inside a 36°C incubator having an atmosphere of 5% CO_2 in humidified air. The nutrient medium consisted of 25% calf serum (heat-inactivated for 30 min at 56°C) and 75% Gey's balanced salt solution (BSS), the glucose level in the net medium being raised to 5.5 mg/ml. The pH of the medium, which was close to 7.0, was maintained at this value by the 5%-CO_2-in-air atmosphere. The medium was changed weekly. The high concentration of glucose was found to be necessary for the differentiation of nerve cells and myelin formation (7). Even with such enriched medium healthy cultures may not be obtained if too many nerve cells have been irreparably damaged by crushing or tearing the explant during the cutting process. It is also important to keep the explant size down to approximately 1 mm^3 to ensure the accessibility of oxygen and nutrients by diffusion to the central part of the explant as well as efficient removal of toxic waste products elaborated by the cells. All glassware, dissecting instruments, and anything that comes directly or indirectly in contact with the cultures should be scrupulously clean, since even the smallest amount of toxic impurities is detrimental to the differentiation and survival of the cultures. Since no antibiotics are used in the BSS or nutrient media, the danger of bacterial contamination is always present at all phases of the culturing process.

The cover slips carrying the cultures can be removed from the culture tubes and examined on a bridge mount filled with BSS by phase-contrast or polarization microscopy. If the examination has been done under sterile conditions, the culture can be returned to the original test tube, either directly or after being subjected to some experimental factor, and incubated further if so desired. At the start or at various times during growth the explant can be exposed to irradiation (results to be published elsewhere) or radioactive tracers, or tested for bioelectric activities (see companion paper, page 9), and then fixed and stained with or without sectioning of the culture, by use of classical staining methods. Whole-mount autoradiography by the dipping technique (8) was done on a few of our cultures to investigate uptake of uridine-^{14}C and synthesis of RNA. Bodian silver staining (9) was done routinely. Sudan Black B was used as a myelin stain (10). Methylene blue (1:50,000 in BSS) was used as a supravital stain for nerve cells to reveal the path of cell processes in the living culture (5).

RESULTS AND DISCUSSION

About 24 hours after explantation glia and mesodermal elements as well as neurites start emerging from the explant. During the next few days more cells emigrate and neurites and glial processes (Fig. 1) increase in density, but no neurons are yet evident. This is because neurons migrate least if at all and so remain inside the explant. Nerve cells (Fig. 2) become visible under a phase-contrast microscope after about 12 days in culture when the explant has become thin enough for transillumination. The nerve cells appear embedded in an extensive network of glial and neuronal processes. They are easily spotted because of their characteristic

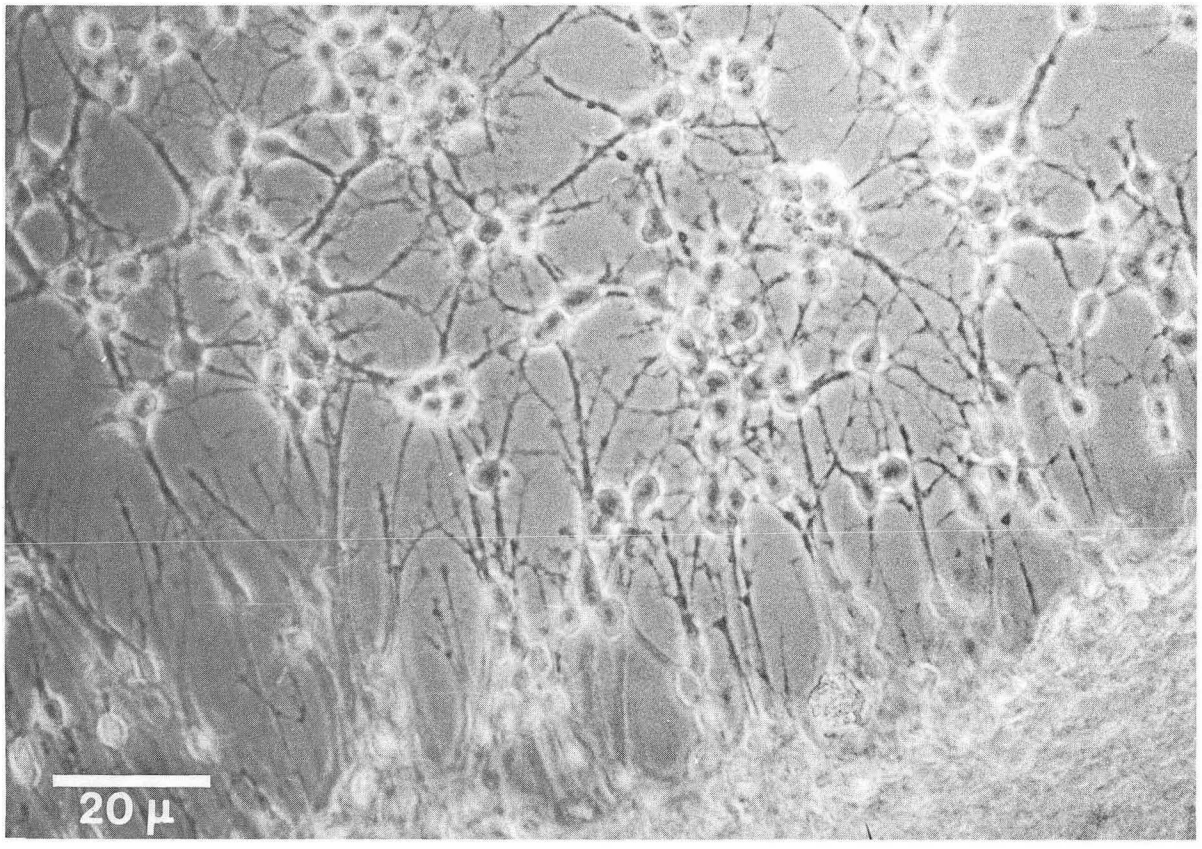

Fig. 1. Explant from newborn rat cerebellum at 4 days in vitro. Notice small cells (mostly glia) as well as glial processes and neurites emerging from the explant. Phase. XBB 695-3451

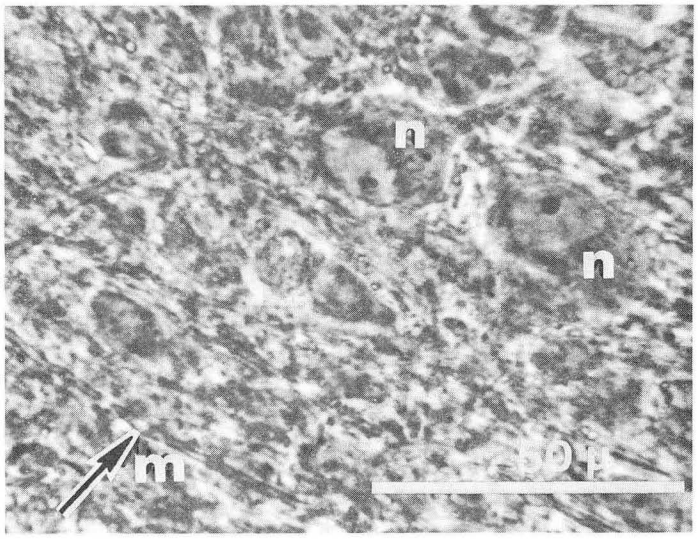

Fig. 2. Newborn rat cerebellum culture at 12 days in vitro. Two visible nerve cells (n). Notice peripheral nuclei in both cells. Myelin (m) is already present at this stage. Phase. XBB 695-3452

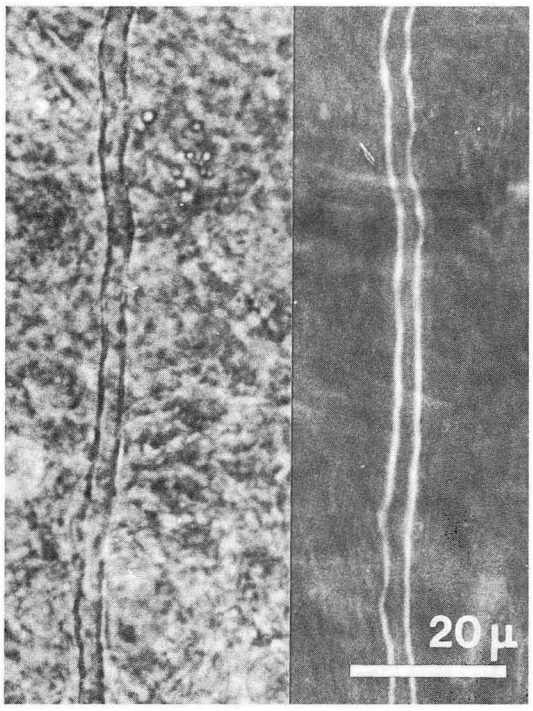

Fig. 3. Myelin in 55-day newborn rat cerebellum culture. Left side shows a myelinated axon in phase. Right side shows the same axon in polarized light.
XBB 695-3453

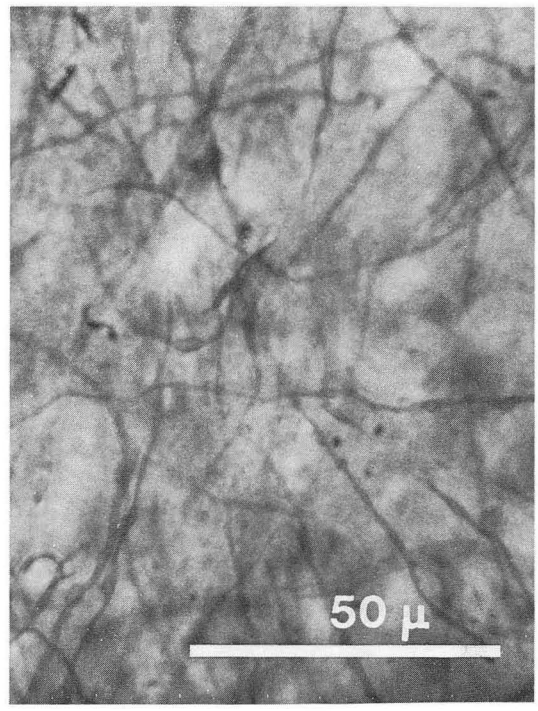

Fig. 4. Myelinated axon after fixation and staining of a 14-day-old rat midbrain culture with Sudan Black B.
XBB 695-3454

shape, their usually large size (about 25 μ at this stage) compared with the majority of other cells in the culture, and their very distinct usually single nucleolus. At this stage the nerve cell nucleus may occupy a peripheral location and Nissl substance may still be not well formed. Also about the 12th day in culture many axons acquire a myelin sheath, which is easily visible due to its high refractivity in ordinary light and its birefringence in polarized light (Fig. 3). Since the elaboration of a myelin sheath requires the collaboration of both the nerve cell, particularly its axon, and the glial cell, its occurrence is considered to be a sign of the general health of culture, particularly when it appears at a time corresponding to that in vivo, i.e., at about two weeks postnatally. The number of our explants that myelinate is upwards of 90% of the total number explanted, and myelination is abundant at 15 days in vitro. Staining for myelin by Sudan Black B (Fig. 4) showed sometimes irregularities which may not be a sign of abnormalities, since they were also seen in vivo in apparently healthy nervous tissue. About the beginning of the third week in vitro the outgrowth zone has become more advanced and extensive glial processes forming networks are apparent. About this time also many of the neurons are more developed (Fig. 5), the nucleus is now centrally located, and Nissl substance is distinct and uniformly distributed in the soma. Although most nerve cell processes were not easily delineated in the living state, yet incubating the culture for about 20 min at 36°C in a very dilute solution of methylene blue in BSS (5) followed by examination by phase-contrast or ordinary-light microscope reveals clearly many of these processes (Fig. 6). Bodian silver

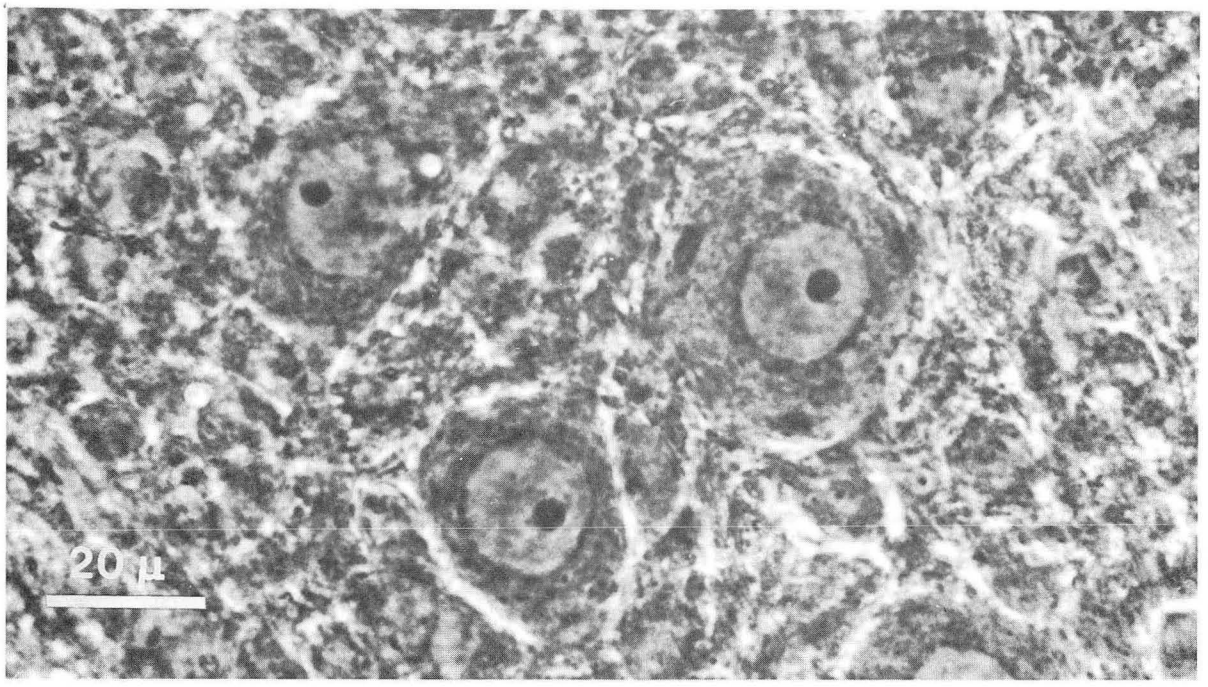

Fig. 5. Newborn rat cerebellum culture showing apparently healthy nerve cells at 21 days in vitro. XBB 695-3455

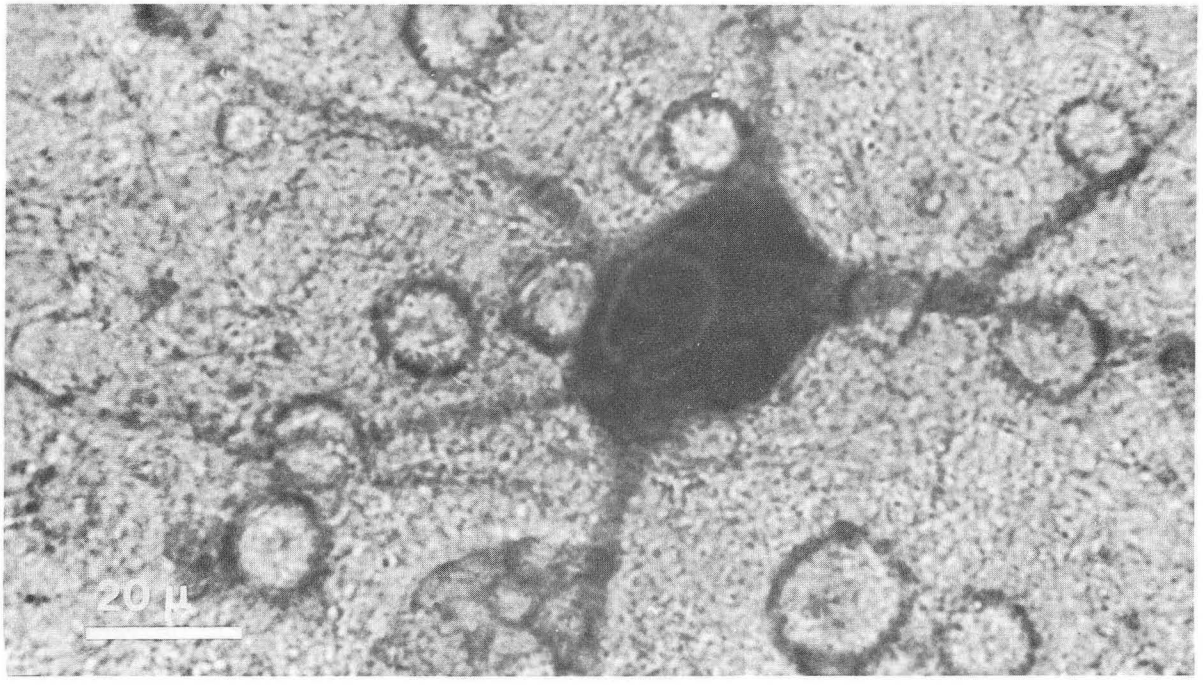

Fig. 6. Living newborn rat midbrain culture at 14 days in vitro, stained supravitally with methylene blue (1:50,000 in BSS). Notice heavy uptake of dye by nerve cell body and its processes. Due to very little uptake by other cells present in the culture, they were not visible in ordinary light. XBB 695-3456

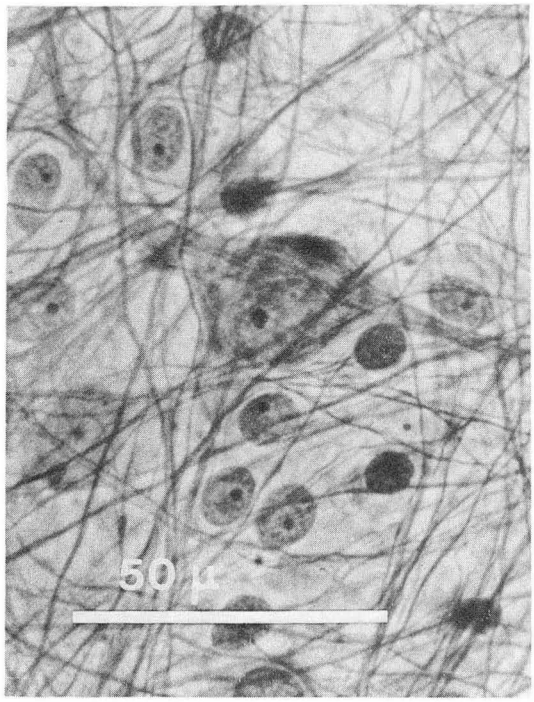

Fig. 7. Newborn rat cerebellum culture at 15 days in vitro, Bodian stained. Notice neuron at center with axons crisscrossing all over the area.

XBB 695-3457

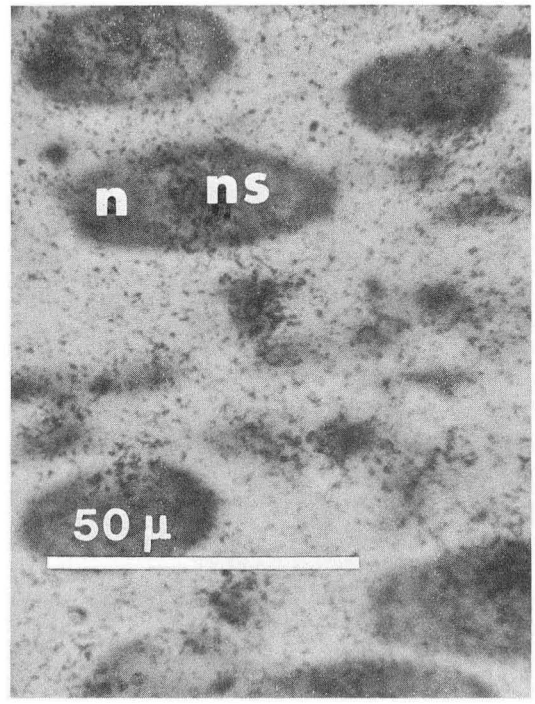

Fig. 8. A newborn rat cerebellar culture at 16 days in vitro, after incubation with uridine-^{14}C, fixation, autoradiography, and staining with Einarson's technique for nucleic acid (12). Notice nerve cell (n) with grains mainly over nucleus (ns).

XBB 695-3458

staining applied at this stage reveals extensive network of interlacing axons and nerve cell bodies (Fig. 7). Frequently some areas in cultures from both midbrain and cerebellum exhibited ciliary activity. The cilia are believed to be of ependymal origin and were observed by Hild (11). The ciliary beating was greatly slowed when the culture temperature was lowered to 4°C. The activity resumed, however, when the culture temperature was raised to 37°C. At about one month in vitro the cultures seem to be stabilized and no major further development occurs. Dead cells and debris are phagocytized by macrophages at all stages of the culture development. The cultures in general can be maintained in an apparently healthy condition for a period of about two months, a period long enough for investigating the effects of many factors on the structure and function of this tissue. However, chromatolysis of the neuron perikarya followed by degeneration, as well as degeneration of the myelin sheaths, generally occurs more frequently in older cultures. In view of the complexity of interconnections between cells in nerve tissue, even at the earliest postnatal stage, and their interdependence, which is undoubtedly greatly disrupted during the cutting process, it is amazing that any nerve cells survive at all. Glial cells proliferate a little but mature neurons do not divide. The nerve cells, however, have a great capacity for regeneration provided their injury is not too severe. This plus the presence of some immature nerve cells or neuroblasts in young animals may explain the success of cultures from nervous tissue.

Since the regeneration and maintenance of nerve tissue explants involve great synthetic capacities, the possibility for investigating this in our system was checked. It was found that nerve cells and glia actively synthesize RNA from uridine-2 ^{14}C (sp. act. 55 mCi/mmol) added to the culture medium at a final concentration of 1.25 μCi/ml and incubated for 30 min at 36°C, as revealed by autoradiography and staining (Fig. 8). Most of the grains were over the nucleus. However, because of the relatively long range of ^{14}C betas, good resolution was not obtained. Future work in this area is planned with tritiated RNA precursors.

SUMMARY

Our experiences and observations with nerve tissue cultures support earlier reports by others concerning the successful maintenance in vitro of nerve tissue in an apparently healthy condition for a period long enough to be useful for important investigations relevant to this tissue.

ACKNOWLEDGMENTS

We are greatly indebted to Professor Walther Hild of the University of Texas Medical Branch, Galveston, Texas, for his encouragement and help in improving our culture techniques. Helpful discussions with Professor M. R. Murray and Professor R. P. Bunge of Columbia University, College of Physicians and Surgeons, by Professor S. M. Crain of Albert Einstein College of Medicine, and by Dr. D. E. Rounds of Pasadena Foundation for Medical Research, Pasadena, California, are gratefully acknowledged. Special thanks is expressed to Miss Roseanne Stevens for her assistance in the preparation of the cultures.

This research was jointly supported by the U. S. Atomic Energy Commission and the National Aeronautics and Space Administration.

REFERENCES

1. Murray, M. R.: Nervous tissues in vitro. In Biology of Cells and Tissues in Culture, Vol. II, edited by E. N. Willmer. Academic Press, New York, 1966.
2. Lumsden, C. E.: Nervous tissue in culture. In The Structure and Function of Nervous Tissue, Vol. I, edited by G. H. Bourne. Academic Press, New York, 1968.
3. Bornstein, M. B.; and M. R. Murray: Serial observation on patterns of growth, myelin formation, maintenance, and degeneration in cultures of new-born rat and kitten cerebellum. J. Biophys. Biochem. Cytol. 4: 499-504 (1958).
4. Hendelman, W. J.; and J. Booher: Factors involved in the culturing of chick embryo dorsal root ganglia in the Rose chamber. Texas Rept. Biol. Med. 24, No. I: 83-89 (Spring 1966).
5. Costero, I.; and C. M. Pomerat: Cultivation of neurons from the adult human cerebral and cerebellar cortex. Am. J. Anat. 89: 405-467 (1951).
6. Hild, W.; and I. Tasaki: Morphological and physiological properties of neurons and glial cells in tissue culture. J. Neurophysiol. 25: 277-304 (1962).
7. Murray, M. R.; E. R. Peterson; and R. P. Bunge: Some nutritional aspects of myelin sheath formation in cultures of central and peripheral nervous system. In Proceedings of the IV International Congress of Neuropathology, Vol. II, edited by H. Jacob. Georg Thieme, Stuttgart, Germany, 1962. P. 267.

8. Rogers, A. W.: Techniques of Autoradiography. Elsevier, New York, 1967.
9. Murray, M. R.; and A. P. Stout: Adult human sympathetic ganglion cells cultivated in vitro. Am. J. Anat. 80: 225 (1947).
10. Peterson, E. R.; and M. R. Murray: Myelin sheath formation in cultures of avian spinal ganglia. Am. J. Anat. 96: 319-355 (1955).
11. Hild, W.: Ependymal cells in tissue culture. Z. Zellforsch. 46: 259 (1957).

Bioelectric Activity of Neurons in Tissue Culture: Synaptic Networks and Effects of Divalent Cations

Werner T. Schlapfer, Abdel-Megid Mamoon, Paul H. O'Lague and Cornelius A. Tobias

Nervous tissue grown and maintained in vitro represents a model system for the study of some of the properties of neurons and their interactions under relatively simple and controllable conditions. The important physiological properties of nerve cells are well retained in culture; thus neurons differentiate and mature in vitro (1, 2), their electrical properties correspond well to the in vivo situation (3, 4), and sympathetic ganglion nerve cells take up catecholamines (5). Organotypic cellular interactions such as the formation of myelin sheaths around axons (6, 7) and the establishment of synaptic structures as seen with the electron microscope (8, 9) are very similar to their in vivo counterparts. In thick cultures obtained by the Maximow technique (10) complex bioelectric activities--e.g., long-lasting oscillatory afterdischarges in response to electrical stimulation and spontaneous complex potentials--are found (11, 12), providing ample evidence for the existence of functional synaptic connections. In similarly cultured fetal material the onset of this complex electrical activity corresponds to the morphological development of clear-cut synaptic profiles as seen in the electron micrographs (13, 14). However, these thick cultures exhibiting complex bioelectric activities do not seem to allow good visualization of individual neurons and their processes at the recording site (15). On the other hand, the flying cover slip technique used by Hild and Tasaki (5), which favors rapid flattening of the explant into a thinly spread layer of neurons and glial cells, is accompanied by a considerable disruption of the normal architecture of the explant, but has the advantage of making individual neurons, dendrites, and axons easily visible under the phase-contrast microscope and accessible to exploration with microelectrodes. An additional advantage of this technique is the relative ease of preparation and maintenance of the cultures. Although Hild and Tasaki (5) have found no evidence for the presence of functional synapses in areas of the explant with low cellular density where dendrites could be clearly seen, slightly denser areas of similar cultures showed morphological evidence for synaptic structures (2, 9). These seem to be functional (16), and the investigation presented here attempts to further establish and examine the properties of synaptic interactions of neuronal nets in thin nerve-tissue cultures.

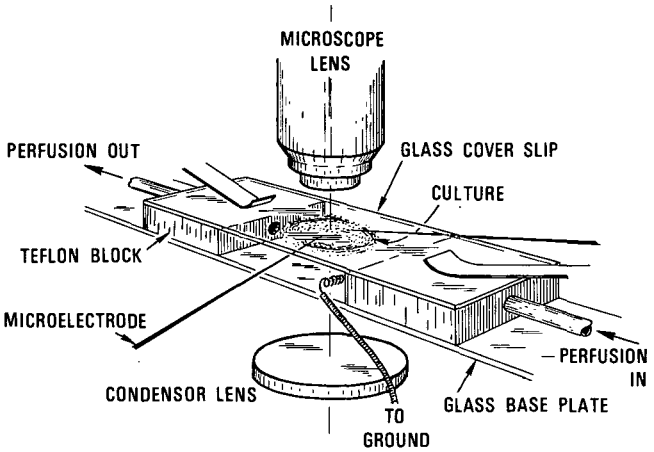

Fig. 1. Microscope stage for electrophysiological experiments on cultured nerve tissue.
DBL 694-4639

MATERIALS AND METHODS

Cultures of cerebellum and midbrain of new-born rats were prepared in plasma clots on flying cover slips in roller tubes (5, 17). They were fed weekly with a medium containing 75% Gey's balanced salt solution (BSS) and 25% calf serum, with glucose increased to 550 mg%. They were incubated at 36.5°C. By 14 to 16 days in vitro (DIV) the cultures had usually spread into a two-dimensional matrix of nerve and associated cells. A modified Bausch and Lomb microscope with Zeiss phase-contrast optics was used to view the cultures during electrophysiological experiments. The cover slip bearing the culture was mounted on a bridge (Fig. 1) which allowed the positioning of microelectrodes under visual control through the open sides. Ports for perfusion and exchange of the bathing solution (usually Gey's BSS enriched with glucose, or modifications thereof) were provided through the bridge mounts. A syringe pump facilitated the exchange of the bathing solution during electrophysiological experiments. All experiments were carried out at room temperature. For extracellular recordings glass capillary microelectrodes with tips of 3–6 μ filled with 0.9% NaCl were connected through low-noise ac preamplifiers (Applied Cybernetics Model 4UAH) to a storage oscilloscope and a tape recorder. Ultrafine glass microelectrodes (tip diameter < 1 μ) filled with 3 M KCl and connected via Ag-AgCl electrodes to a high-input impedance amplifier were used to record intracellular signals.

RESULTS

The growth patterns of the cultures used in these experiments are discussed in the companion paper beginning on p. 1 of this report.

SPONTANEOUS BIOELECTRIC ACTIVITY FROM SINGLE CELLS By positioning the tip of a microelectrode under visual control within a few micra of the soma of a neuron, spontaneous extracellular action potentials were recorded from most of the nerve cells tested. The spikes were usually negative (Fig. 2A), sometimes biphasic negative-positive (Fig. 2B), often with an inflection in the leading edge similar to in vivo recordings from cerebellar Purkinje cells (18), but at times large positive-negative spikes were seen (Fig. 2C) resembling the

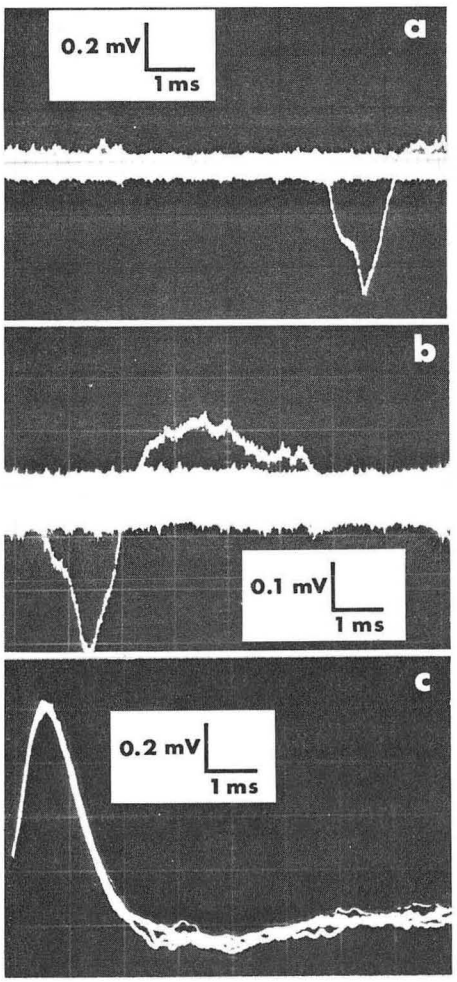

Fig. 2. Extracellular action potentials. A: Midbrain, 27 days in vitro (DIV); B: cerebellum, 20 DIV; C: midbrain, 27-DIV.

XBB 696-3544

extracellular potentials found by Woodward et al. (19) in the Purkinje cell layer of rat cerebellum. The average spike frequency ranged from a few spikes per minute to about 10 spikes per second, with interval distributions that were quite often nonrandom (Fig. 3A). Spikes often occurred in trains, with silent periods of sometimes several seconds between bursts (Fig. 3B). Frequencies as high as 100 impulses per second were observed during such bursts. The interval distribution is at present being analyzed in a more formal fashion. This spontaneous activity was found in cultures of 14 to 30 days in vitro and persisted for up to 5 hours at room temperature in balanced salt solution. No spontaneous extracellular spikes have been detected as yet in neurons located in very thin areas of the explant, where the density of cells and cellular processes is very low. Although the relationship of cellular density (neuron-glial interaction) to electrical activity warrants further study, it appears that a certain critical cellular density favors spontaneous activity, or assists in the maintenance of functional neuronal nets, or both.

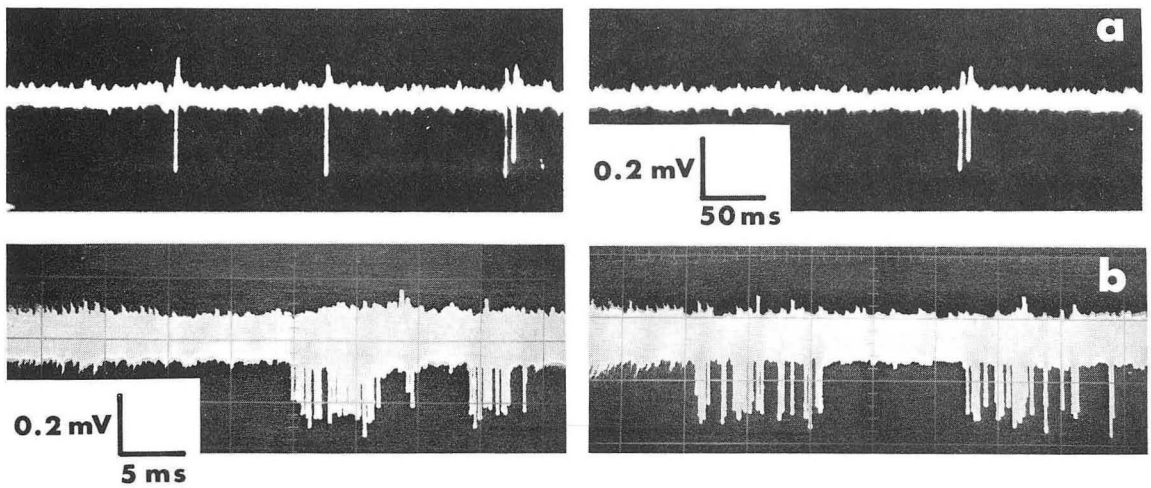

Fig. 3. Spontaneous spike activity. A: Doublet spikes from cerebellum, 30 DIV; B: bursting activity from midbrain culture, 17 DIV.
XBB 696-3545

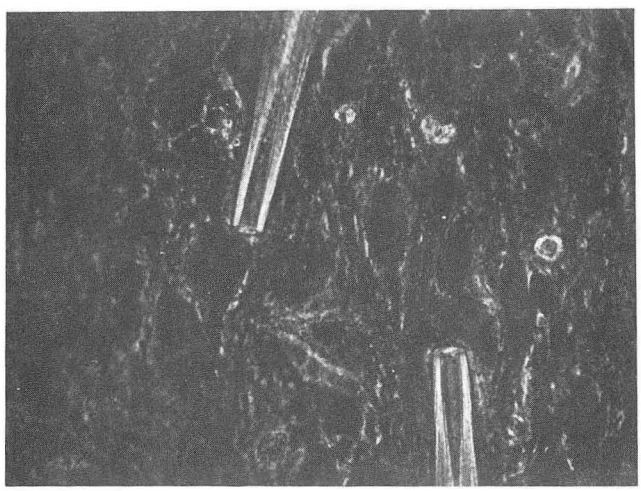

Fig. 4. Typical arrangement of electrodes for recording of extracellular bioelectric potentials.
XBB 696-3543

EXTRACELLULAR RECORDS FROM TWO NEURONS WITHIN THE SAME MICROSCOPIC FIELD When unit activity was simultaneously recorded with two microelectrodes from two randomly selected neurons separated from 20 μ to 200 μ (Fig. 4) their spike activities were very often correlated. Figure 5A shows correlated bursting, while detailed examination of the spikes within each burst (Fig. 5B) reveals a certain independence of individual spikes. Figure 6 is the oscilloscope record of another culture in which the two neurons tested fired very often within very short times. Here again, the correlation was not perfect, since there was no fixed temporal relation between the two firings. The degree of correlation is presently under study with the aid of a computer.

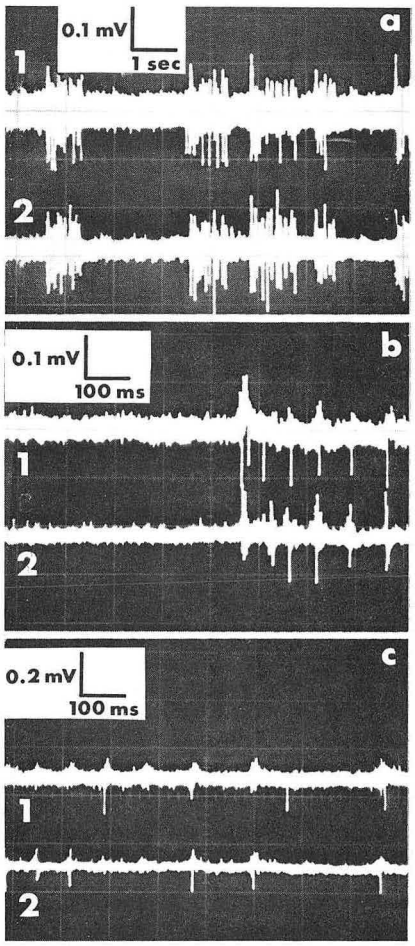

Fig. 5. A: Correlated bursting activity simultaneously recorded with two extracellular microelectrodes from two neurons approximately 50 μ apart. Upper trace is recording from first neuron, lower trace from the second. Cerebellum, 25 DIV. B: Similar sample record from the beginning of a burst. C: From within the burst. (Note the good correlation of the bursts and of some of the individual spikes.)

XBB 696-3546

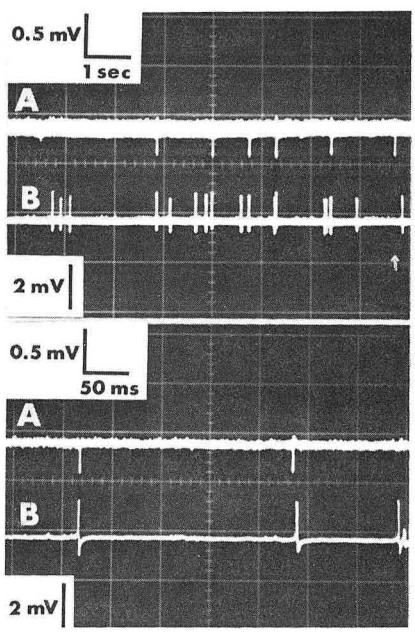

Fig. 6. Correlated spike activity from two neurons (simultaneous recording with 2 extracellular microelectrodes; upper and lower trace); midbrain culture, 22 DIV.

XBB 696-3547

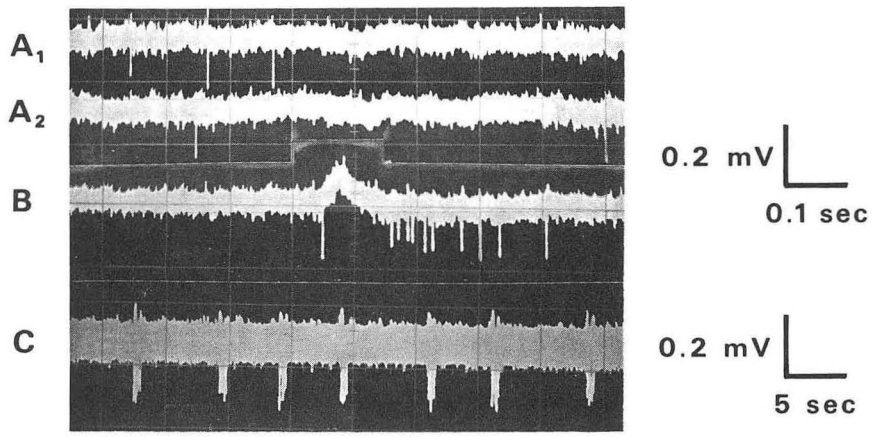

Fig. 7. Effect of injection of 10 μg/ml strychnine in balanced salt solution. A: Control with single spikes of low frequency. B and C: After injection of strychnine.
XBB 696-3542

EFFECTS OF STRYCHNINE The addition of 10 μg/ml strychnine to the bathing medium increased and altered the pattern of spike activity of single neurons in cultures. Unit spike activity of low frequency changed to a bursting pattern within less than a minute after injection of the drug. The pattern was rather stereotyped (Fig. 7B), consisting of a single spike followed by a slow positive wave and a series of 6–12 spikes. Such spontaneous bursts occurred at intervals of 4–8 sec (Fig. 7C).

INTRACELLULAR RECORDINGS FROM SINGLE NEURONS Microelectrode penetrations were made on histologically identifiable neurons. Membrane potentials ranged from -40 to -77 mV (inside negative), which, in a few cases, could be held for as long as 30 min. Figure 8 shows a group of living neurons from a 19-DIV cerebellar culture. A stable membrane potential of -77 mV was recorded for 22 min from one neuron (arrow). During the penetration, signals, presumably EPSP's, were recorded, suggesting the presence of functioning synapses in these cultures. No suprathreshold signals were observed.

EFFECTS OF VARYING THE CONCENTRATION OF MAGNESIUM AND CALCIUM The spontaneous spike activity of our cultures is very sensitive to changes in the concentration of magnesium and calcium in the bathing medium. Lowering the calcium concentration from 2.55 m$\underline{M}$ (normal amount of Ca^{++} in Gey's balanced salt solution) to 1.2 m$\underline{M}$ reversibly increased the unit spike frequency by a factor of 3–5. A reduction to 0.5 m$\underline{M}$ resulted in a large transitory increase of the firing rate lasting about a minute, followed by a depression to a level lower than the control value (Fig. 9). The effect was reversible: a return to balanced salt solution with 2.55 m$\underline{M}$ Ca^{++} restored the spike frequency more or less to control level. Injecting bathing medium lacking Ca^{++} caused a short burst of activity of even higher frequency, with a subsequent cessation of the spontaneous activity. The activity could be restored by returning to the control Ca^{++} level within a few minutes. No change in spike activity was noted after an increase of the calcium concentration from 2.55 to 3.55 m$\underline{M}$.

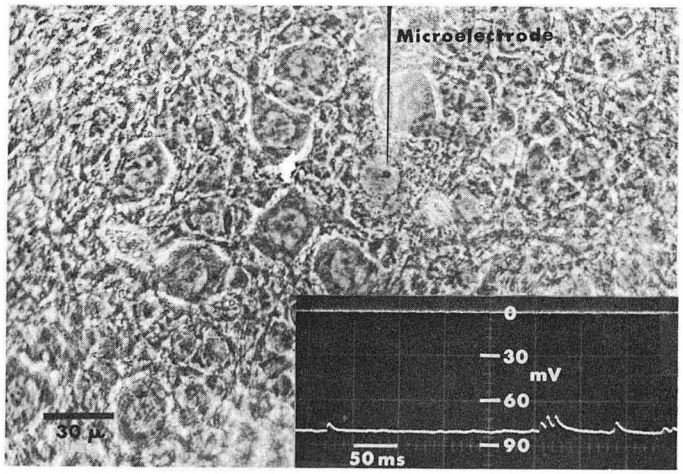

Fig. 8. Group of living neurons (phase contrast) from cerebellum, 19 DIV, showing position of intracellular microelectrode. Inset: Intracellular record from one neuron (arrow) showing membrane potential of -77 mV and subthreshold signals (presumably EPSP's). XBB 696-3548

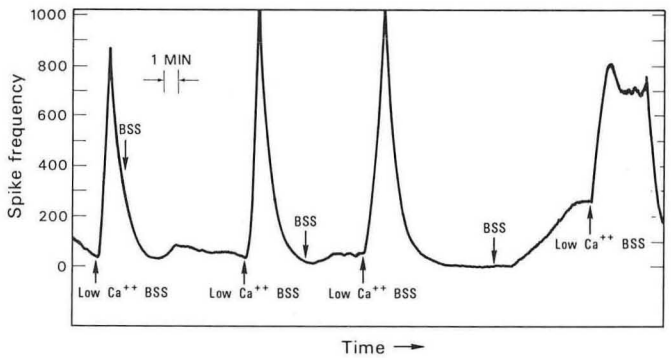

Fig. 9. Effect of lowering the calcium concentration of the balanced salt solution (BSS) from 2.55 mM to 1.2 mM (midbrain culture, 20 DIV). DBL 694-4638

Varying the concentration of magnesium in the presence of Ca^{++} had a much less pronounced effect. Reduction of the magnesium concentration from its normal level (1.07 mM in Gey's BSS) resulted in a reversible increase of the unit spike frequency, while an increase from 1.07 to 2.14 mM caused a reversible decrease of the spontaneous bioelectric activity by a factor of about 2.

DISCUSSION

The in vitro culture of small explants of nervous tissue is an attempt to isolate, simplify, and control the environment of an otherwise hopelessly complex biological structure. Extreme care must be taken to ensure the retention of the essential structural and functional aspects of the tissue, otherwise its simplification would be a vain and useless exercise. Most investigations of cultured nervous tissue are still concerned with demonstrating the integrity of its crucial cellular and organotypic parameters. The initial concern was with the cytology and morphology of neurons and glial cells in vitro (see reviews 20, 21), later with ultrastructure (1, 8, 9, 13). Electrophysiological investigations show that individual neurons retain their characteristic bioelectrical properties, such as membrane potentials, all-or-none action potentials, postspike soma refractoriness, and temporal summation of subliminal stimuli (3, 4). Recently some of the biochemical parameters of cultured nervous tissue have been measured and compared to in situ tissue (5, 22, 23).

Proper communication within the nervous system depends upon synaptic organization. The maintenance of functional synapses in culture is therefore of utmost importance if they are to be used to investigate nervous tissue function. In thick cultures, there is no doubt about the maintenance and even about the de novo formation of functional connections (12, 14). In thin cultures as prepared in this Laboratory, on the other hand, the degree of disruption of functional synapses has been highly controversial (24).

The rhythmic bursting activity, the existence of well-correlated spike activities among individual neurons, the presence of apparent intracellular EPSP's, and the action of strychnine and magnesium all strongly suggest the presence of functional synapses forming nets of nerve cells in densely packed areas of our cultures. The bursting activity of many of our cultures is similar to the spontaneous activity found by others (16), and is likely to correspond to the complex spontaneous bioelectric activity found with larger electrodes in thick nervous-tissue cultures (11, 12, 25). It seems probable that this rhythmic bursting activity is due to a neuronal network of multiple excitatory and inhibitory synapses (12, 26). Alternatively, local fluctuations of the molecular or ionic composition (or both) of the environment could possibly account for the rhythmic bursting activity. The strong correlation found between the extracellular spike activities of two different neurons is also good evidence for functional synaptic connections. The well related silent periods (Fig. 4A) suggest common inhibitory inputs, whereas the correlated individual impulses of the two simultaneous spike trains (Fig. 5) indicate excitatory connections to a network. Intracellular recordings are a powerful tool for the further investigation of the characteristics of individual neurons and their connections. The preliminary results obtained with intracellular electrodes in these investigations need more elaboration, especially to ascertain the origin of the "EPSP's." Variation of the external ionic environment, control of the membrane potential with a second intracellular electrode, or selective stimulation of the presynaptic neuron should be attempted in future experiments. Due to the delicate nature of cultured neurons, intracellular recordings are technically still very difficult to perform at present.

The action of strychnine points to the presence of inhibitory synapses, since it is thought that strychnine selectively inhibits these synapses (27). The effect of strychnine on the bioelectric activity of thicker cultures has been described by Crain (11), and is essentially similar to our findings. Further experimentation is needed in this kind of investigation. Finally, the action of magnesium is compatible with the presence of neuronal nets in our cultures. Although magnesium affects the excitability of the neuronal membrane, its main action is presumably on the synaptic transmission (28, 29). Again, more work is required, but the electrophysiological experiments with strychnine, magnesium, and calcium demonstrate the feasibility of using nerve tissue cultures for pharmacological studies on mammalian central nervous tissue.

SUMMARY

These experiments show that neurons in densely packed areas of thin cultures as prepared in our Laboratory exhibit bioelectric activities similar to the in vivo situation, and that these cultures contain functional synapses forming nets of interconnected neurons even though some of their normal architecture has been destroyed. Perfusion with bathing solutions of varying

concentration of Mg^{++} and Ca^{++} causes large changes in the average spike frequency. These cultures therefore represent a simplified system well suited for the study of some of the functions of the central nervous system. Since the environment can be controlled, effects on these neuronal nets of various chemical compounds, ions, and drugs, as well as of physical parameters such as temperature and radiation, can be studied.

ACKNOWLEDGMENTS

We thank Professor Walther Hild, University of Texas, Medical Branch, Galveston, Texas, for his encouragement and his invaluable help in the improvement of our culture techniques. Special thanks are expressed to Miss Roseanne Stevens for her great help in preparing the cultures for these experiments, and to Dr. C. T. Gaffey for his criticisms and suggestions regarding the electrophysiological techniques.

This research was jointly supported by the U.S. Atomic Energy Commission and the National Aeronautics and Space Administration.

REFERENCES

1. Bunge, M. B.; R. P. Bunge; E. R. Peterson; and M. R. Murray: A light and electron microscope study of long-term organized cultures of rat dorsal root ganglia. J. Cell Biol. 32: 439-466 (1967).
2. Hild, W.: Cell types and neuronal connections in cultures of mammalian central nervous tissue. Z. Zellforsch. 69: 155-188 (1966).
3. Crain, S. M.: Resting and action potentials of cultured chick embryo spinal ganglion cells. J. Comp. Neurol. 104: 285-326 (1956).
4. Hild, W.; and I. Tasaki: Morphological and physiological properties of neurons and glial cells in tissue culture. J. Neurophysiol. 25: 277-304 (1962).
5. Burdman, J. A.: Uptake of [^{3}H] catecholamines by chick embryo sympathetic ganglia in tissue culture. J. Neurochem. 15: 1321-1323 (1968).
6. Peterson, E. R.; and M. R. Murray: Myelin sheath formation in cultures of avian spinal ganglia. Am. J. Anat. 96: 319-355 (1955).
7. Hild, W.: Myelogenesis in cultures of mammalian central nervous tissue. Z. Zellforsch. 46: 71-95 (1957).
8. Bunge, R. P.; M. B. Bunge; E. R. Peterson; and M. R. Murray: Ultrastructural similarities between *in vitro* and *in vivo* central nervous tissue. J. Cell. Biol. 19: 11a (1963).
9. Callas, G.; and W. Hild: Electron microscopic observations of synaptic endings in cultures of mammalian central nervous tissue. Z. Zellforsch. 63: 686-691 (1964).
10. Bornstein, M. B.; and M. R. Murray: Serial observation on patterns of growth, myelin formation, maintenance, and degeneration in cultures of newborn rat and kitten cerebellum. J. Biophys. Biochem. Cytol. 4: 499-504 (1958).
11. Crain, S. M.; and M. B. Bornstein: Bioelectric activity of neonatal mouse cerebral cortex during growth and differentiation in tissue culture. Exptl. Neurol. 10: 425-450 (1964).
12. Crain, S. M.: Development of "organotypic" bioelectric activities in central nervous tissues during maturation in culture. Intern. Rev. Neurobiol. 9: 1-43 (1966).

13. Bunge, M. B.; R. P. Bunge; and E. R. Peterson: The onset of synapse formation in spinal cord cultures as studied by electron microscopy. Brain Res. 6: 728-749 (1967).
14. Crain, S. M.; and E. R. Peterson: Onset and development of functional interneuronal connections in explants of rat spinal cord-ganglia during maturation in culture. Brain Res. 6: 750-762 (1967).
15. Crain, S. M.: in T. H. Bullock (ed.), Simple Systems for the Study of Learning Mechanisms. Neuroscience Res. Progr. Bull. 4, 2: 160 (1966).
16. Cechner, R. L.: Personal communication (Manuscript of Ph. D. Thesis, 1967).
17. Mamoon, A.; W. T. Schlapfer; and C. A. Tobias: Mammalian nervous tissue in culture. Page 1 of this report.
18. Eccles, J. C.; R. Llinas; and K. Sasaki: The action of antidromic impulses on the cerebellar Purkinje cells. J. Physiol. (London) 182: 316-345 (1966).
19. Woodward, D. J.; B. J. Hoffer; and L. W. Lapham: Postnatal development of electrical and enzyme histochemical activity in Purkinje cells. Exptl. Neurol. 23: 120-139 (1969).
20. Murray, M. R.: Nervous tissues in vitro. In Biology of Cells and Tissues in Culture, Vol. II, edited by E. N. Willmer. Academic Press, New York, 1966.
21. Lumsden, C. E.: Nervous tissue in culture. In The Structure and Function of Nervous Tissue, Vol. I., edited by G. H. Bourne. Academic Press, New York, 1968.
22. Cechner, R. L.; H. M. Geller; and D. G. Fleming: Primary pathways for glucose metabolism in CNS tissue cultures. Biophys. J. 9: A-61 (1969).
23. Appel, S. H.; and D. H. Silberberg: Pyrimidine synthesis in tissue culture. J. Neurochem. 15: 1437-1443 (1968).
24. Hild, W.: Electrophysiological phenomena observed in single neurons and neuroglial cells in cultures of central nervous tissue. In Brain Function, Vol. II, edited by M. A. Brazier. University of California Press, Berkeley and Los Angeles, 1964.
25. Cunningham, A. W. B.: Qualitative behavior of spontaneous potentials from explants of 15-day chick embryo telencephalon in vitro. J. Gen. Physiol. 45: 1055-1076 (1962).
26. Farley, B. G.: In Computers in Biomedical Research, Vol. I, edited by R. W. Stacy and B. Waxman. Academic Press, New York, 1962. Chap. 11, P. 265.
27. Bradley, K.; D. M. Easton; and J. C. Eccles: An investigation of primary or direct inhibition. J. Physiol. 122: 474-488 (1953).
28. Somjen, G. G.; and G. Kato: Effects of magnesium and calcium on neurons in the central nervous system. Brain Res. 9: 161-164 (1968).
29. Desmedt, J. E.: L'action des cations alcalino-terreux sur les transmissions neuromusculaire et synaptiques. In Ions Alcalino-Terreux, Handbuch der experimentellen Pharmakologie, Vol. 17/1, edited by Z. M. Bacq. Springer-Verlag, Berlin, 1963.

Isolation of Disomics in *Saccharomyces cerevisiae*

Patric Tauro, Ubaldo S. Rodarte-y-Ramon, Tommy J. McKey and Robert K. Mortimer

In synchronous cultures of yeast, the syntheses of DNA and several enzymes are periodic (1-3). The number of periods of synthesis of a given enzyme is equal to the number of structural genes present (4). The synthesis of two other primary gene products--namely, ribosomal and transfer RNA (t-RNA)--is, however, continuous during the cell cycle (5). By DNA-RNA hybridization, it has been shown that there are large numbers of cistrons for both ribosomal and t-RNA in S. cerevisiae (6, 7). The continuous synthesis of stable RNA during the cell cycle of yeast may be due to either (i) scattering of these cistrons on the 16 chromosomes of yeast, with each of these cistrons being periodically transcribed, or (ii) a different type of control for these cistrons than for the structural genes for enzymes.

Lack of techniques to isolate large-molecular-weight DNA from yeast makes it difficult to estimate the number of cistrons for stable RNA on any given chromosome. Although determination of the genetic locations of these cistrons may be difficult, by the use of yeast strains having known extra chromosomes (disomics) it should be possible to estimate the number of cistrons for each of the RNA species on the different chromosomes of yeast. The disomic strains are also suitable for genetic mapping (8) and for the isolation of mutants defective in recombination (9). A technique for the construction of disomic strains with the extra chromosome identified was suggested by the findings of Pittenger (10) and Case and Giles (11) on pseudowilds in Neurospora. Some wild-type spores from heterokaryons that carried two complementing alleles at a locus were found to be disomic for the chromosome carrying these alleles. The wild-type response in these cases was due to complementation and not to intragenic recombination or conversion. This paper summarizes our initial studies concerning the construction of disomics (n+1) in S. cerevisiae using this approach. A similar procedure has been used by Fink (12) for construction of other disomics in this yeast.

MATERIALS AND METHODS

The stocks were maintained on YEPD agar slants by regular transfers. The media and the procedures for mating, isolation of zygotes, and sporulation of hybrids are described by Manney (13) and Hawthorne and Mortimer (14).

For this experiment a diploid D1 with the following genotype was constructed:

$$\frac{a}{\alpha}\ \frac{trp5\text{-}1}{+}\ \frac{leu1\text{-}19}{leu1\text{-}5}\ \circ\ \frac{ade6\text{-}121}{ade6\text{-}23}\ \frac{+}{can^r}\ \frac{ura1\text{-}1}{+}\ .$$

The genes trp5, leu1, and ade6 are located on chromosome VII (8). The centromere of this chromosome is located between leu1 and ade6. The alleles leu1-19 and leu1-5 complement, whereas ade6-121 and ade6-23 are noncomplementing alleles that are widely separated in the ade6 gene (15); can^r is a recessive mutation that confers resistance to canavanine. Its incorporation in this diploid allowed selection of spores in the presence of unsporulated diploids (16). The leu1 allele pair provided a means for selection of spore clones with chromosome VII in diploid condition. However, conversion and recombination between these alleles also would yield wild-type spores. The ade6 allele pair was included to confirm the presumed disomics. Only leucine-independent spore clones that exhibited a high frequency of reversion to adenine independence were selected for further characterization as presumed disomics. The high frequency of adenine reversion is characteristic of a heteroallelic condition and would not be expected if chromosome VII were in haploid condition. Additional characterization of the presumptive disomics depended on tetrad analysis. Hybrids carrying three instead of two chromosomes are expected to exhibit irregular segregation ratios for genes on this chromosome.

RESULTS

ISOLATION OF DISOMICS FROM DIPLOID D1 Cells of diploid D1 were sporulated. The sporulated sample, which contained approximately 30% asci, was treated with glusulase (Endo Labs) and then sonicated to yield a suspension of single spores (≈60%), unsporulated cells, and cell debris. This suspension was plated on a synthetic medium that contained adenine, tryptophan, uracil, and canavanine (i.e., leucine-deficient). This medium permits the growth of (i) unsporulated diploids that are homozygous for can^r, for example, as a result of a previous mitotic segregation event, (ii) spores that are disomic for chromosome VII and also carry the can^r gene, and (iii) haploid spores that are leucine-independent as a result of conversion or recombination within the leu1 gene, and also carry the can^r gene. The colonies that developed on this medium were replica-plated to adenine-deficient medium and the replicas exposed to X rays (4 krads) to induce heteroallelic reversion. Only unsporulated diploids and disomics are expected to yield revertants on this medium. Of 1.4×10^8 cells plated originally, 50 leucine-independent canavanine-resistant clones were obtained that showed reversion on adenineless medium. These were tested for mating response, with both a and α mating-type testers, as well as for uracil requirement. Only disomics are expected to exhibit a mating response. In addition some disomics express the uracil mutation. Of the 50 clones tested 16 were tentatively identified as disomics by use of these criteria.

GENETIC ANALYSIS OF A PRESUMPTIVE DISOMIC One of the presumptive disomics DS-542-VII, was crossed to X2180-1A (a mating type, wild). The resulting hybrid D2 was sporulated and the spores analyzed for segregation of the trp5, leu1, ade6, and mating-type genes. If Ds-542-VII is disomic, the expected genotype of the cross D2 is

$$\frac{a}{\alpha}\ \frac{\begin{matrix}\text{trp5} & \text{leu1-19} & + & & \text{ade6-21} & +\end{matrix}}{\begin{matrix}+ & + & \text{leu1-5} & \circ & + & \text{ade6-23}\end{matrix}}\ \frac{\text{can}^r}{+}.$$

$$\begin{matrix}+ & + & + & & + & +\end{matrix}$$

The expected frequencies of segregation ratios (nonrequirement: requirement) of a gene in duplex condition in a trisome, such as for trp5, are

$$P(4:0) = (1/3)(2-x),\ P(3:1) = 2/3\ x,\ P(2:2) = (1/3)(1-x), \tag{1}$$

where P(4:0), P(3:1), P(2:2) are the probabilities of the corresponding segregation ratios and x is the second-division segregation frequency; for trp5, x = 0.33 (8). At the leu 1 locus there is one dominant allele (simplex) and two complementing mutant alleles. It can be shown that the segregation ratios for leucine independence: leucine dependence are described by

$$P(4:0) = (1/3)(1-x),\ P(3:1) = 2/3\ x,\ P(2:2) = (1/3)(2-x). \tag{2}$$

The second-division segregation frequency, x, for leu1 is 0.05 (8). For the calculation of Eqs. 1 and 2 it has been assumed that crossing-over occurs randomly among two of the trisomic chromosomes. For ade6 only 2:2 segregation is expected because only one dominant allele is segregating. Mating type is expected to segregate 2a, 2α in each ascus if only two copies of the chromosome are present. Deviations from these expected ratios can result from gene conversion (17). The segregation ratios for the different genes for a sample of 28 asci are presented in Table 1. Included in this table are the expected numbers of asci for each of the ratios. It can be seen that the data agree quite well with the predictions based on the assumption that DS-542-VII is disomic for chromosome VII. The spore viability of D2 was high (greater than 90%). This in addition excludes the possibility that DS-542-VII was diploid. If this were the case, D2 would be triploid, and very low spore viability would have been encountered (18).

Table 1. Segregation ratios of markers in D2.

Marker	+:-	Number of asci observed	Number of asci expected
leu	4:0	7	9
	3:1	4	1
	2:2	17	18
trp	4:0	11	16
	3:1	13	6
	2:2	4	6
ade	4:0	0	0
	3:1	3	0
	2:2	25	28
Mating type	4:0	0	0
	3:1	0	0
	2:2	28	28

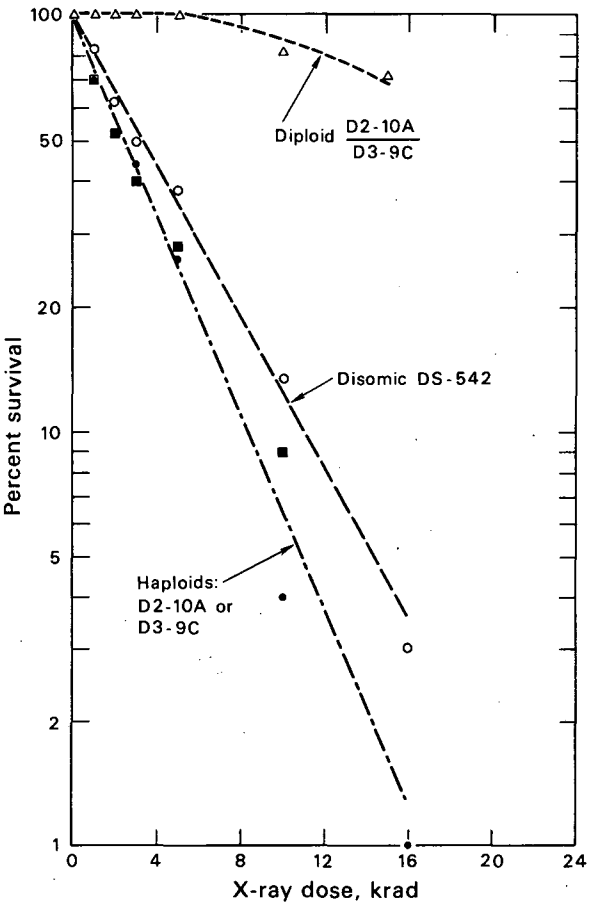

Fig. 1. X-ray sensitivity of disomic DS-542-VII and parental strains. Washed cells were plated on YEPD agar plates and irradiated as indicated.
DBL 693-4609

RADIATION SENSITIVITY Radiation sensitivity in yeast is ploidy-dependent (19). This property is therefore useful in distinguishing haploids from strains of higher ploidy. Genetic analysis described before indicates that the strain DS-542-VII is disomic for chromosome VII and the rest of the genome is expected to be in haploid configuration. If this is the case the radiation sensitivity of the disomic strain should be similar to that of the haploids. Figure 1 illustrates the results of an experiment in which the radiation sensitivity of the disomic strain was compared with that of its parental haploid and diploid strains. It is seen that the radiation sensitivity of the two haploid parental strains is identical and, as expected, the diploid strain is considerably more resistant to X-ray irradiation than the haploids. The disomic strain is slightly more resistant to X-ray inactivation than the parental haploids and still has exponential survival.

INDUCTION OF PROTOTROPHS It has been observed that X-ray induction of prototrophs in heteroallelic disomics follow a linear kinetics for low X-ray doses (9). Induction of adenine prototrophs was tested in the strain DS-542-VII and found to follow a linear relationship for a dose range of 0 to 3 krads. The slope of the line is 55 prototrophs/10^8 survivors/rad. The corresponding frequency for this allele pair in diploids is 120 prototrophs/10^8 survivors per rad. This result also supports the conclusion that the strain is disomic.

STABILITY OF THE DISOMIC DS-542-VII If disomics are used to determine the number of cistrons for stable RNA on each of the yeast chromosomes, some estimate of stability is required. DNA-RNA experiments require large number of cells and prolonged periods of growth in liquid medium. Nondisjunction could lead to reversion of a fraction of the population of cells to a haploid state. Haploidization of chromosome VII on DS-542-VII leads to cells that are leucine-dependent. Some of those also may be tryptophan-dependent. A sample of 241 clones grown for 10 generations in liquid medium were tested and not one showed a tryptophan or leucine requirement. In addition, all still reverted to adenine independence at a high frequency. This suggests that, at least for this case, the disomic condition is quite stable.

DISCUSSION

Our knowledge of aneuploids and in particular disomics is to a large extent based on investigations carried out in plants. In yeast, a few disomics accidentally observed have been reported (14). The method described herein to isolate disomics in yeasts is simple and allows easy construction and detection of disomics for any given chromosome. The data obtained from the genetic analysis, radiation sensitivity, and prototroph induction with DS-542-VII confirm that the strain is disomic for chromosome VII.

In plants, aneuploids have been observed to possess lower vigor than the normal diploids (20). However, different aneuploids behave differently, depending on which of the chromosomes is in triplicate. The disomic DS-542-VII described in this study displays normal growth compared to the parental haploids and displays a relatively high degree of stability during prolonged periods of culture. The complementing nature of leu1-5 and leu1-19 in the disomic, as in the diploid parent, suggests that both genes are functional. It therefore suggests that the entire chromosome VII is also functional. Furthermore, the segregation of several markers investigated indicates normal replication of the extra chromosome during meiosis. The high degree of stability and the fact that the extra chromosome is functional makes this strain extremely useful for biochemical studies. In addition to being useful in determination of stable RNA cistrons in yeast, disomics are also useful in determining genetic linkage (8) and detection of translocations.

SUMMARY

A method for the isolation of disomics in yeast by the use of a system containing a set of noncomplementing alleles is described. The disomic isolated by this procedure has been investigated for its disomic status. The data suggest that the extra chromosome present in DS-542-VII is functional and that the strain is stable.

ACKNOWLEDGMENTS

The cooperation of Dr. E. Jones and Dr. S. Nakai, who supplied the strains used in this experiment, is gratefully acknowledged.

REFERENCES AND NOTES

1. Williamson, D. H.: J. Cell. Biol. 25: 517 (1965).
2. Gorman, J.; P. Tauro; M. Laberge; and H. O. Halvorson: Biochem. Biophys. Res.

Commun. 15: 43 (1964).

3. Halvorson, H. O.; J. Gorman; P. Tauro; M. Laberge; and R. Epstein: Fed. Proc. 23: 1002 (1964).
4. Tauro, P.; and H. O. Halvorson: J. Bacteriol. 92: 652 (1966).
5. Tauro, P.; E. Schweiser; R. Epstein; and H. O. Halvorson: in Cell Cycle: Genetic and Developmental Aspects. Edited by G. M. Padilla, G. L. Whitson, and I. L. Cameron. Academic Press, New York, 1969.
6. Fukuhara, H.: Proc. Natl. Acad. Sci. U.S. 58: 1065 (1967).
7. Schweiser, E.; C. MacKechnie; and H. O. Halvorson: J. Mol. Biol. 40, 261 (1968).
8. Mortimer, R. K.; and D. D. Hawthorne: Genetics 53: 165 (1966).
9. Rodarte, U. S.; R. K. Mortimer; P. Tauro; and S. Fogel: Isolation and characterization of recombination-defective mutants in Saccharomyces cerevisiae. In preparation.
10. Pittenger, T. H.: Genetics 39: 326 (1954).
11. Case, M.; and N. Giles: Proc. Natl. Acad. Sci. U.S. 46: 659 (1960).
12. Fink, G. (Cornell University): private communication.
13. Manney, T. R.: Genetics 50: 109 (1964).
14. Hawthorne, D. C.; and R. K. Mortimer: Genetics 45: 1085 (1960).
15. Jones, E.: Ph.D. thesis, University of Washington, 1965.
16. Sherman, F.; and H. Roman: Genetics 48: 225 (1963).
17. Roman, H.: Cold Spring Harbor Symp. Quant. Biol. 23: 155 (1958).
18. Mortimer, R. K.: Radiation Res. 9: 312 (1958).
19. Mortimer, R. K.: in Fundamental Aspects of Radiosensitivity. Brookhaven Symposia in Biology No. 14, 1961.
20. Burnham, C. R.: in Discussions in Cytogenetics. Burgess Publishing Co., Minneapolis, 1962.

Patric Tauro's present address is Department of Microbiology, Punjab Agricultural University, Ludhiana, India.

Ubaldo Rodarte-y-Ramon holds a Fellowship of the Comisión Nacional de Energía Nuclear, Mexico.

Fluorescence of Serum High-Density Lipoprotein

Norman K. Freeman and Alex V. Nichols

Fluorescence has in recent years assumed increasing importance as a property of proteins which can provide evidence regarding their structural and conformational changes in a variety of circumstances. The use of fluorescence in the study of proteins has many aspects, which have been discussed in considerable detail by Konev (1) and by Chen (2). Wavelength shifts and intensity changes of the native protein fluorescence can be observed; it is also possible to attach fluorescent dye molecules to proteins in various ways. If noncovalently bound, such complexes may be used to investigate binding properties. If they are covalently bound, polarization measurements permit certain inferences regarding the rotational properties of protein molecules.

Very little has been reported on the fluorescence of lipoproteins. Margolis and Langdon (3) presented fluorescence emission curves for low-density lipoproteins (from human serum) in 0.15 M NaCl and in 8 M urea. Only small differences were noted in peak wavelengths (2-3 nm) and in fluorescence intensity (≈ 5%). It was suggested on the basis of this observation that whatever structural alteration resulted from urea denaturation did not radically change the polar character of the immediate environment of the aromatic amino acids; i.e., they were not originally buried in a lipid matrix.

We have set out to study the fluorescence properties of lipoproteins more extensively. Our primary interest is the set of human serum lipoproteins that are customarily isolated by ultracentrifugal procedures. It is contemplated that a variety of techniques involving fluorescence will be used, and that the information obtained will be pertinent to such structural features as molecular size and shape, arrangement of lipid and protein components, and nature of lipid-protein binding. The data presented in this paper, however, are limited to measurements of the intrinsic fluorescence spectra and quantum yields of serum high-density lipoprotein (HDL) and its delipidized apoprotein counterpart (apo-HDL).

EXPERIMENTAL PROCEDURE

MATERIALS High-density lipoprotein (d 1.063–1.21 g/ml) was prepared from human serum by the standard ultracentrifugal techniques employed in this Laboratory (4). Apo-HDL

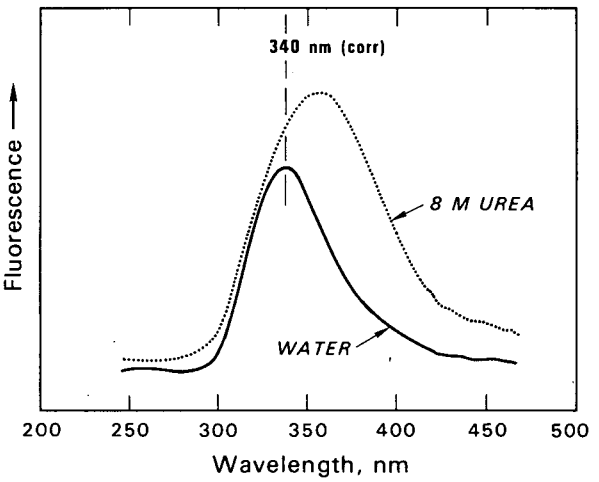

Fig. 1. Fluorescence emission spectra of high-density lipoprotein, 0.23 mg/ml. Excitation at 280 nm.

DBL 694-4643

was obtained by a delipidization procedure which consisted of extraction by alcohol and ether at low temperature as described by Scanu (5). Bovine plasma albumin (Armour, crystallized) was used without further purification.

APPARATUS Fluorescence measurements were made with an Aminco-Bowman Spectrophotofluorometer, Model 4-8106. Its emission wavelength scale was calibrated with a mercury lamp and appropriate corrections were applied. Fluorescence emission curves were recorded on a Sanborn X-Y Recorder, Model 670 A. Ultraviolet absorption measurements were made on a Cary Model 14 Spectrophotometer.

RESULTS AND DISCUSSION

The principal observations are essentially those shown in Figs. 1, 2, and 3. These are fluorescence emission spectra of HDL, apo-HDL, and albumin (BSA) respectively, both in water and in 8 M urea. In all cases the excitation wavelength was 280 nm. Wavelengths of fluorescence maxima and estimated quantum yields are given in Table 1.

The calculations of quantum yield (ϕ, fluorescence efficiency) were made relative to BSA, which was assumed to have the value 0.152 determined by Teale (6). No corrections of the spectra were made, but since the positions of both absorption and fluorescence maxima are nearly the same for the different proteins the equation given by Parker (7) should be valid:

$$\frac{F_{HDL}}{F_{BSA}} = \frac{A_{HDL}\phi_{HDL}}{A_{BSA}\phi_{BSA}},$$

where A and F are measured absorbance and fluorescence (at their respective maxima) for the two protein solutions at suitable concentrations. Areas of the fluorescence curves would be preferable to peak heights, but since only ratios are involved and the band shapes are similar, peak heights may be used.

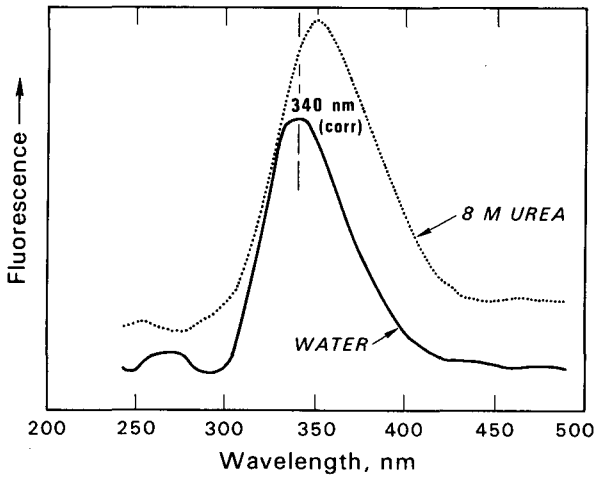

Fig. 2. Fluorescence emission spectra of delipidized high-density lipoprotein, 0.2 mg/ml. Excitation at 280 nm.
DBL 694-4644

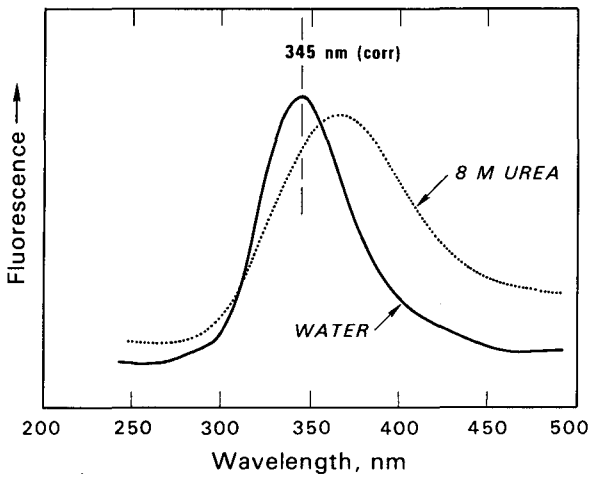

Fig. 3. Fluorescence emission spectra of bovine serum albumin, 0.066 mg/ml. Excitation at 280 nm.
DBL 694-4645

The interpretation of these data hinges on the postulate--discussed by Konev (1)--that the tryptophan residues in a protein can be either on the surface where they are exposed to an aqueous environment, or buried in the hydrophobic interior of the molecule. Since the fluorescence peak of tryptophan itself has been observed to shift from about 350 nm in water to 329 nm in dioxane, it is inferred that the dielectric constant of the medium has a significant effect on the wavelength of maximum fluorescence. When tryptophan is incorporated into a protein, its quantum yield is also determined to a considerable extent by the degree of polarity of the microenvironment. The yield tends to be lower in hydrophobic regions, higher in hydrophilic regions.

In a lipoprotein there is an obvious additional hydrophobic milieu that is available for interaction with the protein. Still it may not be possible to distinguish the lipid hydrophobic region from the interior of the protein itself as a microenvironment. Our data for the effects of 8 M urea on HDL are consistent with most proteins, i.e., there is a shift of about 15 nm

Table 1. Fluorescence of high-density lipoprotein.

	λ_{max}		
	absorption (nm)	fluorescence (nm)	Quantum yield
HDL (in water)	280	340	0.12
HDL (in 8 M urea)		355	0.15
apo-HDL (in water)	278	340	0.18
apo-HDL (in 8 M urea)		355	0.23
BSA (in water)	278	345	0.15[a]
BSA (in 8 M urea)		365	0.13

a. From Teale, Ref. 6.

toward longer wavelengths, and there is an increase in quantum yield. (For a number of proteins the wavelength shift is fairly uniform, whereas the change in quantum yield is irregular, and in a few cases negative--BSA, for example.) Thus this observation gives no indication of any special effect of lipids on the tryptophan fluorescence. Neither does the position of the fluorescence maximum, which is if anything slightly higher than the range (328–339 nm) of several simple proteins. The effect of 8 M urea seems to be essentially the same in apo-HDL as it is in HDL.

The 50% increase in quantum yield as a consequence of delipidization must have some significance, although it is not accompanied by a wavelength shift. Konev suggests that a tryptophan residue in a hydrophilic environment has a quantum yield of 0.20–0.25, which is close to that of free tryptophan. In a hydrophobic environment the value drops to about 0.08. Intermediate values represent a distribution of tryptophans between the two states. In many proteins in which such intermediate values occur they can be raised to the free tryptophan range by exposure to 8 M urea. However, as pointed out by Konev, the quantum yield of a particular protein probably reflects some mean value of the yields of all the tryptophan residues as they are influenced by various kinds of constant or induced dipole-dipole or ion-dipole effects of the surrounding groupings. The quantum yields of HDL (0.12) and apo-HDL (0.18) are both in the intermediate range, and the higher value of the latter suggests that delipidization does indeed transfer some tryptophan residues from less polar to more polar environments. There is no wavelength shift, however, so the process must differ from that resulting from the action of urea. Since there is a further effect of urea on apo-HDL, it is tempting to speculate that intact HDL has three classes of tryptophans: (i) at a protein-water interface; (ii) at a protein-lipid interface; (iii) in the interior of the protein. Although the present evidence is consistent with this hypothesis, it is still inconclusive.

SUMMARY

Measurements have been made of the intrinsic fluorescence of high-density lipoprotein and delipidized high-density lipoprotein. Spectra of both substances in water and in 8 M urea

were compared, and quantum yields were estimated. The data have been interpreted in terms of a hypothesis that the tryptophan residues are distributed among three distinct kinds of local environment in the lipoprotein macromolecule.

REFERENCES

1. Konev, S. V.: Fluorescence and Phosphorescence of Proteins and Nucleic Acids. Plenum Press, New York, 1967.
2. Chen, R. F.: in G. G. Guilbault, Fluorescence: Theory, Instrumentation, and Practice. Dekker, New York, 1967. P. 443-509.
3. Margolis, S.; and R. F. Langdon: J. Biol. Chem. 241: 477 (1966).
4. Lindgren, F. T.; A. V. Nichols; and R. D. Wills: Am. J. Clin. Nutr. 9: 13 (1961).
5. Scanu, A.: J. Lipid Res. 7: 295 (1966).
6. Teale, F. W. J.: Biochem. J. 76: 381 (1960).
7. Parker, C. A.: Photoluminescence of Solutions. Elsevier, Amsterdam, 1968. P. 262.

Ultracentrifuge Data Acquisition from a Central Control System

Alfred A. Windsor, Lin C. Jensen, David A. Hoopes and Frank T. Lindgren

In an earlier study (1) automatic acceleration to full speed was provided for an analytic ultracentrifuge using a modified electronic speed-control system. However, during an ultracentrifuge run it is useful and frequently necessary to obtain accurate information about the acceleration phase, full-speed stability, and rotor temperature, and the exact time that schlieren photographs are taken. The present automatic system is designed to provide all such data from one or more analytic ultracentrifuges.

When data are collected from several devices and channeled into one recorder, a method of coding and collating is required. We have chosen to use a master clock to synchronize the start of each machine and to code the data by the time at which measurements are taken. A time sequencer strobes the measurements by switching from machine to machine in a one-two-three sequence. This data-collecting system is available for any one or all three ultracentrifuges, which may run on totally independent operation schedules.

A digital clock (Parabam Model DA 24, Hawthorne, California) reading hours, minutes, and seconds on a 24-hour basis controls the timing. An interface coupler (Dymec Model 2526, Hewlett-Packard, Palo Alto, California) operates with an IBM summary punch machine to store and record 12 input characters. The IBM patchboard determines the card format containing the time, machine number, rpm, and rotor temperature. Each card also has the date punched from a master card.

Figure 1 shows the progression of data from the centrifuges to the summary punch machine. Mercury reed relays select signals from gear-tooth counters (Electro Model 3010-A, Chicago, Ill.) for rotor speed information and from radiometers for rotor temperature information. A gear attached to the drive motor has teeth which are counted to give impulses proportional to rotor speed. The radiometer (Beckman Instruments, Palo Alto, California) is the total radiation heat-balance type used in the Model L2-65B preparative ultracentrifuge. A 0.5-in.-diameter aluminum disk receives the energy, and thermocouple wires support and measure the temperature of the disk. The outer structure defines the area from which the receiving ele-

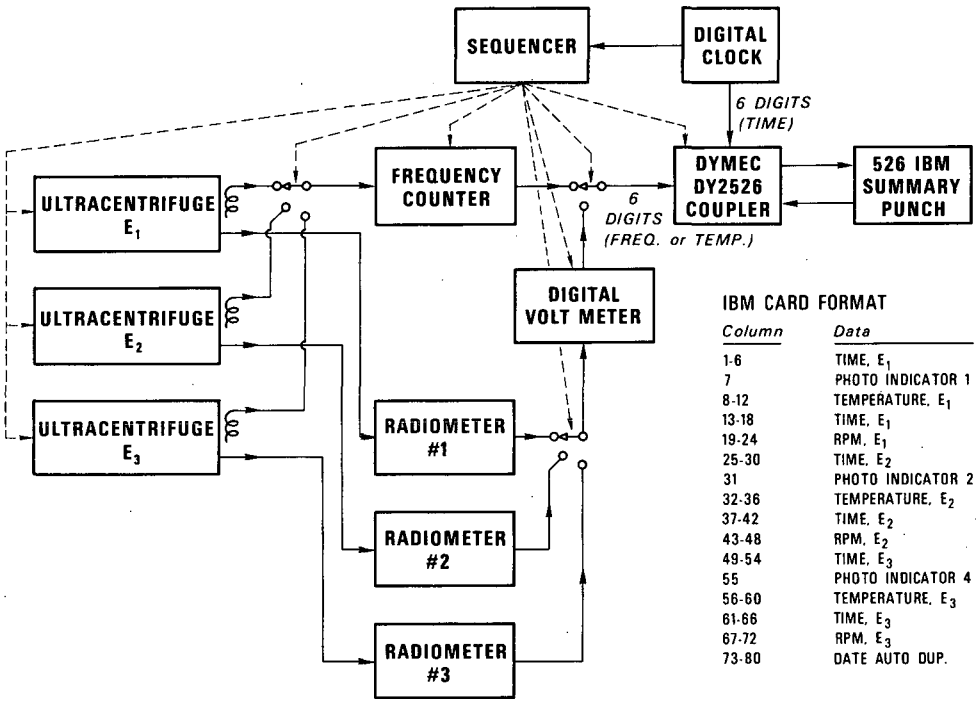

Fig. 1. Overall block diagram.

DBL 695-4698

ment or disk receives the infrared radiation. This structure or shield also has a thermocouple for comparison with the disk thermocouple; a thermoelectric module heats or cools the shield to the same temperature as the disk in a closed-loop system.

Reed relays select radiometer outputs to channel the corresponding ultracentrifuge temperature analog voltage to a digital voltmeter (Model 3460B, Hewlett-Packard, Palo Alto, California). The bottom of the analytic rotor is recessed 40 thousandths and painted flat black to optimize radiation exchange between the rotor and the radiometer; the latter is offset 3/4 in. from the axis of the rotor and spaced 1/4 in. from the rotor bottom. Five digits of binary coded decimal (BCD) temperature information are available at the digital voltmeter output. A counter (Model 5246L, Hewlett-Packard, Palo Alto, California) with a preset unit converts rotor speed pulses to BCD revolutions per minute. Six digits are available at the output, and reed relays select between speed and temperature digital output for the interface coupler.

The sequencer chassis converts timing signals from the master clock to instructions to the system. All ultracentrifuges are scanned; if one is not in operation the numbers corresponding to the static condition are recorded by the printing summary punch machine. Each time a picture is taken an indicator is punched just before the temperature as shown in the card format (Fig. 1). Machines are coded by punching a 1, 2, or 4. If pictures are taken by one or by two or three machines simultaneously, it is still possible to know which machines took pictures because the coupler decodes these numbers as the sum.

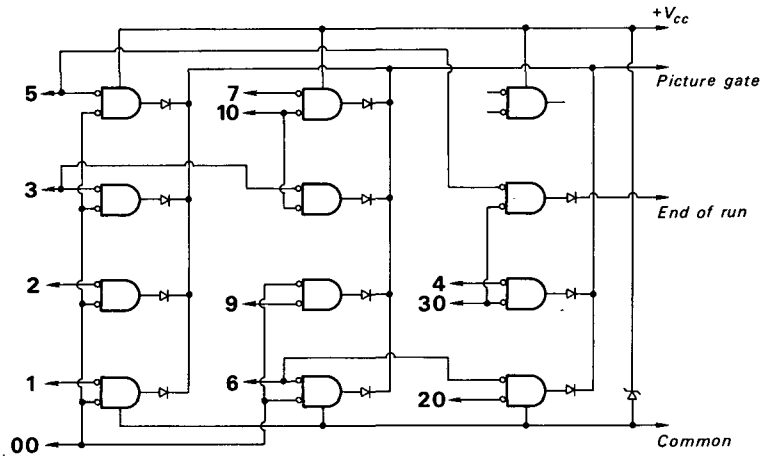

Fig. 2. Circuit diagram of program card.
DBL 695-4699

MACHINE 3, STARTED AT 14H37M 0S 02/11/69

FRAME	CLOCK	TIME	RPM	TEMP	EQV. UTS
1	14H40M30S	-2.00	34731	25.41	.4951
2	14H42M30S	0.	52687	25.00	1.9670
3	14H44M30S	2.00	52639	24.91	3.9674
4	14H48M30S	6.00	52639	24.91	7.9673
5	14H50M30S	8.00	52640	24.93	9.9672
6	14H56M30S	14.00	52640	24.95	15.9671
7	15H 4M30S	22.00	52639	24.99	23.9667
8	15H12M30S	30.00	52639	25.02	31.9664
9	15H30M30S	48.00	52639	25.06	49.9655
10	15H46M30S	64.00	52639	25.13	65.9648

UP-TO-SPEED RPM = 52638.9 (+- .63) N = 32

M-C TEMPERATURE AVERAGES..
D-RUN, FRAMES 5-10 25.04
G-RUN, FRAMES 2- 7 24.95

Fig. 3. Computer evaluation of a successful ultracentrifugal run. DBL 695-4700

Each ultracentrifuge is designed to operate wholly independently of the system (if desired) when the connector leading to the central system is replaced by an appropriate jumper plug. A timed cycle of acceleration and photography is determined by a program card in each centrifuge, and the cycle is initiated by a push button on each centrifuge whether controlled locally or by the central system. The Beckman commutator timer has been replaced by an integrated circuit, giving flexibility of 99 possible picture times. Pictures may be taken at any 2-minute interval over a period of 200 minutes. Figure 2 shows the present program card, which consists of three integrated circuit NAND gates providing permissive gates for ten pictures followed by an end-of-run gate.

Each machine is started at a coded time, with machine number 1 beginning 10 or 40 sec after the minute, number 2 at 20 or 50 sec after the minute, and machine 3 at zero and 30 sec after the minute. After starting, temperature and speed are measured every half minute for the first 5 min during acceleration and every 2 min during the run. Detailed measurements of rotor speed are required during 5 min of acceleration to full speed, because within this period two schlieren pictures are taken. A Fortran IV computer program processes the punched data, yielding graphs of rotor speed and temperature versus time and the accumulated value of $\omega_{FS}^{-2} \int \omega^2(t)dt$ for the mean time of each schlieren photograph.

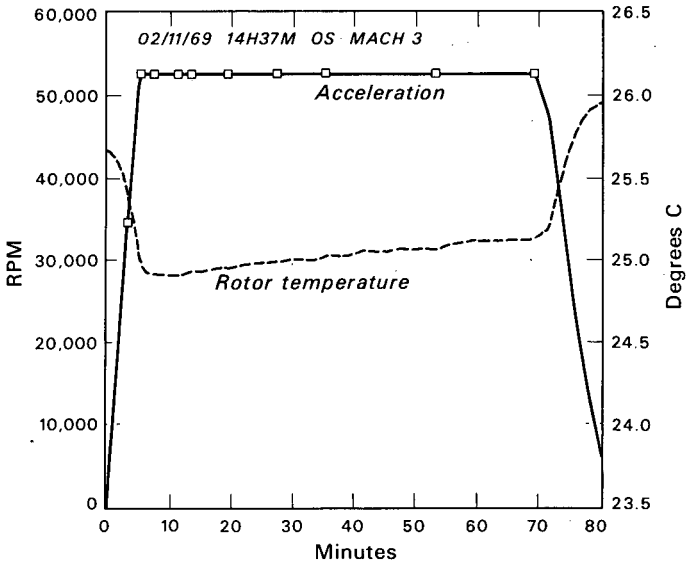

Fig. 4. CRT plot of acceleration and rotor temp. Each small square represents the taking of a photograph. DBL 695-4701

A typical computer evaluation of a successful ultracentrifugal run is shown in Fig. 3. Had there been any failure, an error message or messages would describe the difficulty. An additional feature of the computer analysis is shown in Fig. 4. Here a cathode ray tube (CRT) plot gives a visual profile of acceleration and rotor temperature, as well as showing at what time schlieren photographs were taken.

DISCUSSION

The automatic control and data-acquisition system as described here is a useful application of computer techniques to simple electromechanical devices. Data obtained directly in the form of IBM punched cards allow convenient and direct submission of data for computer analysis. Such data permit quick computer evaluation of each day's runs, machine performance, and error-detection capability. Where needed, the equivalent up-to-speed centrifugation during the acceleration phase of each run is available with great accuracy. Such information is essential in very-low-density lipoprotein analysis, where significant migration of molecules occurs during the acceleration phase of the run. Also, the system permits great flexibility in the actual ultracentrifugal run itself, for example, nonlinear acceleration or a run consisting entirely of programed acceleration. The latter capability may be useful in minimizing the effects of adiabatic temperature changes during acceleration to full speed. Finally, such a system should potentially increase the accuracy of sedimentation and flotation rates, particularly at low rotor speeds.

SUMMARY

Three analytic ultracentrifuges are controlled and useful operating measurements recorded by a central control and data-acquisition system. Rotor speed, temperature, picture number of each schlieren photograph, and the time of each measurement are recorded on punched cards and processed by a computer program. These data permit error detection as well as more accurate schlieren analysis of lipoprotein distributions and flotation rates.

ACKNOWLEDGMENTS

We wish to thank Frank T. Upham, Electronics Department, for his valuable assistance and advice. This work was supported in part by Research Grant 5-R01-HE-01882-15 from the National Heart Institute, U.S. Public Health Service, Maryland, and by the U.S. Atomic Energy Commission.

REFERENCE

1. Windsor, A. A.; T. H. Rich; R. E. Doyle; and F. T. Lindgren: Rev. Sci. Instr. 38 [7]: 949-952 (1967).

The Scanning Electron Microscope: A High-Information-Content Image of Biological Systems

Thomas L. Hayes

The principal value of the scanning electron microscope (SEM) lies in the instrument's ability to produce high-information-content images. It is not, in general, an instrument of higher resolving power than the conventional transmission electron microscope, but the SEM can add useful information that is not available in the transmission electron microscope image. The resolving power of current scanning electron microscopes is about 100 Å.

The information-rich image of the SEM is made possible by an imaging technique that allows uncoupling of the two functions of a microscope: localization and information transfer. The light microscope and the conventional transmission electron microscope utilize a lens system for image formation. Such a system makes use of the same radiation both to localize the points of the specimen and to carry information about each point. As a result, the parameters of resolution and image information are linked together by the type of radiation used. For example, the light microscope produces an image that is rich in information (spatial, chemical, physiological) but low in resolution, whereas the conventional transmission electron microscope produces an image that is high in resolution but low in information (chemical bonds do not influence the image, the image is two-dimensional, the specimen is not living).

The SEM, on the other hand, uses a nonfocused system of image formation, which allows the uncoupling of resolving power and information content. One kind of radiation (electrons) can be used to localize the specimen points at high resolution, and another kind of radiation (visible light, secondary electron, etc.) can be used to transfer the information about these points to the image. By utilizing a time sequence of points (TV) as the imaging system, rather than a lens-focusing system, the SEM permits a great increase in the information transfer from specimen to image.

This information-rich image allows an investigation of the second transfer step: information transfer from image to observer. The usual mode of transfer in scientific studies makes use of a reduction of the image to ideas expressed in words or numbers. In this mode the information is transferred by objective, abstract means. The SEM can provide images that

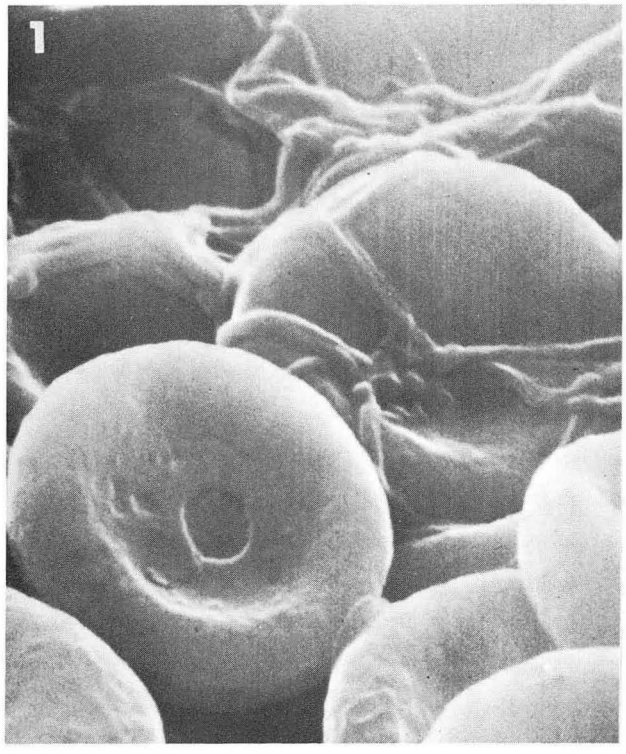

Fig. 1. Human red blood cells in blood clot. L. W. McDonald and T. L. Hayes, Exptl. Mol. Pathol., in press, 1969. ×5800
XBB 686-3441

Fig. 2. Living flour beetle. R. F. W. Pease, T. L. Hayes, A. S. Camp, and N. M. Amer, Science 154, 1185 (1966). ×170
JHL-6424

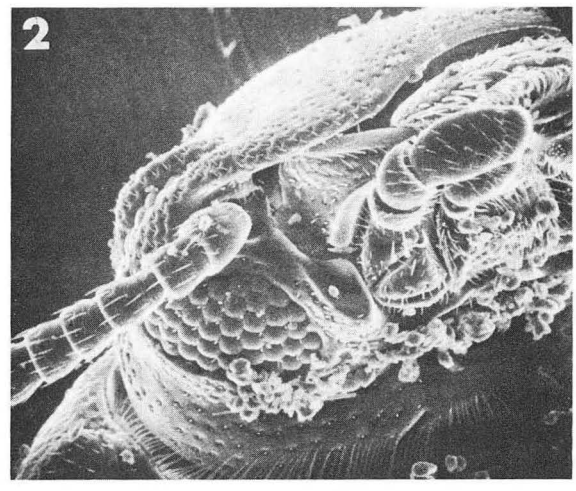

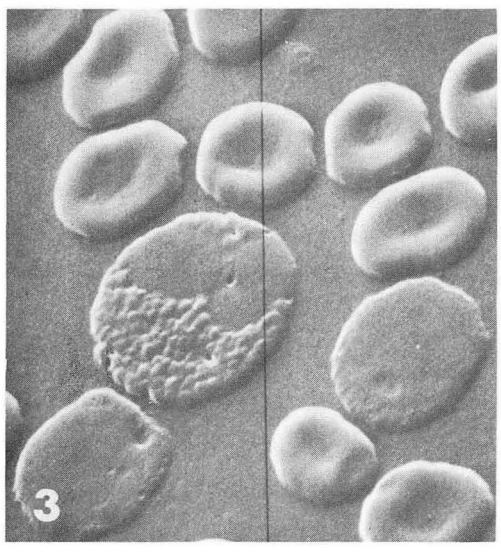

Fig. 3. Eosinophil from peripheral blood of leukemic patient. L. W. McDonald and T. L. Hayes, Exptl. Mol. Pathol., in press, 1969. ×2000. XBB 681-483

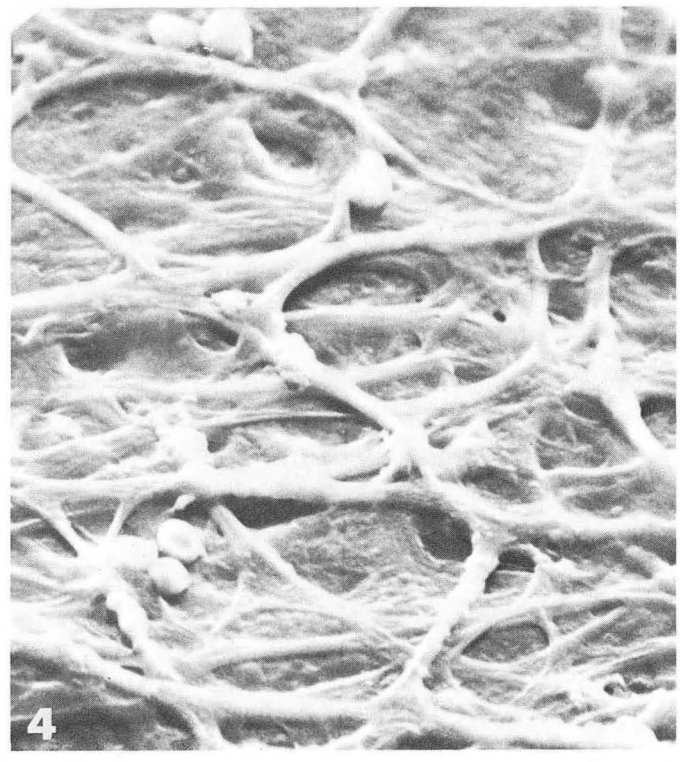

Fig. 4. Trabecular meshwork of human eye. W. H. Spencer, J. Alvarado, and T. L. Hayes, Investigative Ophthalmology 7:651-662 (1968). ×4300.
XBB 688-5137

are suitable for this type of transfer, as illustrated by computer analysis of images, pattern recognition, or chemical analysis by cathodoluminescence or characteristic X rays. The SEM can also provide images that can help us to investigate another mode of information transfer from image to observer: the subjective, experiential mode. In particular, the secondary electron mode of SEM operation produces an image with the important experiential factor of three-dimensional space (Fig. 1). We are often aware that the four-dimensional world is not suited to our experiential understanding, but we sometimes forget that a two-dimensional world is equally foreign. A three-dimensional image provides one important parameter that permits the image to approximate experienced vision (Figs. 2, 3).

The value of experiential information transfer depends somewhat on the definition of reality that we prefer. Many may not agree with Soren Kierkegaard when he suggests that existence precedes essence, but the influence of his thoughts is an existential fact. It would seem that at least we should investigate the possible value of adding subjective information transfer to the analytic, objective modes already familiar to us. It is possible that in addition to writing the analytic program notes, we should try to listen to the symphony. Particularly in dealing with the very complex systems found in biology (Fig. 4), subjective, experiential information transfer may add significantly to our understanding of the system.

SUMMARY

We would suggest that high information as well as high resolution should be considered in the evaluation of a microscope's image, and that the scanning electron microscope is a valuable instrument for the production of such high-information-content images of biological systems. We would also like to suggest that subjective as well as objective criteria be considered when we evaluate the transfer of this information from image to observer.

ACKNOWLEDGMENTS

The Scanning Electron Microscope Program at Berkeley has been supported by the United States Atomic Energy Commission, the Joint Services Electronics Program, the United States Air Force Avionics Laboratory, and the National Institutes of Health (Grant #GM5536-01).

REFERENCES

1. Hayes, T. L.; and R. F. W. Pease: The scanning electron microscope: Principles and applications in biology and medicine, in Advances in Biological and Medical Physics, edited by J. Lawrence and J. Gofman, Vol. 12. Academic Press, New York, 1968. Pp. 85-137.
2. Oatley, C. E.; W. C. Nixon; and R. F. W. Pease: Scanning electron microscopy, in Advances in Electronics and Electron Physics, edited by L. Marton, Vol. 21. Academic Press, New York, 1965. Pp. 181-247.
3. Everhart, T. E.; O. C. Wells; and C. W. Oatley: Factors affecting contrast and resolution in the scanning electron microscope. J. Electronics and Control 7: 97-111 (1959).
4. Pease, R. F. W.: The scanning electron microscope. IEEE Spectrum 4 [10]: 96-102 (1967).

Distribution of Spleen Colony Forming Units in Bone and Marrow

Donald C. Van Dyke

In spite of 100 years of intense investigation of marrow physiology and pathology since Neumann's discovery (in 1868) that blood cells develop in the red bone marrow (1), little light has been shed on the possible importance of the surrounding bone in the process. The fact that under normal and pathological circumstances hematopoiesis may occur in extramedullary sites probably explains why bone has not been attributed great importance in the maintenance of marrow function. On the other hand, in most adult mammals it is within a surrounding of bone that marrow thrives. The question as to what a surrounding of bone may contribute to the welfare of its contained marrow has been the subject of recent investigations in this Laboratory (2, 3). Rohlich's original studies on this question (4) led him to conclude that the bone was important in modifying the blood supply of the medullary cavity and that regeneration of marrow following mechanical removal occurred in tissue which apparently had its origin in the Haversian canals. The study presented here was undertaken to test the possibility that the marrow colony-forming units (CFU) have their origin in the surrounding bone.

MATERIALS AND METHODS

The spleen CFU assay technique of McCulloch and Till (5) was employed, using female LAF_1 mice and 1100 rad ^{60}Co. Bone and marrow cells were obtained from the mid-shaft of the femur, which in the adult mouse contains rich red marrow and a smooth endosteal surface, allowing a clean separation of marrow and bone. The proximal and distal thirds of the femur were removed by using a small electric saw. Marrow was washed from the mid-shaft by attaching a syringe and vigorously flushing with Eagle's medium (6). In some experiments a small pledget of cotton attached to a wire drill was then forced through the medullary cavity with rotation to insure that no fragment of marrow remained. The dense cortical bone was ground, using 100 strokes of a pestle in a mortar with a small amount of Eagle's medium. Bone fragments were removed by decanting and the cell content determined by counting in a standard hemacytometer after 1:1 dilution with white cell diluting fluid. The cell suspension derived from bone (usually 10–20 bones) was diluted to 6 ml with Eagle's medium, and 0.5 ml was given by tail vein to each of 10 radiated recipients.

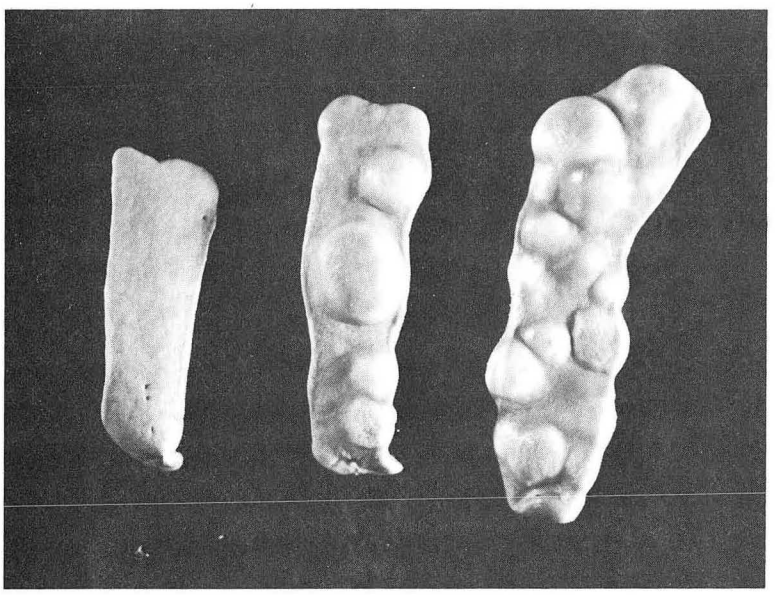

Fig. 1. Spleen colonies from equal numbers (35,000) nucleated cells from marrow (center) and bone plus endosteum (right). The spleen of the control given no exogenous cells is shown on the left.
XBB 692-914

Marrow was dispersed, analyzed for cell content, diluted to the same concentration as the final bone-cell suspension, and 0.5 ml injected.

Eosin staining demonstrated 8.5% nonviable cells whether derived from grinding bone or by suspending marrow. To demonstrate that viable cells rather than nonspecific materials were responsible for colony formation when bone was the source, one group of recipients was given cells derived from grinding bone from radiated (1100 rad) donors.

Gross evaluation of the erythropoietic competence of the spleen colonies formed was made by ^{59}Fe uptake. Five hours prior to autopsy (10 days after radiation and inoculation) the recipients were given ^{59}Fe IV, and at autopsy the mice were carefully perfused with saline through the inferior vena cava while the heart was still beating. Spleens were removed and weighed, and ^{59}Fe content was determined by use of a standard well counter.

RESULTS

Marrow flushed from each mid-femoral shaft yielded approximately 8×10^6 nucleated cells. When bone was ground after the marrow was washed out but the endosteal surface was not scrubbed, each mid-femoral shaft yielded approximately 60,000 nucleated cells, of which one in 3000 formed a spleen colony, Fig. 1. When bone was washed free of marrow and the endosteal surface scrubbed with cotton before being ground, each shaft yielded an average of 20,000 nucleated cells of which again one in 3,000 formed a colony. Under the experimental conditions used the number of colonies formed from suspensions of marrow cells was one per 6,500 nucleated cells injected, Fig. 2. Thus the cells derived from grinding bone were more than twice as rich in stem cells as marrow itself. Scrubbing the endosteal surface reduced the number of nucleated cells recovered after grinding to 30% without reducing the ratio of nucleated cells to CFU.

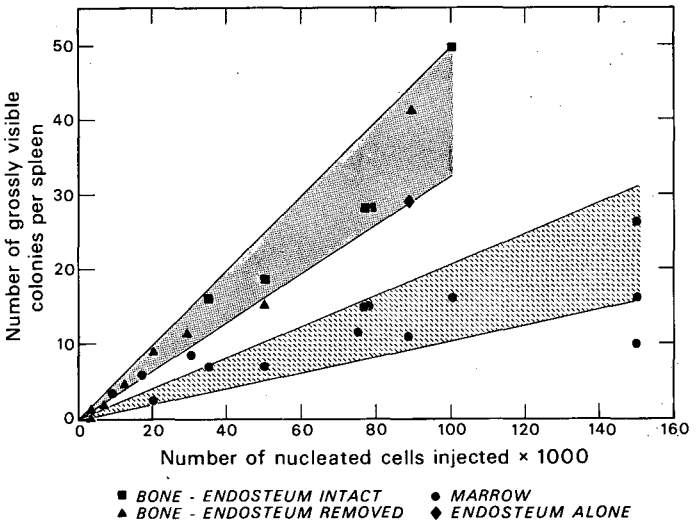

Fig. 2. Comparison of the number of colonies produced after injection of cells derived from grinding bone or suspending marrow.

DBL 692-4576

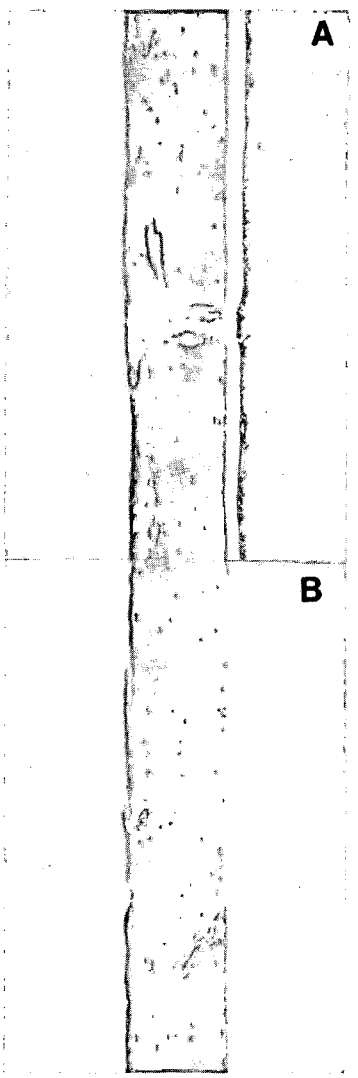

Fig. 3. A: Segment of mid-femoral shaft after flushing out of marrow. Most of the endosteum remains with the bone and a thin layer of hematopoietic cells remains adherent to the endosteum. The space between endosteum and bone is an artifact of preparation.

B: Similar segment after scrubbing endosteal surface with cotton. Endosteum with attached hematopoietic cells is completely removed. Cellular material remains only in the Haversian canals.

XBB 695-3460

Figure 3 shows the appearance of the bone after flushing out the marrow (top) and after scrubbing the endosteal surface with cotton (bottom). After flushing, most of the endosteum remains with the bone, with a thin layer of marrow cells attached. After scrubbing with cotton, the endosteum and adherent marrow are completely gone, cells remaining only in the Haversian canals. In all cases the periosteum has been removed by scrubbing with cotton in the process of isolating the bone.

Material derived from grinding irradiated bone produced no colonies, nor did it enhance the colony formation when added to viable marrow suspensions.

Microscopic examination of spleens and femurs of the recipients showed a similar variety of colony types in the spleen and the presence of colonies in the marrow whether the inoculum was from marrow or bone. Spleen uptake of ^{59}Fe was similar for both groups.

DISCUSSION

Carsten and Bond (6) have stated that thorough grinding of the entire bone with its contained marrow gave a higher yield of CFU's than did the aspiration technique, which did not recover marrow from trabecular portions of the bone. These authors did not indicate that bone itself contributed significantly, and the results of these experiments show that the contribution from bone and endosteum would be 1/60 of the total CFU's recovered.

Jacob et al. (7) state that they were unable to effect marrow growth in the dog spleen by direct insertion of marrow without bone or bone alone without periosteum or endosteum, but when bone with its contained marrow was implanted proliferation of marrow occurred. In contrast, Tavassoli and Crosby (8) have found that autologous fragments of marrow have survived in various extramedullary sites in the rat, rabbit, and dog. The process originates from a network of surviving reticular cells which proliferate and differentiate into osteoblasts and give rise to trabecular bone followed by repopulation of the marrow. Tavassoli states "we have never been able to achieve the growth of ectopic marrow without bone despite many efforts in this line of work" (personal communication).

In studying regeneration of marrow following mechanical removal, Rohlich (4) found: After removal of the bone marrow the medullary cavity was first filled with blood. Granulation tissue from the connective tissue in the environment and from the Haversian canals in the compacta proliferated into this coagulated blood. Not only did the proliferating connective tissue from the Haversian canals grow into the medullary cavity, but in addition, bone tissue had been resorbed from the Haversian canals, causing the latter to become markedly dilated, Fig. 4.

The ingenious series of experiments by Friedenstein et al. (9) appears to give direct proof that bone provides the microenvironment attractive to hematopoietic marrow independent of any hematopoietic stem-cell contribution. Transplants of bone marrow from partially inbred (semisyngenetic) donors formed bone of donor origin harboring marrow of recipient origin.

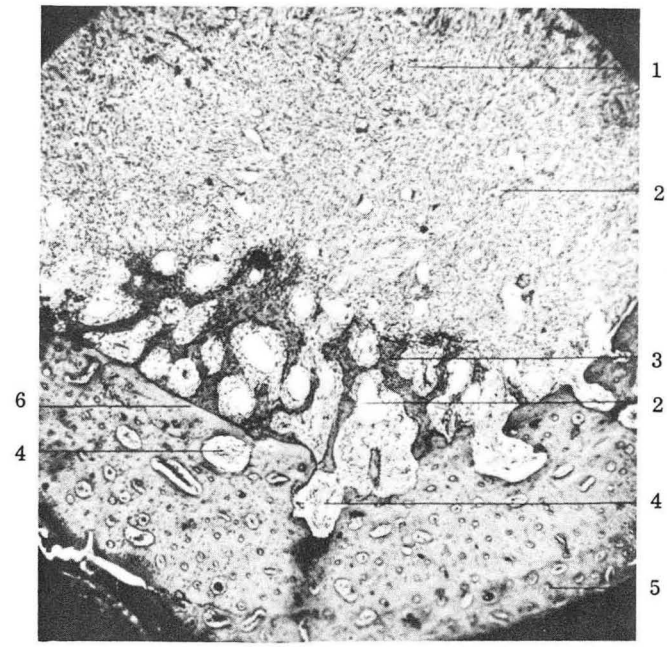

Fig. 4. Transverse section through diaphysis from which the red bone marrow had been removed 14 days earlier: (1) front of the granulation tissue; (2) blood vessesl; (3) bone trabeculae; (4) abnormally dilated Haversian canals; (5) periosteal formation of new bone tissue; (6) border line. (Reproduced from Rohlich--Ref. 4.) XBB 6812-7645

CONCLUSIONS

Spleen colony-forming cells have been shown to be found in bone. The total number is small, but the ratio of CFU to nucleated cells is greater than in marrow. The results would seem to indicate that bone either collects or generates marrow colony-forming cells.

REFERENCES

1. Neumann, E.: Ueber die bedeutung des knochenmarkes für die blutbildung. Zentral. Med. Wiss. 6: 689 (1868).
2. Van Dyke, D.: Similarity in distribution of skeletal blood flow and erythropoietic marrow. Clin. Orthoped. 52: 37-51 (1967).
3. Van Dyke, D.; and N. Harris: Bone marrow reactions to trauma. Submitted to Blood, 1969.
4. Rohlich, K.: Uber die beziehungen zwischen der knochensubstanz und der blutbildung im knochenmark. Z. Mik.-Anat. Forsch. 49: 425-64 (1941).
5. Till, J. E.; and E. A. McCulloch: A direct measurement of the radiation sensitivity of mouse and bone marrow cells. Radiation Res. 14: 213-22 (1961).
6. Carsten, A. L.; and V. P. Bond: Viability of stored bone marrow colony-forming units. Nature 219: 1082 (1968).
7. Jacob, S. W.; W. C. Moloney; E. M. Barsamian; O. E. Owen; and J. E. Dunphy: Histologic sequences following implantation of the autologous canine rib into the spleen. Surg. Gynecol. Obstet. 109: 697-702 (1959).
8. Tavassoli, M.; and W. H. Crosby: Transplantation of marrow to extramedullary sites. Science 161: 54-56 (1968).
9. Friedenstein, A. J.; K. V. Petrakova; A. I. Kurolesova; and G. P. Frolova: Heterotopic transplants of bone marrow. Transplantation 6: 230-47 (1968).

Clinically Applicable Fluoro-Kinetic Method for Bone Blood Flow Determination

Donald C. Van Dyke and Jean-Pierre Naets

Intravenously administered fluoride rapidly leaves the blood, approximately half being excreted by the kidneys and half being taken up by bone (1-3). The short-lived isotope of fluorine, ^{18}F, is routinely prepared carrier- and contamination-free (4) and provides an ideal isotope for clinical application of the kinetic determination of blood flow to the total skeleton.

Because blood clearance of fluoride is dominated by urinary excretion and uptake by bone, uptake by bone can be computed from information on blood clearance and urinary appearance during the first hour after intravenous administration. Bone uptake in the initial period can be converted to total skeletal blood flow, since the extraction of fluoride by bone is virtually complete on a single passage (3).

Because of its 111-min half-life, the radiation dose to the patient from ^{18}F is relatively small (3), and if desired the study could be repeated after an interval of a few hours. Except for currently limited availability of the isotope, the method is simple and requires no special equipment. Growing interest in the use of ^{18}F as a bone-scanning agent suggests that ways of increasing its availability to departments of nuclear medicine will be found in the near future. Multiple-head in vivo continuous recording counting equipment or a positron scintillation camera can be used to simplify the determination, but is not essential to the method.

This report demonstrates the fluoro-kinetic method for bone blood flow measurement in dog, rat, and man.

MATERIALS AND METHODS

Analysis of the fluoro-kinetics data depends on accurately determining the initial blood clearance rate and the amount of isotope appearing in the urine during the initial period. The blood disappearance rate may be obtained graphically, using the values after equilibration in the ^{18}F "space" and before reentry from bone becomes significant. A simple method for determining when equilibration in the ^{18}F space is complete is to place a counter over some fleshy portion of the patient's body and record the counts at 60-sec intervals until no increase

in counting rate occurs. This will normally take from 5–25 minutes. Maximum counting occurs at the time ^{18}F equilibration in the body fluids is complete, and the time determined in this way indicates when to start plotting the rate of loss of label from blood due to bone uptake and urinary excretion.

The minimum number of blood samples should be at 5, 10, 20, 30, 40, 50, 60, 80, and 100 minutes. After mixing (5–25 min) the values should fall exponentially during the first hour. Points between 20 and 60 minutes usually provide the $t_{1/2}$ of the initial blood curve after mixing, but the timing must be determined for each patient.

Adequate hydration of the patient is necessary to insure a urine collection at the time desired. Urine should be collected at a time as close to the $t_{1/2}$ of the initial blood curve (30–60 min for most patients) as possible.

If an Anger positron scintillation camera is available, the initial tissue-mixing curve and the buildup curve in the urine can be obtained by splitting the camera field just lateral to the bladder (at the line of the inguinal crease) and recording count rate from each half. Subtraction of the lateral half (tissue background) from the medial half (tissue plus bladder) should give the bladder buildup curve. This curve can be used to correct the urine value if voiding is delayed well beyond the time when blood disappearance is exponential.

The number of counts per ml obtained by extrapolation of the first blood exponential to zero time divided into the counts injected gives the initial mixing "volume." The rate of clearance after mixing times the mixing volume gives the volume of blood cleared (by bone and kidney) per minute. This figure divided by the cardiac output (measured or estimated) gives the fraction of the cardiac output cleared (by bone and kidney) of ^{18}F per minute.

Since the $t_{1/2}$ of clearance from blood equals the $t_{1/2}$ of appearance in bone and urine, urine collected at a time similar to the blood $t_{1/2}$ can be used to determine the theoretical total that would be excreted if these initial rates prevailed to infinity (no feedback from bone). This value (urine at infinity) can be determined graphically or by the formula

$$U_\infty = \frac{u(t)}{[1 - \exp(-693/t_{1/2})t]}$$

$1 - U_\infty$ equals the theoretical (no secondary loss from bone) fraction of the injected dose accumulating in the skeleton. This number times the fraction of the cardiac output cleared per minute gives fraction of cardiac output to bone (assuming 100%) clearance in a single passage through bone).

In experimental animals, on which serial autopsies can be done, the bone accumulation curve and fraction of injected dose in the skeleton may be used in the calculations rather than the values obtained from urine.

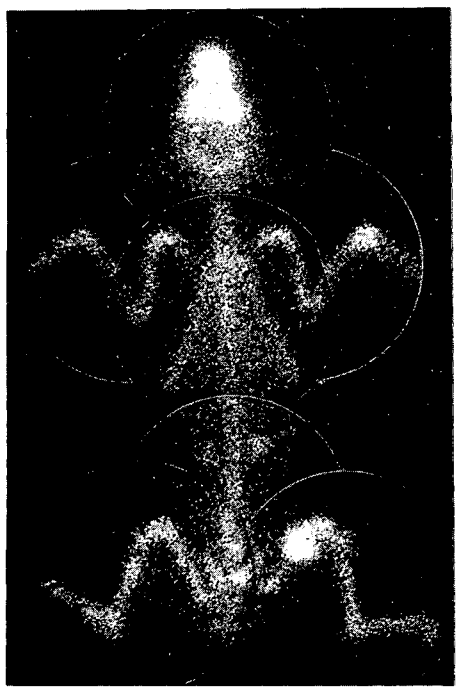

Fig. 1. Composite positron scintillation camera pictures of ^{18}F distribution in the female radium-burdened beagle of Table 1. The bladder had been irrigated with saline just prior to taking pictures over the pelvis. High uptake in an osteosarcoma of the right femur as well as unusually high uptake in the region of the jaws can be seen. A second bone lesion in the right wrist is suspected. Visualization of both kidney pelvises is due to continued excretion of the isotope. The picture is compatible with the 3-compartment model presented (extracellular fluid, urinary excretion, and rapid initial skeletal uptake with slow release) in Fig. 3 2 hr after injection.

XBB 691-526

PROCEDURE

DOG A 10.9-kg female beagle dog was anesthetized with 5 ml Diabutal given intravenously. An intravenous infusion (40 ml/hour) of normal saline containing 4000 units heparin was started and an intravenous plastic cannula was inserted at another site for ease of blood sampling. A catheter was placed in the bladder and 1000 units of heparin was given intravenously. Three millicuries ^{18}F was given IV at the start of the experiment. One-ml samples of blood were taken at frequent intervals over a 10-hr period, and the hematocrit was determined at beginning, middle, and end of the experiment. The bladder was irrigated at frequent intervals and the ^{18}F content of each sample and of the accumulated sample was determined. Previous determinations had shown the blood volume of the adult female beagle to be 98.4 ml/kg (1070 ml for this dog). According to Dukes (5) cardiac output would be 1450 ml/10 kg (1580 ml/min for this dog).

Positron scintillation camera pictures showing distribution of ^{18}F carried by the blood to various parts of the skeleton were routinely taken 2 hours after injection, when blood levels were low, skeletal uptake was near maximum, and physical decay had not reduced the isotope below efficient recording levels. An example of the pictures obtained from a dog having a high radium burden over a 5-year period is shown in Fig. 1. Abnormally high uptake in the jaws and in an osteosarcoma in the right femur is apparent. A lesion in the right wrist is suspected, and both kidney pelvises can be seen as a result of continuing excretion of the isotope. The bladder had been irrigated just prior to taking of the pictures. The dog had been given 300 μCi of ^{18}F.

RATS Analysis of fluoro-kinetics in rats was based on measurement of blood disappearance and bone uptake rather than on blood disappearance and urine excretion, as in the dog.

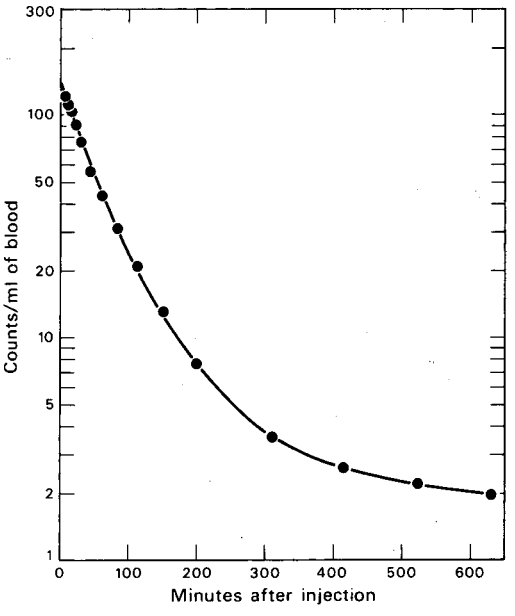

Fig. 2. Loss of ^{18}F from blood during the 10 hr following an intravenous injection. Mixing in the extravascular space was apparently complete by the time of the first sample (5 min). Loss was exponential during the first hour.
DBL 691-4513

The data used are from the same animals from which previously published data were obtained (3). Rats of the Long-Evans strain with an average weight of 277 g were given ^{18}F via the tail vein and then at intervals killed so as to obtain measurements of blood content, uptake by one tibia, and uptake by the entire skeleton (cleaned of as much soft tissue as possible). The published value of 21 ml of blood per 100 g per min (6) was used for cardiac output (58 ml/min of blood or 31 ml/min of plasma for the rats in this study). Plasma volume was assumed to be 2.8% of body weight or 7.8 ml.

MAN Patients referred to the Donner Laboratory Clinic for investigation of abnormalities involving bone were studied by this technique. Mark II whole-body scans and positron scintillation camera pictures to demonstrate distribution of ^{18}F to parts of the skeleton were done at completion of the fluoro-kinetic studies. Patient B. W., studied because of a parathyroid adenoma without associated bone disease, will serve as an example of application of the method.

This 65-year-old, 77-kg man had a pulse of 72 and blood pressure of 150/90. (Cardiac output was calculated to be 5600--Ref. 5). For greater accuracy, and especially where abnormalities in blood volume and cardiac output are suspected, direct measurement by the RISA method should be done (7), as follows.

1. Hydrate patient adequately and advise not to urinate.
2. When patient feels he could urinate at any time, place under camera with bladder in one half of the field and hip in the other. Start continuous recording from both halves. (Check accuracy of bladder positioning by a picture during procedure.)
3. Place plastic needle (for sampling) in one arm and inject ^{18}F in other.
4. Collect blood samples at approximately 5, 10, 20, 30, 40, 60, 80, 100, and 120 min.
5. Have patient void completely at 30 minutes.

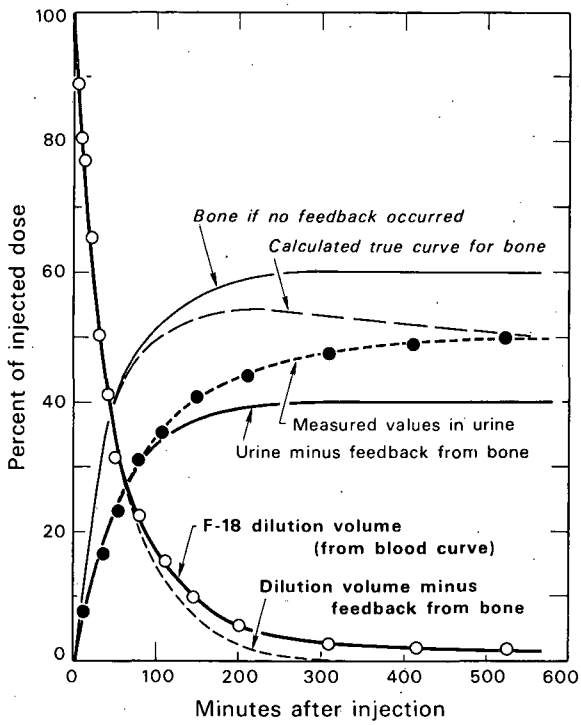

Fig. 3. An attempt to account for 100% of the injected ^{18}F in a 3-compartment model (^{18}F dilution space, urinary excretion, and skeletal uptake).
DBL 691-4511

RESULTS

DOG In the dog the ^{18}F content of the blood decreased exponentially during the period of 5–60 min, with a half-time of 34 min (Fig. 2). The initial rate of appearance in the urine was compatible with a 34-min $t_{1/2}$, and by 3.5 hours 48.6% of the injected dose was excreted (Fig. 3). Slowing of the rate of loss of label from the blood after the first hour, associated with a slow but continuing appearance in the urine, was indicative of "feedback" from bone to blood. Loss from bone with concomitant appearance in urine between 4 and 9 hours has been reported by Durbin (1). The half-time of 34 min (before feedback becomes significant) can be used to calculate what the final value for ^{18}F in urine would be if no feedback occurred. (The amount appearing in urine at the blood half-time (15.5%) would be half the final theoretical value of 31%--Fig. 3). The difference between this theoretical value of 31% and the observed value of 48.6% is due to feedback of fluoride from bone, Fig. 3. Since that ^{18}F which is not excreted goes to bone, the theoretical final value must be 69%, having the same $t_{1/2}$ as the initial blood and urine curves, 34 min (Fig. 3). The actual rate of appearance of ^{18}F in bone would be the difference between the sum of the observed values for extracellular fluid and the observed values for urine.

The sustained extracellular fluid (blood) level and the continually rising total urinary excretion are both presumed to be functions of loss from bone. The actual skeletal content of ^{18}F must therefore be the difference between the sum of the observed extracellular fluid content plus the observed urine content and 100% (Fig. 3). The slope of the later portion of this curve, between 4 and 8 hr, indicates an elution rate from bone of 0.75% per hr (Fig. 3).

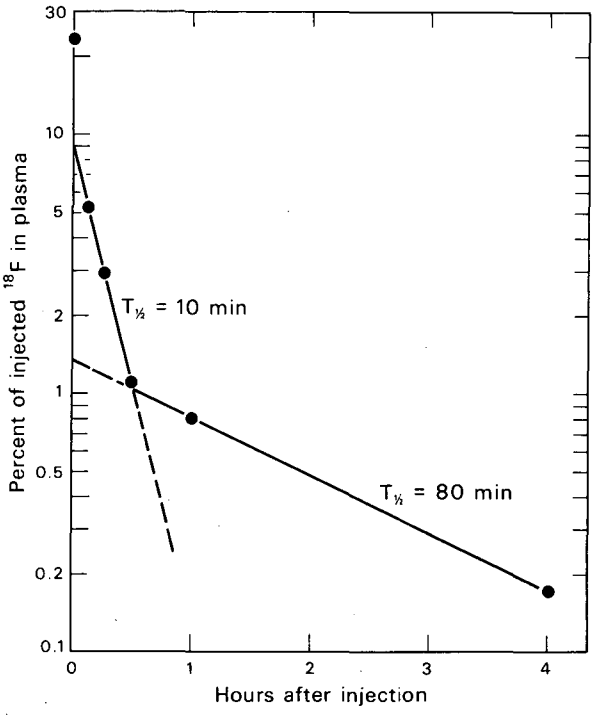

Fig. 4. Pattern of loss of ^{18}F from the blood of rats after an intravenous injection. Initial loss from plasma was compatible with the 10-min halftime of uptake measured in the tibias of the same animals if the high first point (0.5 min) is assumed to be due to incomplete mixing. The rats received 8 semimonthly injections of ^{226}Ra (1.25 μCi/kg/inj.) 3.2 years prior to this scan. This figure was obtained through the cooperation of M. Bulgin, Radiobiology Laboratory, University of California at Davis as part of a collaborative study of bone seeking radionuclide effects.

DBL 691-4512

The zero-time extrapolate of the blood curve indicates an ^{18}F "space" of 2957 ml. As the initial rate constant for the blood and extracellular fluid is 2.04%, then 60.3 ml per min is cleared by bone plus kidney. (Clearance is from blood, so 60.3 ml blood cleared per minute.) Assuming the cardiac output to be 1580 ml per min, then 3.8% of cardiac output is cleared per minute. Assuming a bone extraction efficiency of 100% and having found a 69/31 distribution between bone and kidney (Fig. 3), one knows that bone blood flow is 69% of 3.8, or 2.6% of cardiac output.

RAT Accumulation of ^{18}F in excised rat tibia was exponential, with a half-time of 10 min. Initial loss from plasma was compatible with a 10-min half-time if the high first point is assumed to be due to incomplete mixing at 0.5 min (Fig. 4). These data are very similar to the blood disappearance curve presented by Durbin. Although the blood curve was a composite of rapid early and slower late components, suggesting re-entry from bone, uptake by bone was a single exponential 10-min doubling time, with no apparent loss during the following 7 hr. Thus, fluoro-kinetics in the normal rat was dominated by a 10-min half-time or a rate constant of 6.93% per min. Extrapolation of this portion of the plasma curve to time zero showed 9% of the injected dose in plasma (7.8 ml) giving an ^{18}F "space" equal to 86 ml or 31% of body weight; 6.93% of this "space" or 5.9 ml is cleared per minute. Cardiac output is calculated to be 58 ml per min, giving 10% of cardiac output cleared of ^{18}F per minute. Measured uptake by the skeleton was 30% without evidence of significant feedback, indicating a 30/70 distribution of ^{18}F between bone and urine, or 3% of cardiac output to bone. This value is somewhat smaller than that previously obtained (4.4%) by graphic analysis.

MAN In patient B. W. (hyperparathyroid) the blood curve showed mixing to be complete by 15 min, with decline following a single exponential with a 48-min half-time during the subsequent 45 min. Extrapolation of that portion of the curve to zero time indicated a mixing "volume" of $\left(\frac{\text{cpm injected}}{\text{cpm/ml blood at } t_0}\right)$ 1.53×10^4 ml. The rate of clearance from this volume ($0.693/t_{1/2}$) was 1.44% per min, or 220 ml. This value divided by the estimated cardiac output (5600 ml) gives the fraction of the cardiac output cleared by bone and kidneys per minute = 3.7%.

Table 1. Fluoro-kinetic determinations of fraction of cardiac output going to bone in different species and diseases in man.

Species, disease	Fraction of cardiac output going to bone (%)
Normal rat	3.0
Normal beagle (female)	2.6
	2.9
Normal beagle (male)	2.7
	2.7
	3.5
	3.7
Radium-burdened beagle (female)[a] with osteosarcoma	1.9
Radium-burdened beagle (male)[a]	2.2
Normal men	7.6
	7.2
	7.8
Normal woman	6.0
Acromegaly	1.9
Hyperparathyroid without bone disease	3.3
Aplastic anemia	3.4
Severe diabetes	5.9
Acromegaly with hyperparathyroid	6.7
Chronic blood-loss anemia	7.5
Fracture, nonunion	8.0
Acromegaly + limited Paget's	8.2
Severe diabetes	8.5

a. From Radiobiology Laboratory, University of California-Davis (USAEC [AT 04-3] 472); Ref. 8.

The example is simplified by the fact that the patient voided at 50 min, which is approximately the half-time of the initial blood component. At that time (the $t_{1/2}$), 8.4% of the injected dose appeared in the urine, indicating that if that rate prevailed to infinity (no feedback from bone) 16% of the injected dose would be excreted by the kidneys and the remaining 84% would be deposited in bone. Thus 84% of 3.9% (the fraction of the cardiac output cleared per min), or 3.3% of cardiac output goes to the skeleton.

DISCUSSION

Measurement of bone blood flow in the living animal or patient has not previously been possible. Availability of a simple and reliable technique should provide better insight into the relationship of bone blood flow to a variety of disturbances involving the skeleton, and should be a valuable aid in differential diagnosis once the characteristic findings in different disease conditions have been established. Table I gives the values found for adult rats, adult beagle dogs, and 9 human patients with diseases known to affect the skeleton.

SUMMARY

Because the rapid initial clearance of fluoride from blood is dominated by urinary excretion and uptake by bone, uptake by bone can be computed from information on blood clearance and urinary appearance during the first hour after intravenous administration. Since the extraction of fluoride by bone is virtually complete on a single passage, bone uptake in the initial period can be converted to total skeletal blood flow. The short-lived isotope of fluorine, ^{18}F, is ideal for clinical application to the kinetic determination of blood flow to the skeleton. Study of normal rats and dogs by this method indicates that the effective circulation to the skeleton is approximately 3% of cardiac output. Values from 1.9 to 8.5% of cardiac output going to bone have been found in nine patients with different diseases associated with vascular or skeletal abnormalities. Application of this technique should provide better insight into the relationship of bone blood flow to a variety of disturbances involving the skeleton, and should be a valuable aid in differential diagnosis once the characteristic findings in different disease conditions have been established.

REFERENCES AND NOTE

1. Wallace-Durbin, P.: The metabolism of fluorine in the rat using ^{18}F as a tracer. J. Dental Res. 33: 789-800 (1954).
2. Carlson, C. H.; L. Singer; and W. D. Armstrong: Radiofluoride distribution in tissues of normal and nephrectomized rats. Proc. Soc. Exptl. Biol. Med. 103: 418-20 (1960).
3. Van Dyke, D.; H. O. Anger; Y. Yano; and C. Bozzini: Bone blood flow shown with ^{18}F and the positron camera. Am. J. Physiol. 209: 65-70 (1965).
4. Thomas, C. C., Jr.; I. A. Sondel; and R. C. Kerns: Production of carrier-free ^{18}F. Western New York Nuclear Research Center. Personal communication.
5. Dukes, H. H.: The Physiology of Domestic Animals, 7th edition. Comstock Publishing Associates, Ithaca, New York, 1955. P. 111.
6. Bullard, R. W.: Maintenance of arterial pressure and cardiac output in the hypothermic rat. Federation Proc. 15: 28 (1956).

7. Donato, L.; R. A. Holmes; and H. N. Wagner, Jr.: The circulation. In Principles of Nuclear Medicine, W. B. Saunders Co., Philadelphia, 1968. P. 531-83.
8. Radiobiology Laboratory Annual Report, USAEC Doc. UCD 118-472 (1968).

Jean-Pierre Naets is a visiting scholar at the Donner Laboratory from Université Libre de Bruxelles.

Urinary Erythropoietin Assay in the Diagnosis of Hematologic Disease

Donald C. Van Dyke and Mary Lou Nohr

In the absence of methods for measurement of serum erythropoietin when it is low, normal, or only slightly elevated, the ability to measure daily erythropoietin excretion becomes important; we assume either that urinary excretion can be relied upon as a reflection of the concentration of erythropoietin in the body fluids, or that a reliable comparison between erythropoietin excretion of normal and erythropoietically abnormal human beings can be made. In testing the validity of this assumption, several practical problems have arisen. The extraction method previously used by Van Dyke et al. (1) varies in recovery, and Marver and Gurney have shown (2) that ingestion of sodium bicarbonate may increase excretion 3–10 times. Does bacterial contamination of the urine lead to significant loss of erythropoietin? Does the level of urinary erythropoietin depend on fluid intake and urine volume?

If these problems are resolved satisfactorily, then a stringent examination should be made of the reliability of the urinary erythropoietin assay in the differential diagnosis of relatively difficult diagnostic problems. Can this measurement be relied upon to differentiate between an erythropoietin-producing tumor or cyst (3) and benign cyst in a patient with polycythemia? Can it distinguish unequivocally between primary polycythemia and polycythemia secondary to cardiac or pulmonary disease (4), or abnormalities in the hemoglobin molecule which interfere with oxygen delivery to the tissue (4, 5)?

The object of this study was to clarify as many of the practical problems as possible in an attempt to standardize procedure and evaluate measurement of erythropoietin in the urine as a meaningful clinical test and research tool.

MATERIALS AND METHODS

COLLECTION AND CONCENTRATION OF URINE Complete 24-hour collections of urine were made from patients with various hematologic diseases and from normal volunteers. The urine was frozen immediately after voiding and stored at -18°C until concentrated. All samples were processed within 2 months after collection and stored after processing at -20°C until assay.

Two methods of concentration were compared, the collodion-adsorption method (1) and dialysis against Carbowax (6). The first required concentration of 3 days' urine output by exposure of the urine to a collodion membrane in a high-pressure filter. The membrane was dissolved in ether-alcohol, and the precipitate was washed three times in ether-alcohol and once in ether and then dried under vacuum. The total solids obtained were diluted in 11 ml for assay in 10 mice. The second method required a 24-hour urine collection which was dialyzed against Carbowax overnight in the cold. The following day the contents of the bag were washed out, the bag was washed twice with a small volume of saline, and the contents and wash centrifuged in the cold for 20 minutes. The supernatant was redialyzed against Carbowax overnight in the cold. The next day the volume in the bag was measured and brought to a total of 12 ml. This was divided into samples equivalent to 60- and 18-hour excretion, which were diluted to 11 ml for assay. Assay of a concentrate of the full 24-hour output frequently resulted in death of recipient mice.

Dose-response curves were determined by using 3-day collections of urine from an anemic pregnant woman, from a patient with erythrocytosis, and from a normal male, each dialyzed against Carbowax.

Recovery of erythropoietin by the collodion adsorption method or by Carbowax dialysis was compared in two ways. Urine from two patients whose erythropoietin titer was high was processed by both methods, and the concentrates were brought to the original volumes and compared directly with a sample of the unmodified urine. When erythropoietin was too low to be measured in unmodified urine, a 4-day collection was pooled; 3/4 was concentrated by collodion adsorption, 1/4 was concentrated by Carbowax dialysis.

In further studies of the Carbowax method, a known amount of erythropoietin was added to half of a 24-hour collection. Both 12-hour equivalents were then carried through the concentration procedure. For control the same amount of erythropoietin was diluted in saline, left in the refrigerator for 2 days, and frozen when the urine was frozen.

METHOD OF ASSAY Female mice of the Balb/c strain rendered polycythemic by hypertransfusion according to the method of DeGowin et al. (7) were used routinely for all assays. This assay was compared directly with the method described by Adamson et al. (6), which utilizes posthypoxic protein-depleted mice injected with test material every 12 hours for 4 days.

SPECIAL STUDIES The effect of fluid intake on erythropoietin excretion was studied in a normal male volunteer. Urine was collected on consecutive days for one day of ad lib. water intake, two days of severe fluid restriction, and a fourth day of increased water intake. At the time of processing, erythropoietin was added to half the base-line sample to determine recovery.

The effect of alkalinization on excretion of erythropoietin was studied, using the alkalinization procedure described by Marver and Gurney (3). Base-line studies were made of 1–4-day urine collections. Six grams $NaHCO_3$ were taken orally t. i. d. for 2–4 days. At the time of processing, erythropoietin was added to half of one day's prealkalinization urine. Acetazol-

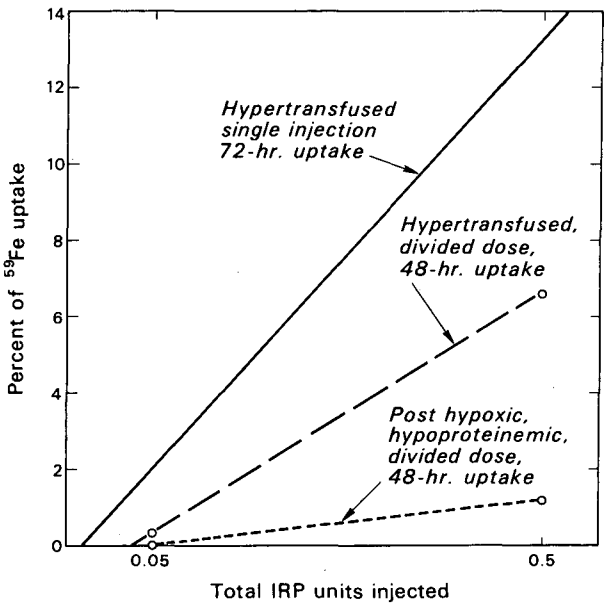

Fig. 1. Response of hypertransfused or post-hypoxic, protein-depleted mice to a dose of erythropoietin divided and injected every 12 hr for 4 days. The curve obtained with the standard assay (hypertransfused, single injection) is included for comparison.

DBL 680-5478

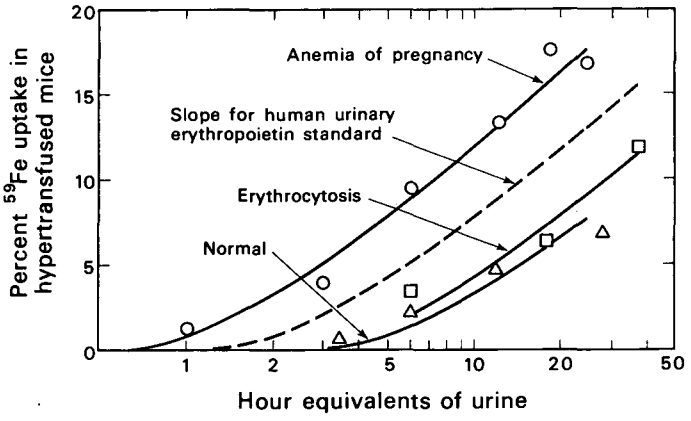

Fig. 2. Parallelism of slope obtained with increasing concentrations of urine to that obtained with increasing dose of erythropoietin. Individual symbols refer to data from the same subject.

DBL 689-5439

amide (Diamox®) was tested as an alkalinizing agent in one patient whose urine after alkalinization with $NaHCO_3$ had previously been assayed. Diamox® did not cause the degree of alkalinization obtained with $NaHCO_3$, and erythropoietin excretion increased less with Diamox® than with $NaHCO_3$, so $NaHCO_3$ was retained as the standard alkalinizing agent.

RESULTS

TECHNIQUES The hypertransfused mouse assay of DeGowin et al. showed a steeper slope than the method described by Adamson, but an equal minimum effective dose (Fig. 1). Also shown in Fig. 1 is a comparison of dose divided into eight injections employing either hypertransfused or posthypoxic, protein-depleted recipient mice (Adamson's method). There was no advantage in dividing the dose.

With the hypertransfused mouse assay it was possible with increasing amounts of urine dialyzed against Carbowax to obtain a dose-response relationship that was parallel to that

obtained with standard erythropoietin (8). Figure 2 illustrates this with urine from three subjects.

Dialysis against Carbowax was selected as the most convenient and reliable method of concentration of urine, providing virtually 100% recovery of erythropoietin. This was demonstrated with urines of high erythropoietic activity processed by the two methods. In this study less than 50% of erythropoietin measured in unmodified urine was recovered by collodion adsorption, whereas virtually 100% (80-100%) was recovered by Carbowax dialysis. When erythropoietin was too low to be measurable in unmodified urine, concentrates of urine prepared by Carbowax dialysis showed a higher level of erythropoietin than collodion-adsorbed urine concentrates in 9 of 10 patients. The exception was a case in which a 24-hr collection concentrated by dialysis was negative and the 3-day concentrate by collodion showed a minimal erythropoietin level.

In another study a known amount of erythropoietin was added to half of a 24-hour urine collection prior to dialysis against Carbowax. In 17 cases in which there was no detectable erythropoietin in half the urine concentrate, there was 100% recovery of added erythropoietin from the second half. In eight cases with no detectable erythropoietin there was no recovery of added erythropoietin. Subsequently one of the eight patients was reassayed and 100% of added erythropoietin was recovered from the urine.

To determine if bacterial contamination was deleterious to urinary erythropoietin or a factor in failure to recover added erythropoietin, bacterial cultures were made of most urine samples studied. The results of the assay were plotted against the numbers of colonies of bacteria, and no correlation was found. From three urine samples which showed massive bacterial contamination, 100% of added erythropoietin was recovered. Bacteria, obtained from a culture of urine from which added erythropoietin was not recovered, were added to standard erythropoietin and incubated at 37°C for 2 hours. This resulted in no loss of activity of the standard. Occasionally we have found normal or high levels of urinary erythropoietin when there was massive bacterial contamination.

SPECIAL STUDIES In the one subject studied for this effect, dehydration resulted in decreased erythropoietin excretion to levels not measurable on the first day of dehydration,

Table 1. Effect of fluid intake on urine volume and excretion of erythropoietin.

Procedure	Volume of urine excreted (ml)	IRP units of erythropoietin excreted/day
Normal (base-line)	1280	1.32
Day 1 of dehydration	700	not detectable
Day 2 of dehydration	480	0.77
Excessive fluid intake	4040	2.52

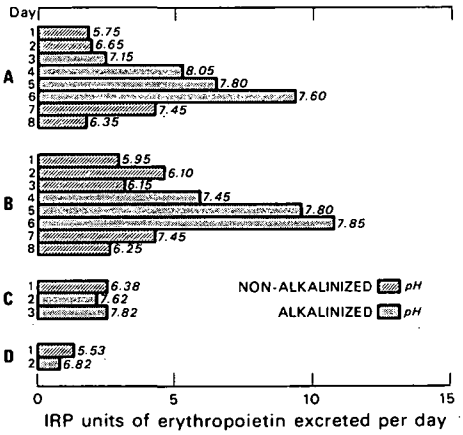

Fig. 3. Effect of alkalinization on daily excretion of erythropoietin by normal, adult male volunteers.

DBL 689-5440

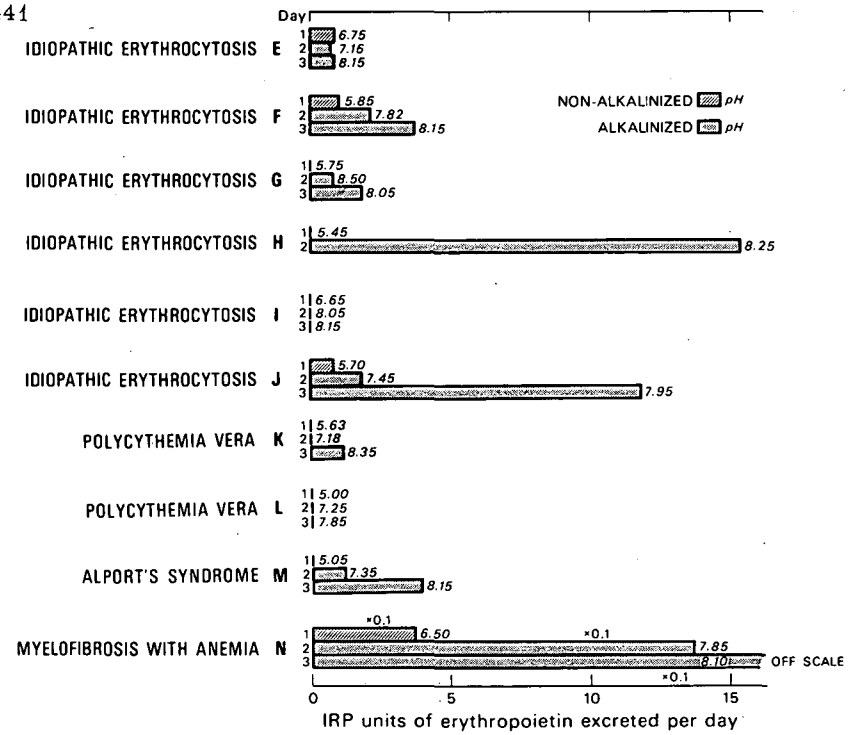

Fig. 4. Effect of alkalinization on daily excretion of erythropoietin by patients with hematologic disease.

DBL 689-5441

and low but measurable values on the second day (Table 1). On the third day, when fluid intake was greatly increased, the urinary excretion of erythropoietin rose slightly. Adamson et al. (6) report no correlation between erythropoietin excretion and urine volume, determined in a single individual as a function of normal urine volume variation. However, Van Dyke (9) reported that when one patient with a high level of urinary erythropoietin developed unexplained polyuria, erythropoietin content per ml of urine was essentially unchanged, resulting in an increase in erythropoietin excretion with increasing urinary volume in this (isolated) case.

Four normal subjects and 10 patients with various hematologic diseases were given 6 g $NaHCO_3$ orally t.i.d. for 2 or more days. The results of assays of each day's urine output are shown in Fig. 3 for normals and Fig. 4 for patients. The pH is shown next to the bar for

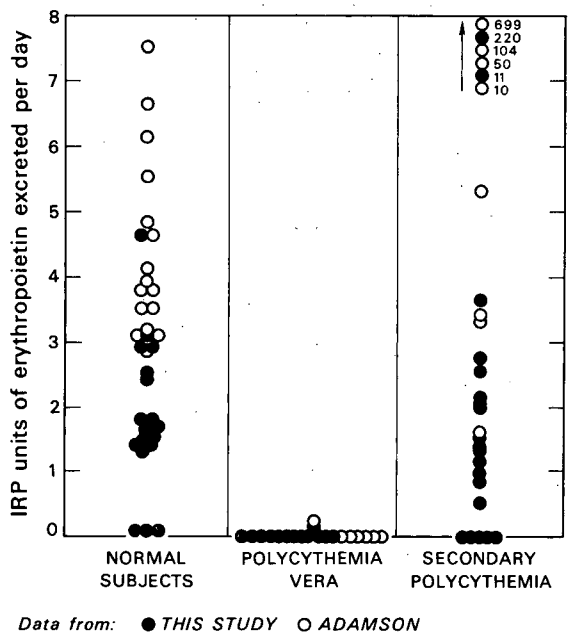

Fig. 5. Erythropoietin excretion of normal human beings or patients with primary or secondary polycythemia. Included in the figure are data presented by Adamson (10). DBL 689-5442.

each day. There was no correlation between urine volume and erythropoietin excretion, and added erythropoietin was quantitatively recovered from all but one base-line collection. In normal subjects erythropoietin excretion may remain unchanged following alkalinization, as in subjects C and D, or it may increase with duration of alkalinization. It can be seen that pH of subject A did not continue to rise during alkalinization although erythropoietin excretion was progressively increased.

Excretion of erythropoietin during alkalinization by patients with a variety of hematologic disorders is presented in Fig. 4. Urinary erythropoietin excretion in patients E, I, and L was unchanged. The remaining patients had moderate to marked increase in erythropoietin excretion. Serum erythropoietin of patient J was measured one week before alkalinization and on the second day of alkalinization. The serum level rose from "not detectable" to 0.044 unit/ml in spite of continuing polycythemia. Added erythropoietin was not recovered from the base-line sample of patient I, and it was not surprising to find no measurable erythropoietin in alkalinized samples.

Each of the topics discussed above was a practical problem arising from work done in this Laboratory or by others in attempting to use the urinary erythropoietin assay in clinical studies. With no manipulation of the patient the results are sometimes equivocal, as shown in Fig. 5. No data are included in the figure where it is known that added erythropoietin was not recovered. As can be seen, 28% of patients diagnosed as secondary polycythemia (hypoxia, cyst or tumor, or idiopathic) had no detectable erythropoietin in urine concentrates, and occasionally only slight or no erythropoietin was found in normal urine concentrates. All patients diagnosed as having polycythemia vera had a low erythropoietin level. Hence, a normal or high level of erythropoietin established the diagnosis of secondary polycythemia and appeared to negate a

diagnosis of polycythemia vera. Values obtained from results described by Adamson (10) were included in the figure for comparison.

In a study of a series of pregnant women, normal or anemic from iron deficiency or from causes unknown, it was found that 4 of 14 anemic women had no detectable erythropoietin. There was no recovery of added erythropoietin in the one case tested. Results from those anemic women with measurable erythropoietin are included in Fig. 6. Erythropoietin excretion in three normal pregnant women was in the range for normal females (0.5–1.6 IRP units per day), and one normal pregnant woman had slightly elevated excretion (Fig. 6). An abstract of these data has been presented elsewhere (11).

DISCUSSION

Erythropoietin is normally excreted in the urine and can be measured by using simple concentration procedures and standard bioassay techniques. The method of concentration by dialysis against Carbowax employed by Adamson et al. (6) and Alexanian (12) was found to result in complete recovery of erythropoietin from the urine. The hypertransfused mouse assay provided a sensitive assay method, with increased response to increased dose in a manner parallel to the dose-response curve obtained with human urinary erythropoietin. It was found that bacterial contamination did not significantly affect erythropoietin recovery.

Resolution of technical problems in assaying urine for erythropoietin content has focused attention on the usefulness of the method in diagnosis of hematologic disorders. When erythropoietin is measurable there are few problems in interpretation. Normal or elevated urinary erythropoietin in polycythemic patients indicates secondary polycythemia without implicating the etiologic factors. Work done by Adamson suggests that tumor-induced erythrocytosis may be diagnosed by phlebotomizing the subject and measuring erythropoietin excretion (10). In his series those patients with polycythemia secondary to tumor failed to show any increases in excretion after bleeding, whereas other secondary polycythemics markedly increased their erythropoietin excretion; patients with polycythemia vera phlebotomized showed measurable but not greatly elevated erythropoietin excretion. Adamson's results are in agreement with those previously presented by Nixon et al. (13), who obtained a rise in serum erythropoietin after phlebotomy of secondary polycythemics, but observed only very slight increase in serum erythropoietin in patients with polycythemia vera.

The difficulty in interpreting the meaning of the urinary erythropoietin assay arises primarily when erythropoietin excretion is not measurable. In the presence of elevated blood counts it is possible that the patient has polycythemia vera. In Adamson's studies (see comparison in Fig. 5) patients with polycythemia vera were clearly different from secondary polycythemics on the basis of urinary erythropoietin excretion without phlebotomy. In our series, however, five patients classified as secondary polycythemics had nondetectable erythropoietin levels. Two of them had renal cysts containing erythropoietically active fluid. The patients with typical polycythemia vera had slight or nonmeasurable erythropoietin.

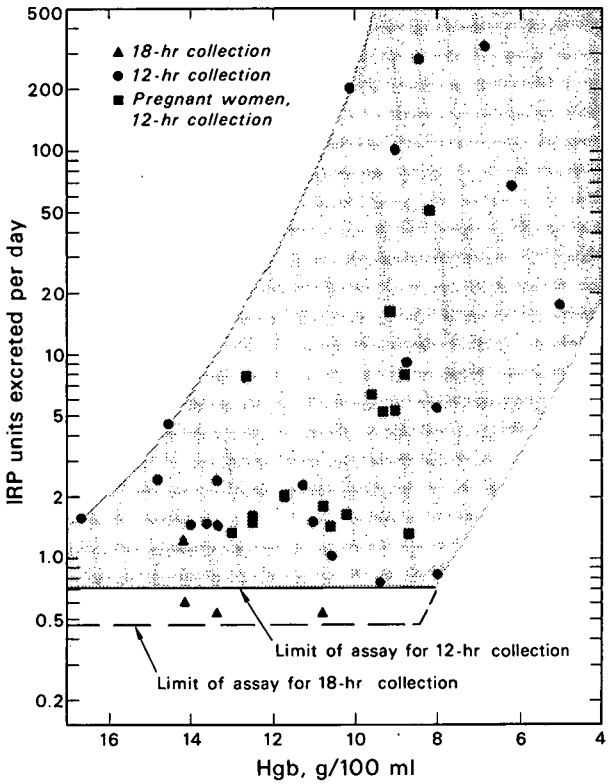

Fig. 6. Range of values obtained for excretion of erythropoietin by normal and anemic subjects. Points between 12-hr and 18-hr collection limits are values obtained from assay of 18-hr collections.
DBL 680-5480

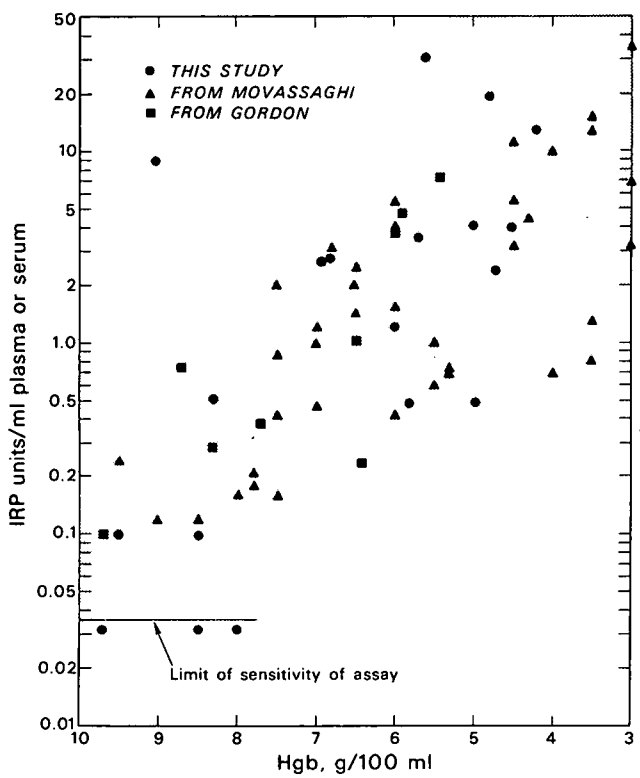

Fig. 7. Range of values obtained from serum erythropoietin of anemic patients. Included are data from Movassaghi et al. (19) estimated from erythropoietin curve (slope 21.6) presented by Shore et al. (25), and data from Gordon et al. (21). The high point just beneath the legend is very atypical. Points below the line of limit of sensitivity were negative in the assay.
DBL 680-5479

During the evolution of the assay procedure, we began to add a known amount of erythropoietin to half of a 24-hour urine collection prior to concentration. In 17 cases with nonmeasurable erythropoietin, recovery after concentration was virtually 100%, and quantitative recovery by this method has been obtained in other laboratories (6, 12). In eight of our cases added erythropoietin was not recovered after concentration, and the urine itself had no erythropoietic activity. This suggested a factor in urine inimical to erythropoietin. Bacterial contamination either was not present or was minimal, and in one case incubation of erythropoietin with bacteria from culture of such a urine resulted in no loss of activity of erythropoietin. Characterization of this factor (inhibitor, antibody?) was not undertaken, but no definitive correlation with the hematologic state could be made. Seven of the eight patients had primary or secondary polycythemia, and the eighth was a woman with slight anemia (hgb 10.4 g%) of pregnancy. (None of these is included in Fig. 6.) Several investigators (14-17) have reported an erythropoietin-inhibitory substance in plasma of polycythemic animals or posthypoxic man, or in thymoma (18), and although our studies do not corroborate this concept, they do not rule out the possibility of the existence of such a substance.

At the least, the studies presented here have led to the conclusion that to begin to evaluate the meaning of a nondetectable erythropoietin level, one must first test for the recoverability of erythropoietin from that urine. If there is no recovery of added erythropoietin, the assay is uninterpretable at present.

Another condition resulting in diminution and possibly loss of erythropoietin in urine was dehydration by severe restriction of fluid intake. It is unlikely that dehydration is a factor in most cases in which urinary erythropoietin is undetectable, but this is easily controlled and should be noted. Normal fluctuation of urine volume did not affect the amount of erythropoietin excreted (6).

Occasionally no erythropoietin was found in urine concentrates from anemic subjects, for example, for four pregnant women suffering moderate anemia of unknown etiology. Erythropoietin was added to the urine of only one of the four and it was not recovered. Moreover, assay of a postpartum urine sample from another of these women, whose hematocrit was 38.5% and hemoglobin concentration 12.2 g%, showed no detectable erythropoietin and very poor recovery (30%) of added erythropoietin. Though the cause of the anemia of these women remains in doubt, a reasonable explanation is insufficient erythropoietin.

Erythropoietin deficiency could feasibly be an etiologic factor in a case of anemia (Alport's syndrome; no uremia) in which erythropoietin was not detectable in a 12-hour urine concentrate (patient M in Fig. 4). In this instance it was determined that added erythropoietin could be recovered. Following alkalinization small amounts of erythropoietin were present, although these amounts were much lower than would be expected judging by the severity of anemia.

Marver and Gurney reported that administration of $NaHCO_3$ to anemic subjects increased the concentration of erythropoietin excreted into the resulting alkaline urine. Our studies utilizing this observation have shown that frequently this is the case (Figs. 3 and 4). Alkaliniza-

tion may serve as a valuable adjunct to the urinary erythropoietin assay, as in the case of anemia described above (patient M) in which erythropoietin became measurable; preliminary studies suggest that this procedure may assist in establishing a differential diagnosis in some cases of polycythemia. However, the essentiality of alkalinization has not been established. Erythropoietin excretion may or may not continue to rise, as shown by the studies of normal volunteers, so that duration of alkalinization necessary to produce maximum erythropoietin excretion may be different for each subject.

Of primary importance in interpretation of all results from serum or urine is the degree of anemia or polycythemia at the time of sampling. Movassaghi et al. (19) have shown a high degree of correlation between serum and urinary concentration of erythropoietin and hemoglobin in iron-deficient children, and Hammond et al. (20) showed a similar relationship in patients with sickle-cell anemia. Other investigators (21-23), measuring serum levels primarily in adult patients, found a rough correlation between hemoglobin and serum erythropoietin levels, and Van Dyke et al. (24) stated that in anemia serum erythropoietin is consistently measurable only when hemoglobin concentration is below 5 g%, and erythropoietin is measurable in unmodified urine only at hemoglobin concentrations of 4 g% or less. These determinations were made in the fasted-rat assay, but utilization of the more sensitive plethoric mouse assay has permitted detection of erythropoietin at only slightly higher hemoglobin concentration. When the hemoglobin concentration is 7 g% or less, erythropoietin can always be detected in the serum, Fig. 7. (Movassaghi's data show that in their assay system erythropoietin can be detected in serum of children with iron-deficiency anemia with hemoglobin concentrations of 9 g% or less.) When hemoglobin concentration is greater than 7 g%, the serum level may not be sufficiently elevated to be assayed, in which case a urine concentrate should be assayed (Figs. 6 and 7). Urine concentrates from patients with hemoglobin above 7 g% showed little correlation between urinary erythropoietin content and hemoglobin concentration.

The patient with polycythemia vera who has been phlebotomized to normal hemoglobin levels shows a normal concentration of erythropoietin in the urine (10). The patient with a measurable level of erythropoietin and secondary polycythemia shows a still higher concentration after phlebotomy unless an erythropoietin-producing tumor is the cause of the polycythemia (10).

Assay of urinary content of erythropoietin will be useful only until assay methods sufficiently sensitive to measure subnormal levels in the serum are developed. Recent progress in purification of erythropoietin (26) provides hope for a sensitive radioimmunoassay in the foreseeable future.

SUMMARY

In the absence of methods for measurement of serum erythropoietin when it is low, normal, or only slightly elevated, the ability to measure daily erythropoietin excretion becomes important. When a patient's hemoglobin is 7 g% or less, the concentration of erythropoietin in the serum is usually sufficiently high so that serum can be assayed. However, if the hemoglobin concentration is above 7 g%, the serum erythropoietin may not be sufficiently elevated

to be measured by present methods. Although erythropoietin concentration in urine is lower than that in serum, the hormone can be quantitatively and conveniently concentrated from urine. The urinary level probably reflects the plasma level, though proof that the urine level accurately reflects plasma level under all circumstances has not been obtained.

Concentrating urine by dialysis against Carbowax provides quantitative recovery and is the method of choice. When erythropoietin is not detectable in urine concentrates, no interpretation is possible unless quantitative recovery of added erythropoietin has been demonstrated. When erythropoietin cannot be demonstrated in concentrates of urine in spite of recovery of added erythropoietin, the patient can be assumed to have a subnormal level. Why added erythropoietin cannot be recovered from some urines has not been determined, but destruction by bacterial contamination has been ruled out as the cause.

Measurable erythropoietin in the urine in the presence of untreated polycythemia is strong evidence in favor of a diagnosis of secondary polycythemia. Adamson has shown that polycythemia secondary to tumor can be further distinguished by failure to increase erythropoietin excretion after phlebotomy.

REFERENCES AND NOTE

1. Van Dyke, D.; M. L. Nohr; and J. H. Lawrence: Blood 28: 535 (1966).
2. Marver, D.; and C. W. Gurney: Ann. N. Y. Acad. Sci. Erythropoietin 149: 570 (1968).
3. Waldmann, T. A.; W. F. Rosse; and R. L. Swarm: ibid. 509.
4. Adamson, J. W.; and C. A. Finch: ibid. 560.
5. Novy, M. J.; M. J. Edwards; and J. Metcalfe: J. Clin. Invest. 46: 1848 (1967).
6. Adamson, J. W.; R. Alexanian; C. Martinez; and C. A. Finch: Blood 28: 354 (1966).
7. DeGowin, R. L.; D. Hofstra; and C. W. Gurney: Proc. Soc. Exptl. Biol. Med. 110: 48 (1957).
8. Human urinary erythropoietin standardized against the International Reference Preparation (IRP) obtained from the Medical Research Council of Great Britain.
9. Van Dyke, D.: In L. W. Jacobson and M. Doyle (eds), Erythropoiesis. Grune and Stratton, New York, 1962. P. 386 (discussion).
10. Adamson, J. W.: Blood 32: 597 (1968).
11. Kosmin, M.; M. B. Fish; R. O. Wallerstein; M. Pollycove; D. C. Van Dyke; and R. Smith: Clin. Res. 15: 132 (Abstract) (1967).
12. Alexanian, R.: Blood 28: 344 (1966).
13. Nixon, J. C.; D. R. Korst; J. Whalen; and R. L. Brandt: Ann. Internal Med. 62: 1084 (Abstract) (1965).
14. Krzymowski, T.; and H. Krzymowska: Blood 19: 38 (1962).
15. Whitcomb, W. H.; and M. Z. Moore: Ann. N. Y. Acad. Sci. Erythropoietin 149: 462 (1968).
16. Reynafarje, C.: ibid. 472.
17. Ramos, J.; E. P. Cronkite; M. L. Greenberg; L. M. Schiffer; and P. Stryckmans (1965): cited in Ref. 16.
18. Field, E. O.; M. N. Caughi; N. M. Blackett; and D. W. Smithers: Brit. J. Haematol. 15:

101 (1968).

19. Movassaghi, N.; N. A. Shore; and D. Hammond: Proc. Soc. Exptl. Biol. Med. 126: 615 (1967).
20. Hammond, D.; N. Shore; and N. Movassaghi: Ann. N. Y. Acad. Sci. Erythropoietin 149: 516 (1968).
21. Gordon, A. S.; A. H. Weintraub; J. F. Camiscoli; and J. F. Contrera: Ann. N. Y. Acad. Sci. 119: 561 (1964).
22. Gurney, C. W.; L. O. Jacobson; and E. Goldwasser: Ann. Internal Med. 49: 363 (1958).
23. Penington, D. G.: Lancet 1: 301 (1961).
24. Van Dyke, D. C.; M. Layrisse; J. H. Lawrence; J. F. Garcia; and M. Pollycove: Blood 18: 187 (1961).
25. Shore, N. A.; N. Movassaghi; and D. Hammond: Ann. N. Y. Acad. Sci. Erythropoietin 149: 46 (1968).
26. Espada, J.; and A. Gutnisky: private communication. Erythropoietin Collection Center, Universidad del Nordeste, Faculdad de Medicina, Corrientes, Argentina.

This work was supported in part by the United States Atomic Energy Commission and in part by Grant #5ROICA08370 from the National Cancer Institute of the National Institutes of Health.

Localization of ^{58}Co and ^{65}Zn Hematoporphyrin Complexes in Canine Lymph Nodes

Rashid A. Fawwaz, H. Saul Winchell, Frederick Frye, William P. Hemphill and John H. Lawrence

Hematoporphyrins and metallo-hematoporphyrins have been found to localize in lymph nodes (1, 2). However, no attempt has hitherto been made to quantitate the fraction of the administered hematoporphyrin or metallo-hematoporphyrin which does so.

In this report we present results obtained with two metallo-hematoporphyrins, ^{58}Co- and ^{65}Zn-hematoporphyrin complexes. A quantitative study has been made of the tissue distribution of these metallo-hematoporphyrins in a series of dogs and in one human subject.

It appears possible to use radioactively labeled metallo-hematoporphyrins in selective lymphatic irradiation.

METHODS

Hematoporphyrin-free base was obtained from K and K Laboratories (Plainview, New York). Carrier-free radioactive cobaltous acetate [$^{58}Co(C_2H_3O_2)_2$] and radioactive zinc acetate [$^{65}Zn(C_2H_3O_2)_2$] (5 Ci per g) were obtained from New England Nuclear Corporation (Boston, Massachusetts).

^{58}Co- and ^{65}Zn-hematoporphyrin complexes were prepared according to the method of Taylor (3).

In one series of studies carrier-free ^{58}Co-acetate was added to an acetate buffer, pH 6, and administered intravenously to two normal dogs. In a second series of studies ^{58}Co-hematoporphyrin was dissolved in 0.05 N sodium hydroxide and administered intravenously to seven normal dogs and to one human patient with carcinoma of the colon. In addition ^{65}Zn-hematoporphyrin was dissolved in 0.05 N sodium hydroxide and administered intravenously to one normal dog. The amount of hematoporphyrin administered varied from 10 to 50 mg, but the amount of metallo-hematoporphyrin was negligible, since carrier-free ^{58}Co and high-specific-activity ^{65}Zn were used in the preparation of the metallo-hematoporphyrins.

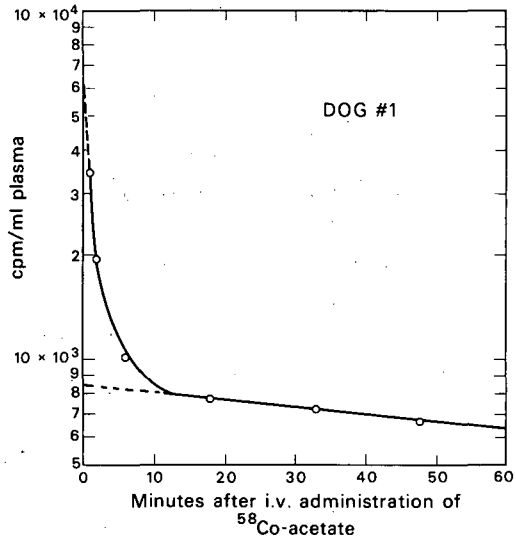

Fig. 1. The disappearance of radioactivity from the plasma in a dog (#1) given ^{58}Co-acetate intravenously. There is an initial rapid disappearance of ^{58}Co from the plasma ($t_{1/2} \approx$ 4 minutes). Thereafter there is a change in the slope of the curve with the appearance of a slower second exponential ($t_{1/2} \approx$ 200 minutes).
DBL 689-5462

In each experiment plasma samples were obtained every 10 min for the first hour of the study, and daily thereafter for 5 days. Radioactivity of samples was determined by utilizing a well-type scintillation counter. The initial distribution volume of the intravenously administered metallo-hematoporphyrin was calculated by dividing the activity administered by the zero-time extrapolate of the single exponential function fitted to the plasma radioactivity clearance curve during the first hour of the study.

In two dogs, plasma samples were obtained on Day 1 following the intravenous administration of the ^{58}Co-hematoporphyrin. In the same dogs, plasma samples were obtained prior to the administration of radioactivity; part of this plasma was incubated with ^{58}Co-acetate and the other part with ^{58}Co-hematoporphyrin. A 16-hr paper electrophoresis was performed on all these plasma samples, using B-2 Veronal buffer, pH 8.6 (Spinco). Following the electrophoresis the distribution of the radioactivity in the paper was determined by dividing the paper into sections and counting each section in a well-type scintillation counter.

The loss of radioactivity from the entire body of two dogs and of one human subject given ^{58}Co-hematoporphyrin was determined by use of the whole-body counter.

At the ends of periods varying from 1 to 18 days the dogs were killed, the tissue samples weighed, and the concentration of radioactivity determined. In one human patient specimens of mesenteric lymph node, fat, and muscle were obtained during an exploratory laparotomy 5 days following the intravenous administration of ^{58}Co-hematoporphyrin. On the day prior to surgery a needle bone-marrow biopsy was obtained from the iliac area. The human tissue samples were weighed and the radioactivity counted by using a well-type scintillation counter.

RESULTS

Figure 1 shows the disappearance of radioactivity from the plasma in a dog (#1) given ^{58}Co acetate intravenously. The abscissa represents time after IV administration of ^{58}Co acetate

and the ordinate the counts per minute per ml of plasma. There is an initial rapid disappearance of ^{58}Co from the plasma ($t_{1/2} \approx 4$ min). Thereafter, there is a change in the slope of the curve, with the appearance of a slower second exponential component ($t_{1/2} \approx 200$ min).

Table 1 shows the tissue distribution of ^{58}Co in the same dog (#1) and in another normal dog (#2). Both dogs were killed on the third day following the IV administration of ^{58}Co acetate. In Table 1, the radioactivity is expressed as the fraction of the administered dose $\times 10^{-6}$ per gram wet weight, and as the ratio of activity per unit weight of the given organ to the activity per unit weight of muscle. The organ containing the highest concentration of radioactivity in these studies is the renal cortex; the organ with the next highest concentration of radioactivity is the liver. The radioisotopic concentration in lymph nodes is low, and comparable to that found in tissues other than kidneys and liver. In these animals little of the administered radioactivity is retained in the body, the major portion having been excreted in the urine.

Table 1.

FRACTION OF ADMINISTERED ^{58}Co ACETATE $\times 10^{-6}$ PER GRAM OF WET WEIGHT OF TISSUE (3 DAYS AFTER ADMINISTRATION)				
	DOG #1	*DOG #2*	*AVERAGE*	*RATIO OF AVERAGE CONCENTRATION IN TISSUE TO AVERAGE CONCENTRATION IN MUSCLE*
MUSCLE	1.1	3.2	2.1	1.0
PANCREAS	3	4.4	3.8	1.8
LUNG	5	8	6.5	3.1
DUODENAL MUCOSA	2.5	6.0	4.2	2.0
SPLEEN	2	3	2.5	1.2
KIDNEY CORTEX	12	40	26	12.4
LIVER	7	22	14.5	6.9
FEMORAL BONE MARROW	1.3	4	2.6	1.2
MESENTERIC LYMPH NODE	2	3	2.5	1.2
ADRENAL	4	4	4	1.9

Figure 2 shows the disappearance of radioactivity from the plasma in a dog (#3) given ^{58}Co-hematoporphyrin. The abscissa represents time after the intravenous administration of ^{58}Co-hematoporphyrin (with only the first hour of the study shown in this figure), and the ordinate represents counts/min per ml of plasma. The plasma disappearance of radioactivity during the first hour is slow, and has a single exponential clearance rate ($t_{1/2} = 85$ min). The initial distribution volume of the intravenously administered ^{58}Co-hematoporphyrin is 1150 ml, which agrees closely with the expected plasma volume of 1200 ml (plasma volume = 5% of body weight). Figure 2 is representative of the pattern of clearance of radioactivity from plasma in the seven normal dogs and the one human patient given ^{58}Co-hematoporphyrin.

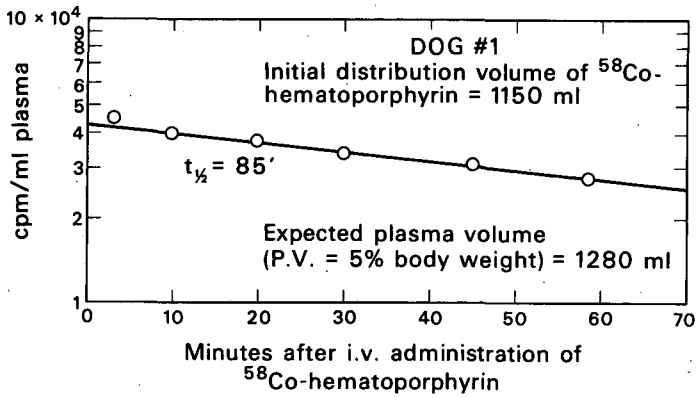

Fig. 2. The disappearance of radioactivity from the plasma in a dog (#3) given ^{58}Co-hematoporphyrin intravenously. The plasma disappearance of radioactivity during the first hour is slow and has a single exponential clearance rate ($t_{1/2}$ = 85 minutes). DBL 689-5461

Figure 3 presents the pattern of radioactivity clearance from the plasma in a dog (#3) during a 5-day period following the IV injection of ^{58}Co-hematoporphyrin. After about 2 hr there is a diminution in the slope of the curve, which eventually corresponds to a $t_{1/2}$ of about 52 hr. This study is also representative of three dogs and one human subject followed for 5 days.

Table 2 represents the tissue distribution in seven dogs and one human patient given ^{58}Co-hematoporphyrin intravenously. The radioisotopic concentration in tissue is expressed as a fraction of the administered dose $\times 10^{-6}$ per gram of wet weight and as the ratio of activity per unit weight of the given organ to the activity per unit weight of muscle. The dogs were killed at intervals ranging from 1 to 18 days after administration of the isotope. The dogs varied in body weight from 32 to 40 lb, and the human subject weighed 160 lb. The results reported under mesenteric lymph nodes are not representative of other nodes obtained from the cervical, inguinal, and paratracheal areas. In the same animal some nonmesenteric lymph nodes attained the same radioisotopic concentration as mesenteric lymph nodes; other nonmesenteric lymph nodes showed much less concentration of ^{58}Co-hematoporphyrin than mesenteric lymph nodes. Whereas some of the nonmesenteric lymph nodes proved to be fibrotic on microscopy, in others the decreased uptake of radioactivity was not commensurate with the degree of fibrosis. Although the absolute concentration of radioactivity in a given tissue varied widely from dog to dog, there appeared to be little change in relative distribution of radioactivity in the various tissues from the 1st to 18th day following IV administration of ^{58}Co-hematoporphyrin. From the averaged relative distribution of radioactivity in different tissues for all dogs studied, expressed as the ratio of averaged activity per gram of the tissue in question to the activity per gram of muscle (last column Table 2), it can be readily appreciated that the highest average relative concentration of activity occurred in the mesenteric lymph nodes, followed by kidney and liver. Additionally, the ratio of activity in lymph node is, on the average, 7.5 times as great as in bone marrow and 16.7 times as great as in duodenal mucosa.

In the human subject the relative distribution of radioactivity in bone marrow, lymph node, muscle, and fat is similar to that exhibited by the dogs. The concentration of radioactivity per gram of lymph node is approximately 6 times as great as in bone marrow.

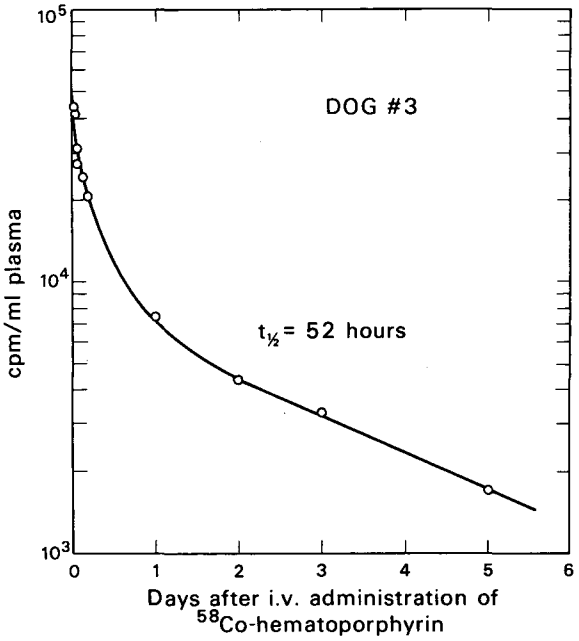

Fig. 3. The pattern of radioactivity clearance from the plasma in a dog (#3) during a 5-day period following the intravenous injection of ^{58}Co-hematoporphyrin. After 2 hours there is a diminution in the slope of the curve which eventually corresponds to a $t_{1/2}$ of 52 hours.
DBL 689-5463

Table 2.

FRACTION OF ADMINISTERED ^{58}Co-HEMATOPORPHYRIN × 10^{-6} PER GRAM OF WET WEIGHT OF TISSUE	DOG								AVERAGE FOR ALL DOGS	RATIO OF AVERAGE CONCENTRATION IN TISSUE TO AVERAGE CONCENTRATION IN MUSCLE
	3	4	5	6	7	8	9	HUMAN		
TIME	1 d	3 d	3 d	4 d	4 d	6 d	18 d	5 d		
MUSCLE	5	20	13	2	6	13	6	1	9.2	1
PANCREAS	12	32	40	15	16	15	20	—	21.4	2.3
LUNG	33	70	80	40	60	40	60	—	54.7	5.9
DUODENAL MUCOSA	40	90	110	50	45	60	120	—	73.5	8.0
SPLEEN	60	130	200	80	80	72	360	—	140	15.2
KIDNEY CORTEX	340	1800	1900	900	570	800	600	—	987	107.3
LIVER	850	760	1000	320	330	1600	1500	—	908	98.6
FEMORAL BONE MARROW	60	220	250	85	48	300	180	11*	163	17.7
MESENTERIC LYMPH NODE	250	2220	1200	500	600	1900	2000	62	1230	133.6
ADRENAL	170	400	40	160	140	—	480	—	290	31
KIDNEY MEDULLA	30	—	—	—	—	—	54	—	42	4.6
BRAIN	6	—	—	—	—	—	3	—	4.5	0.5
BONE	6	—	—	—	—	—	7	—	6.5	0.7
FAT	12	—	—	—	—	—	20	2	16	1.9

*Bone marrow obtained from iliac crest

Figure 4 presents the relationship of plasma radioactivity to migration zones corresponding to various electrophoretically determined plasma protein constituents. The top figure presents results obtained when plasma is incubated with ^{58}Co-hematoporphyrin for 2 hr at 37°C; the lower figure shows results obtained when plasma is similarly incubated with ^{58}Co acetate.

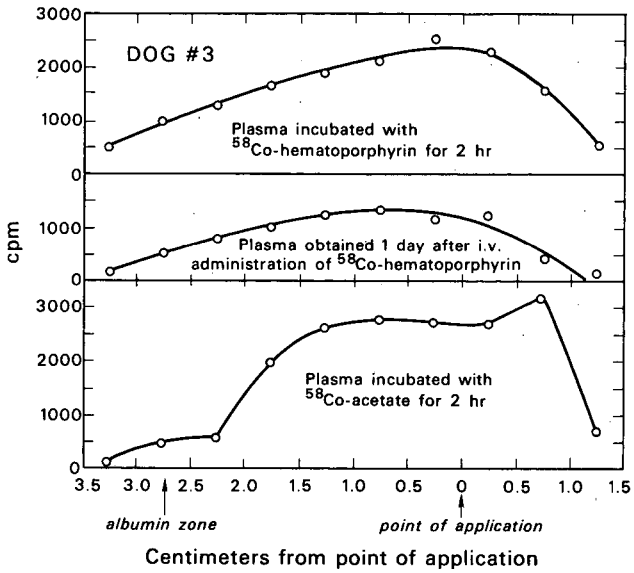

Fig. 4. The relationship of plasma radioactivity to migration zones corresponding to various electrophoretically determined plasma protein constituents. It can be seen that a different distribution pattern results with the use of ^{58}Co-hematoporphyrin as compared to ^{58}Co-acetate and that following in vivo administration of ^{58}Co-hematoporphyrin the distribution or radioactivity in the plasma is similar to plasma incubated in vitro with ^{58}Co-hematoporphyrin.

DBL 689-5459

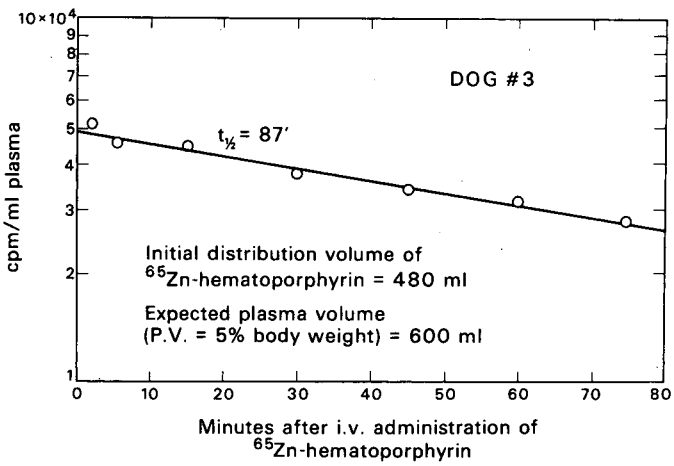

Fig. 5. The disappearance of radioactivity from the plasma in a dog (#10) given ^{65}Zn-hematoporphyrin intravenously. During the first hour of the study the disappearance of radioactivity from the plasma is slow and follows a single exponential function ($t_{1/2} \approx 87$ minutes).

DBL 689-5460

The middle figure presents results obtained from dog plasma 1 day after IV administration of ^{58}Co-hematoporphyrin. It can be seen that a different distribution pattern results with the use of ^{58}Co-hematoporphyrin and with ^{58}Co acetate, and that following in vivo administration of ^{58}Co-hematoporphyrin the distribution of radioactivity in the plasma is similar to the pattern obtained when plasma is incubated in vitro with ^{58}Co-hematoporphyrin.

Figure 5 shows the disappearance of radioactivity from the plasma in a dog (#3) given ^{65}Zn-hematoporphyrin IV. During the first hour of the study the disappearance of radioactivity from the plasma is slow, and follows a single exponential function ($t_{1/2}$ = 87 min), similar to that obtained with ^{58}Co-hematoporphyrin.

Table 3 presents the relative distribution of radioactivity in the tissues of this dog (#3) 3 days after administration of ^{65}Zn-hematoporphyrin. The concentration of radioactivity in this animal's lymph nodes is 8.6 times as great as in the duodenal mucosa and 5 times as great as in bone marrow.

Table 3. Fraction of administered ^{65}Zn-hematoporphyrin $\times 10^{-6}$ per gram of wet weight of tissue (3 days after administration).

	DOG #3	RATIO OF CONCENTRATION IN TISSUE TO CONCENTRATION IN MUSCLE
MUSCLE	16	1.0
PANCREAS	32	2.0
LUNG	30	1.8
DUODENAL MUCOSA	96	6.0
SPLEEN	160	10.0
KIDNEY CORTEX	800	50.0
KIDNEY MEDULLA	16	1.0
LIVER	1600	100.0
FEMORAL BONE MARROW	160	10.0
MESENTERIC LYMPH NODE	830	51.9
ADRENAL	600	37.5

Figure 6 shows the disappearance of radioactivity from the entire body of a human subject (J. D.) given ^{58}Co-hematoporphyrin. The abscissa represents time in days, the ordinate the per cent of activity remaining in the body. For the first 4 weeks the disappearance of radioactivity follows a single exponential with a $t_{1/2}$ of 36 days. The results of this study are similar to those obtained in two normal dogs. The loss of activity occurs both in the urine and in stools, in a ratio of 3:2 urine to stools.

DISCUSSION

Cobalt chelated with porphyrins in vitro appears to be very stable; the metal dissociates from the porphyrin only in the presence of concentrated sulfuric acid (4). The work presented here further suggests that the ^{58}Co-hematoporphyrin complex is stable in vivo, as evidenced by the kinetic studies and tissue-distribution studies.

The clearance of radioactivity from the plasma in dogs injected intravenously with ^{58}Co-hematoporphyrin is described by at least two exponential terms, an initial one with a $t_{1/2}$ of approximately 85 min, and a second one, appearing about the second hour of the study, having a $t_{1/2}$ of approximately 52 hr. The presence of the second exponential component raises two possibilities:

(a) that the ^{58}Co is bound to more than one form of porphyrin;

(b) that there is a feedback of ^{58}Co-hematoporphyrin from tissues into the plasma.

These two possibilities cannot be resolved from the experiments reported here.

The loss of radioactivity from the body of the human and dogs given ^{58}Co-hematoporphyrin, as determined by the whole-body counter, showed a loss of about 2% per day ($t_{1/2}$ = 36 days). In man, this loss during the 1st seven days occurred via the urine and fecal routes in a ratio of 3:2.

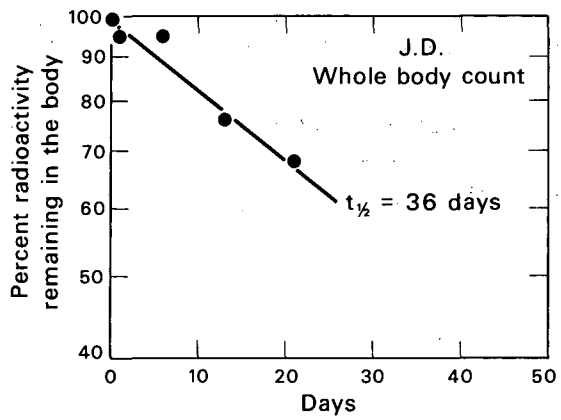

Fig. 6. The disappearance of radioactivity from the entire body of a human subject, J. D., given ^{58}Co-hematoporphyrin intravenously. For the first 4 weeks the disappearance of radioactivity follows a simple exponential with a $t_{1/2}$ of 36 days.
DBL 689-5464

Following the intravenous administration of ^{58}Co-hematoporphyrin to dogs, the lymph nodes, kidney, and liver showed the highest uptake of radioactivity. However, two of the most radiosensitive organs, the duodenal mucosal cells and the bone marrow cells, showed much less concentration of radioactivity, with an average ratio in dogs of lymph node to duodenal mucosal cell of 16:7 and an averaged ratio of lymph node to bone marrow of 7.5:1. These findings, coupled with the marked vulnerability of the lymph cells to irradiation, suggest the possibility of selective lymph-node irradiation, using appropriate radioisotopic metallo-hematoporphyrins. The feasibility of such a procedure would depend on

(a) use of a radioactive metal which is strongly chelated by hematoporphyrin;

(b) use of radioactive metal which decays predominantly by β^- or weak γ emission, since strong γ-emitting isotopes deposit a significant amount of their energy far from the site of their localization.

We are at present engaged in the study of various radioisotopic metallo-hematoporphyrins as possible agents for selective lymphatic irradiation for therapy of lymphatic neoplasma and in suppression of the homograft rejection response.

SUMMARY

Following the intravenous administration of ^{58}Co-hematoporphyrin to a series of dogs the lymph nodes, kidneys, and liver showed the highest uptake of radioactivity. Radiosensitive tissues such as the duodenal mucosa and the bone marrow showed much less concentration of radioactivity. These findings, coupled with the marked vulnerability of the lymph cells to irradiation, suggest the possibility of selective lymph-node irradiation, using appropriate radioisotopic metallo-hematoporphyrins.

ACKNOWLEDGMENT

We would like to thank Johnie A. Maxion for his outstanding assistance in the care and preparation of the animals.

REFERENCES

1. Rassmussen-Taxdal, D. S.; G. E. Wards; and F. H. J. Figge: Fluorescence of human lymphatic and cancer tissues following high doses of intravenous hematoporphyrin.

Cancer 8: 78 (1955).

2. Figge, F. H. S.; G. S. Weiland; and L. O. L. Manganiello: Cancer detection and therapy: affinity of neoplastic, embryonic, and traumatized tissues for porphyrins and metalloporphyrins. Proc. Soc. Exp. Biol. Med. 68: 640 (1948).
3. Taylor, J. F.: Metallo-porphyrins. II. Cobalt and manganese mesoporphyrins in coordination with nitrogenous bases. J. Biol. Chem. 135: 569 (1940).
4. Falk, J. E.: Porphyrins and Metallo-Porphyrins. Elsevier Publishing Company, New York, 1964. P. 33.

Evaluation of ^{111}Ag, ^{113}Sn, ^{90}Yt and ^{109}Pd Hematoporphyrin Complexes for Selective Lymphatic Irradiation

Rashid A. Fawwaz, H. Saul Winchell, Meldrum B. Winstead, Gery C. Armaly, William P. Hemphill and John H. Lawrence

Following the intravenous administration of ^{58}Co-hematoporphyrin to a series of dogs, the mesenteric lymph nodes, kidneys, and liver showed the highest uptake of radioactivity, whereas the duodenal mucosal cells and the bone marrow showed much less concentration of radioactivity (1). These findings coupled with the marked vulnerability of lymph cells to irradiation suggest the possibility of selective lymph-node irradiation using appropriately labeled metallo-hematoporphyrins.

The feasibility of such a procedure would depend upon the use of

(i) a radioactive metal strongly chelated by hematoporphyrin,

(ii) a radioactive metal which decays predominantly by β^- or weak γ emission, as energetic γ's deposit a significant amount of their energy away from the site of localization.

In this report we show that whereas ^{90}Yt, ^{113}Sn, ^{111}Ag, and ^{109}Pd satisfy the second requirement only ^{109}Pd satisfies both requirements.

METHODS

Hematoporphyrin-free base was obtained from K and K Laboratories (Plainview, N. J.). Cobaltous acetate (^{58}Co) (carrier-free), yittrium acetate (^{89}Y) (carrier-free), and stannous acetate (^{113}Sn) (0.2 Ci/g) were obtained from the New England Nuclear Corporation (Boston, Massachusetts). Silver(I) acetate (^{111}Ag) (carrier-free) was obtained from Amersham (England). Palladous chloride (^{109}Pd) (6 Ci/g) was obtained from Nuclear Science Corporation (Pittsburg).

Cobalt-, tin-, silver-, and palladium-hematoporphyrin complexes were prepared according to the methods summarized by Falk (2). An attempt to prepare an ^{89}Yt-hematoporphyrin complex by heating ^{89}Yt acetate with hematoporphyrin dissolved in acetic acid failed.

The radioactively labeled metallo-hematoporphyrins were dissolved in 0.05 N sodium hydroxide and administered intravenously to a series of dogs. The ^{58}Co-hematoporphyrin was also administered to a human patient with carcinoma of the colon.

The amount of hematoporphyrin administered varied from 10 to 50 mg, but the amount of metallo-hematoporphyrin was negligible, since high-specific-activity radioactive metals were used in the preparation of the metallo-hematoporphyrins.

In each experiment plasma samples were obtained every 10 min for the first hour of the study. Radioactivity of samples was determined by utilizing a well-type scintillation counter. The initial distribution volume of the intravenously administered metallo-hematoporphyrin was calculated by dividing the activity administered by the zero-time extrapolate of the single exponential function fitted to the plasma radioactivity clearance curve during the first hour of the study. At the ends of periods varying from 1 to 18 days the dogs were killed, the tissue samples weighed, and water added to bring each sample to a total weight of 2 g. The tissues were then digested with sodium hydroxide and the radioactivity counted. In one human patient, specimens of mesenteric lymph node, fat, and muscle were obtained during an exploratory laparotomy 5 days after the intravenous administration of ^{58}Co-hematoporphyrin. A biopsy was performed on a needle bone-marrow sample from the iliac area on the day before surgery. Tissue preparation for radioisotopic counting was identical to that used in dogs.

RESULTS

The results obtained with ^{58}Co-hematoporphyrin are reported in the preceding paper. During the first hour the plasma disappearance of ^{58}Co-hematoporphyrin injected IV is slow, and has a single exponential clearance rate, $t_{1/2} \approx 85$ min. In these experiments, the mesenteric lymph nodes achieve the highest concentration of activity, followed closely by renal cortex and liver. Additionally the ratio of activity in mesenteric lymph node is on the average 7.5 times as great as in bone marrow and 16.7 times as great as in duodenal mucosa. In the human subject the relative distribution of radioactivity in bone marrow mesenteric lymph nodes, muscle, and fat is similar to that exhibited by dogs. The concentration of radioactivity per gram of lymph node is approximately 6 times that obtained in bone marrow.

Figure 1 shows the disappearance of radioactivity from the plasma in a dog (#1) given ^{111}Ag-hematoporphyrin intravenously. There is an initial rapid disappearance of ^{111}Ag-hematoporphyrin from the plasma ($t_{1/2} \approx 3$ min). Thereafter there is a change in the slope of the curve, with the appearance of a slower second exponential component ($t_{1/2} \approx 60$ min).

Table 1 shows the tissue concentration of ^{111}Ag-hematoporphyrin in the same dog (#1) and in another dog (#2). Both dogs were killed 1 day after the intravenous administration of ^{111}Ag-hematoporphyrin. The organ containing the highest concentration is the liver. The radioisotopic concentration in lymph nodes is low and more or less comparable to that found in organs other than the liver.

Figure 2 shows the disappearance of radioactivity from the plasma in a dog (#3) given ^{113}Sn-hematoporphyrin intravenously. There is an initial rapid disappearance of ^{113}Sn-hematoporphyrin from the plasma ($t_{1/2} \approx 3$ min). Thereafter there is a change in the slope of the curve, with the appearance of a slower exponential component ($t_{1/2} \approx 51$ min).

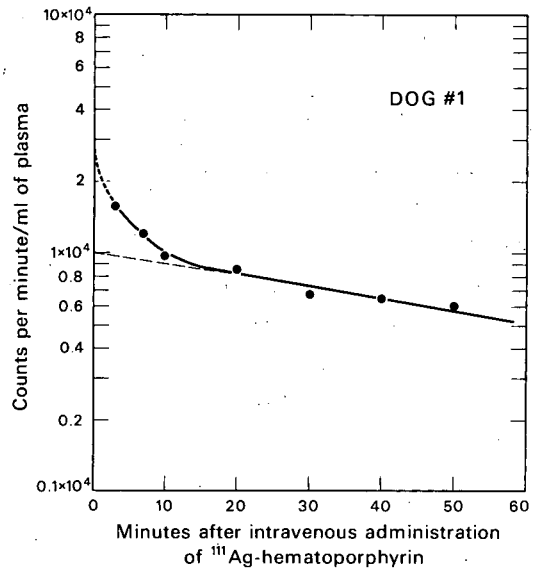

Fig. 1. The disappearance of radioactivity from the plasma in a dog given ^{111}Ag-hematoporphyrin I. V. There is an initial rapid disappearance of radioactivity from the plasma ($t_{1/2}$ = 3 minutes). Thereafter there is a change in the slope of the curve with the appearance of a slower second exponential component ($t_{1/2}$ = 60 minutes).

DBL 691-4503

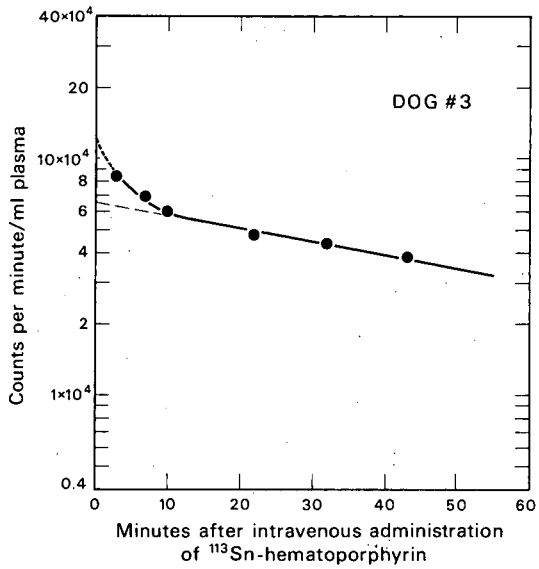

Fig. 2. The disappearance of radioactivity from the plasma in a dog given ^{113}Sn-hematoporphyrin I. V. There is an initial rapid disappearance of ^{113}Sn-hematoporphyrin from the plasma ($t_{1/2}$ = 3 minutes). Thereafter there is a change in the slope of the curve with the appearance of a slower exponential component ($t_{1/2}$ = 51 minutes).

DBL 691-4502

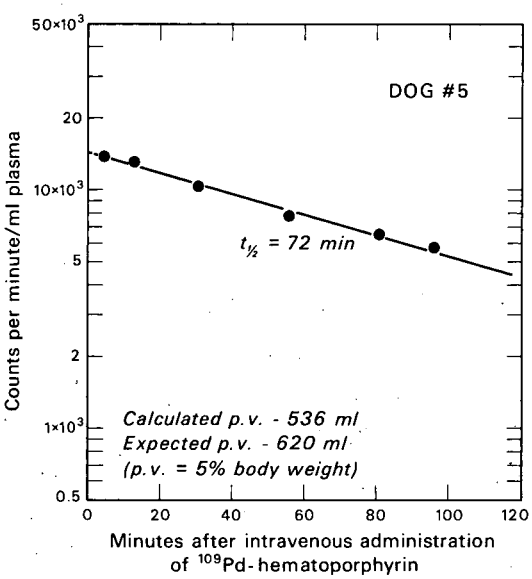

Fig. 3. Shows the disappearance of radioactivity from the plasma in a dog given ^{109}Pd-hematoporphyrin I. V. The plasma disappearance of radioactivity is slow and has a single exponential clearance rate ($t_{1/2}$ = 72 minutes).

DBL 691-4501

Table 1. Fraction of administered ^{111}Ag-hematoporphyrin $\times 10^{-6}$ per gram of wet weight of tissue (1 day after administration).

Tissue	Dog #1	Dog #2	Average	Ratio of concentration in tissue to concentration in muscle
Lymph node	54.6	16	35.3	9.8
Adrenal	52	39	45.5	12.6
Pancreas	8.6	6.9	7.7	2.1
Duodenal mucosa	25.2	48	36.1	10
Kidney cortex	210	195	202.5	56
Spleen	54.6	195	124.8	34.7
Liver	3480	6000	4740	1317
Muscle	4.2	3	3.6	1
Lung	21	69	45	12.5
Salivary gland	---	30	30	8.3
Bone marrow	67	54	60.5	17

Table 2. Fraction of administered ^{113}Sn-hematoporphyrin $\times 10^{-6}$ per gram of wet weight (1 day after administration).

Tissue	Dog #3	Dog #4	Average	Ratio of concentration in tissue to concentration in muscle
Lymph node	98.6	66	82.3	7.1
Spleen	76.5	52	64.2	5.6
Liver	340	258	299	26
Kidney cortex	340	312	326	28.3
Adrenal	136	90	113	10
Pancreas	14	10	12	1.04
Muscle	17	6	11.5	1
Lung	93	110	101.5	9
Bone marrow	34	66	50	4.3
Bone	1054	498	776	67.4

Table 2 shows the tissue distribution of ^{113}Sn-hematoporphyrin in the same dog (#3) and in another dog (#4). Both dogs were killed 1 day after the intravenous administration of ^{113}Sn-hematoporphyrin. The organ containing the highest concentration is the bone, and the organs with the next highest concentration are the liver and renal cortex. The radioisotopic concentration in lymph nodes is low and comparable to organs other than bone, liver, and renal cortex.

Figure 3 shows the disappearance of radioactivity from the plasma in a dog (#5) given ^{109}Pd-hematoporphyrin intravenously. The plasma disappearance of radioactivity is slow and has a single exponential clearance rate ($t_{1/2} \approx 72$ minutes), similar to the plasma clearance of ^{58}Co-hematoporphyrin. The initial distribution volume of the intravenously administered ^{109}Pd-hematoporphyrin is 536 ml, which agrees closely with the expected plasma volume of 620 ml (P. V. = 5% of body weight).

Table 3 shows the tissue concentration of radioactivity in eight dogs injected intravenously with ^{109}Pd-hematoporphyrin. The first two dogs (#5, #6) were less than 1 year old, and all the dogs used in this study were less than 2 years. The weights of the dogs ranged between 25 and 30 lb. The results reported under mesenteric lymph nodes are not representative of nodes obtained from the inguinal, cervical, and paratracheal areas. The uptake of radioactivity by nonmesenteric lymph nodes varied widely, and was consistently lower than that attained by mesenteric lymph nodes.

Table 3. Fraction of administered ^{109}Pd-hematoporphyrin $\times 10^{-6}$ per gram of wet weight (1 day after administration).

Tissue	Dog number 5	6	7	8	9	10	11	12	Average for all dogs	Ratio of concentration in tissue to concentration in muscle
Muscle	7	7	2	10	3	9	9	7	6.6	1.0
Pancreas	14	-	18	2	8	22	20	-	17.5	2.6
Lung	81	28	-	-	-	59	43	-	53.0	8.0
Duodenal mucosa	51	28	100	48	111	60	108	-	72.0	11.0
Spleen	231	141	-	-	-	435	414	-	305.0	46.2
Kidney cortex	990	878	274	256	309	534	405	-	520.0	80.0
Liver	1656	1108	1481	1018	2067	1980	2304	1260	1609.0	244.0
Bone marrow	297	165	289	242	298	132	150	200	221.0	33.5
Mesenteric lymph node	482	475	696	483	1428	528	1530	1400	877.0	133.0
Adrenal	151	99	-	-	-	-	360	-	203.0	30.0

From the averaged relative distribution of radioactivity in different tissues for all the dogs studied, it can be seen that the liver attains the highest concentration, followed by lymph node and then renal cortex. The ratio of activity in mesenteric lymph node is on the average four times as great as in bone marrow and 12 times as great as in duodenal mucosa (last column of Table 4).

Table 4 represents the averaged tissue uptake of ^{109}Pd-hematoporphyrin compared with the averaged tissue uptake of ^{58}Co-hematoporphyrin. Although with ^{109}Pd-hematoporphyrin the relative uptake by the liver and bone marrow is greater, and the relative uptake by the

lymph node and kidney is lower, than that observed with ^{58}Co-hematoporphyrin, the "t" test for small numbers (4) (last column of Table 5) indicates that these differences are not statistically significant.

Table 4. Average tissue uptake of ^{58}Co- and ^{109}Pd-hematoporphyrin complexes.

Tissue	Hematoporphyrin complex		Probability of occurring by chance ("t" test)
	^{109}Pd	^{58}Co	
Muscle	6.6	9.2	0.50
Pancreas	17.5	21.4	0.50
Lung	53.0	54.7	>0.50
Duodenal mucosa	72.0	73.5	>0.50
Spleen	305.0	140.0	0.20
Kidney cortex	520.0	987.0	0.10
Liver	1609.0	908.0	0.02
Bone marrow	221.0	163.0	0.20
Mesenteric lymph node	877.0	1230.0	0.20
Adrenal	203.0	290.0	0.60

DISCUSSION

The metallo-hematoporphyrins have the following order of stability in vitro: Pd > Co ≫ Sn > Ag. The Ag and Sn dissociate from the hematoporphyrin in the presence of water, whereas the Co and Pd dissociate from the hematoporphyrin only in the presence of concentrated sulfuric acid (3). The work presented here suggests that in vivo in dogs ^{109}Pd- and ^{58}Co-hematoporphyrin complexes are much more stable than the ^{113}Sn- and ^{111}Ag-hematoporphyrin complexes, as evidenced by the kinetic and tissue-distribution studies.

The accumulation of ^{109}Pd-hematoporphyrin in the bone marrow was greater than that observed with ^{58}Co-hematoporphyrin, and the uptake of ^{109}Pd-hematoporphyrin by the mesenteric lymph nodes was lower than that observed with ^{58}Co-hematoporphyrin. These differences, however, are not statistically significant. The concentration of ^{109}Pd in lymph nodes was four times as great as in bone marrow and 12 times as great as in duodenal mucosal cells.

The observation that the uptake of ^{109}Pd- and ^{58}Co-hematoporphyrin is greater in mesenteric lymph nodes than in nonmesenteric lymph nodes raises an interesting possibility. Mesenteric lymph nodes are antigenically stimulated continuously, whereas other lymph nodes are so stimulated sporadically (5, 6). Thus it is conceivable that the degree of uptake of metallo-hematoporphyrins by lymph nodes may be a function of antigenic stimulation of the lymph node.

At present we are conducting experiments in which the uptake of ^{109}Pd-hematoporphyrin by antigenically stimulated lymph nodes (foreign protein injected intracutaneously) is being

compared with uptake by nonstimulated lymph nodes in the same animal. We are also testing the usefulness of ^{109}Pd-hematoporphyrin as an agent for selective lymphatic ablation.

SUMMARY

Although ^{111}Ag- and ^{113}Sn-hematoporphyrin complexes failed to show any significant accumulation in lymph nodes, ^{109}Pd (a pure β^- emitter with a 13-hour half-life) complexed with hematoporphyrin showed four times as much accumulation in mesenteric lymph nodes as in bone marrow and 12 times as much accumulation in mesenteric lymph nodes as in duodenal mucosal cells. Compared with ^{58}Co-hematoporphyrin, ^{109}Pd-hematoporphyrin showed less uptake by mesenteric lymph nodes and greater uptake by bone marrow. These differences, however, are not statistically significant. The mesenteric lymph nodes showed greater uptake of ^{109}Pd- and ^{58}Co-hematoporphyrin than did nonmesenteric lymph nodes. This may be a function of antigenic stimulation.

ACKNOWLEDGMENT

We would like to thank Johnie A. Maxion for his outstanding assistance in the care and preparation of the animals.

REFERENCES

1. Fawwaz, R. A.; H. S. Winchell; F. Frye; W. Hemphill; and J. H. Lawrence: Localization of ^{58}Co- and ^{65}Zn-hematoporphyrin complexes in canine lymph nodes. To be submitted to J. Nucl. Med.
2. Falk, J. E.: Porphyrins and Metalloporphyrins. Elsevier Publishing Company, Amsterdam, 1964. P. 138-141.
3. Falk, J. E.: Porphyrins and Metalloporphyrins. Elsevier Publishing Company, Amsterdam, 1964. P. 33-34.
4. Hill, Bradford: Principles of Medical Statistics, 8th Edition. Oxford University Press, N. Y., 1966. P. 146.
5. Yolfey, J. M.; and F. C. Courtice: Lymphatics, Lymph and Lymphoid Tissue. Harvard University Press, Cambridge, Massachusetts, 1956. P 292-293.
6. Micklem, H. S.; and J. F. Loutit: Tissue Grafting and Radiation. Academic Press, New York and London, 1966. P. 57.

The Synthesis of Sodium ^{11}C-Benzoate and Its Use in Renal Visualization

Meldrum B. Winstead, H. Saul Winchell and Rashid A. Fawwaz

The potential usefulness of ^{11}C-labeled compounds in clinical medicine has been previously discussed by Myers and Hunter (1). This positron-emitting radioisotope with a $t_{1/2}$ of 20.4 min is readily produced in large quantities by a variety of nuclear reactions. Although ^{11}C-labeled compounds, including sodium ^{11}C-benzoate, have been synthesized in the past, the only compounds of ^{11}C which have been utilized in vivo for imaging have been ^{11}CO, $^{11}CO_2$, and inorganic ^{11}C carbonates (2, 3). The replacement of ^{12}C in an organic compound by ^{11}C should not alter the biochemistry of the compound. ^{11}C distribution in the body can be accurately delineated by using positronium imaging devices, and large quantities of activity can be administered with little tissue radiation exposure. It is clear that if methods were available for the rapid synthesis of ^{11}C-containing compounds having useful distributions within the body and the logistics of their subsequent distribution to clinical centers were solved, such compounds could become the most useful materials in the armamentarium of the physician practicing nuclear medicine.

In this report we discuss the potential use of sodium ^{11}C-benzoate in renal visualization. Sodium benzoate is a commonly used preservative added to canned foods, soft drinks, bread, etc. It is rapidly detoxified in the human liver by conjugation with a variety of materials, notably glycine. Such conjugation of benzoic acid with glycine yields hippuric acid, which is rapidly excreted by the kidneys. Indeed, excretion of hippuric acid in the urine following oral administration of 6.0 grams or intravenous administration of 1.77 g of sodium benzoate has been used in the past as a measure of hepatic function (4). Labeled benzoic acid can be made in a single-step synthesis by passing labeled carbon dioxide through an ether solution of the Grignard reagent, phenylmagnesium halide. Such reactions have been used for the production of ^{14}C-labeled benzoic acid (5), and similar reactions have been used for the production of ^{11}C-labeled carboxylic acids (6).

MATERIALS AND METHODS

^{11}C was produced as a mixture of ^{11}CO and $^{11}CO_2$, by deuteron bombardment of a fused B_2O_3 target, by the reaction ^{10}B(d, n)^{11}C. B_2O_3 was obtained from 20th Century Electronics

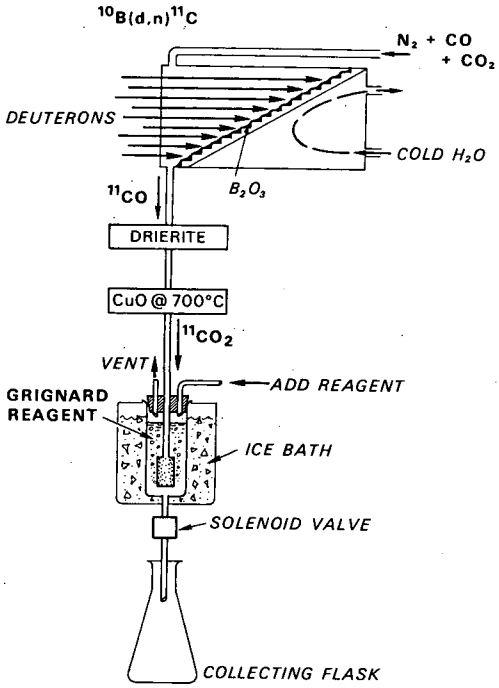

Fig. 1. Deuteron bombardment of a fused B_2O_3 target $^{10}B(d, n)$ ^{11}C yields ^{11}CO and $^{11}CO_2$ liberated from the target by recoil. The ^{11}CO is oxidized to $^{11}CO_2$ in the gas phase by passage over CuO at 700°C. The $^{11}CO_2$ is then reacted with appropriate Grignard reagents or organolithium compounds to form, after acid hydrolysis and extraction with $NaHCO_3$, ^{11}C-labeled sodium carboxylates. Yields are generally in the range of 60-80% of ^{11}C produced and preparation time is approximately 30 minutes. Millicurie quantities of ^{11}C-carboxylic acids have been prepared.

DBL 6810-5512A

Ltd., New Addington, Surrey, England, 90% enriched in the ^{10}B isotope. A 15-MeV deuteron beam from the 88-inch cyclotron at the Lawrence Radiation Laboratory at Berkeley was defocused to cover an area approximately 1 in. in diameter at the point at which it hit the target. Beam currents used varied from 5 to 25 μA. Preparation of the target and extraction of ^{11}CO and its oxidation to $^{11}CO_2$ by passage over hot CuO were similar to those previously described by Kamen (6). The nitrogen gas stream containing $^{11}CO_2$ was passed through a cold solution containing 3 ml of 3 M phenylmagnesium bromide in 20 ml of ether (Arapahoe Chemicals, Boulder, Colorado) (see Fig. 1). The above-noted reaction was cooled by use of an ice-water bath, and carbonation of the Grignard reagent occurred according to the reaction

$$C_6H_5MgBr + CO_2 \rightarrow C_6H_5COOMgBr. \quad (1)$$

When deuteron bombardment of the B_2O_3 target had been completed, reaction 1 was quenched by the addition of 10 ml of 6 N HCl. Nitrogen gas was passed through the reaction mixture during the acid hydrolysis as well as in the subsequent bicarbonate extraction step in order to provide adequate mixing of the reagents. The acid hydrolyzed the excess Grignard reagent to benzene and the product of reaction 1 to benzoic acid, according to the reaction

$$2C_6H_5COOMgBr + 2HCl \rightarrow 2C_6H_5COOH + MgBr_2 + MgCl_2. \quad (2)$$

The resulting two-layer system contained small amounts of benzene and benzoic acid dissolved in the ether layer, and the lower hydrochloric acid layer contained acid aqueous soluble impurities. The acid layer was removed and the ether solution was then extracted by the addition of 20 ml of 6% sodium bicarbonate solution, which again formed a two-layer system, with the

lighter ether solution containing the benzene, and the heavier sodium bicarbonate aqueous layer containing the ^{11}C-labeled sodium benzoate. The lower layer was drawn off, and this solution was collected in an Erlenmeyer flask containing a boiling chip. The solution was heated to boiling in order to remove small amounts of ether or benzene which might be dissolved in the aqueous solution. The remaining solution, containing the sodium benzoate and sodium bicarbonate, was then passed into a serum bottle and sterilized prior to its administration by passing through a Millipore ® filter.

^{131}I Iodohippurate (0.16 mCi/mg) and ^{203}Hg Chlormerodrin (^{203}Hg-Neohydrin) (1.18 mCi/mg) were obtained from E. R. Squibb and Sons, New York, New York. Radioisotope distribution in vivo was determined by using the positron-scintillation camera described previously (7).

RESULTS

Preliminary experiments using ^{14}C-labeled carbon dioxide demonstrated that 60–80% of the $^{14}CO_2$ introduced into the system was converted to benzoic acid. It was also determined that negligible quantities of $^{14}CO_2$ escaped the Grignard reagent solution, and thus essentially all the $^{14}CO_2$ that passed through the solution was trapped by the Grignard reagent. This was determined by placing a 2-methoxyethanol-ethanolamine trap in series with the apparatus in such a way that all gas escaping from the reaction flask passed through the trap. Negligible quantities of radioactivity were recovered in the trap. The percentage recovery of ^{14}C as sodium benzoate was determined by adding carrier benzoic acid to the final bicarbonate solution, acidifying with 6 N hydrochloric acid, separating and recrystallizing from water the benzoic acid crystals thus formed, and measuring the fraction of ^{14}C trapped by the Grignard reagent which was recovered as benzoic acid. Since essentially 100% of the $^{14}CO_2$ was trapped by the Grignard reagent, we conclude that of the radioactivity introduced into the reaction flask, up to 80% could definitely be recovered in the system as benzoic acid.

In preliminary runs we have produced approximately 20–40 mCi of sodium ^{11}C benzoate by the above-noted methods. We expect that this can be readily optimized to produce curie quantities of ^{11}C-labeled sodium benzoate. In the present process, it is possible to produce carrier-free ^{11}C-labeled benzoic acid, but we found it convenient to pass approximately 1 millimole carrier CO_2 through the Grignard reagent to produce a total of approximately 1 millimole of sodium benzoate.

Total elapsed time from addition of acid to the Grignard reagent to preparation of material for administration is 10–20 minutes.

In preliminary experiments with normal dogs it was found that renal visualization began as early as a minute after the intravenous administration of sodium ^{11}C-benzoate. No significant visualization of the liver occurred, suggesting that if hepatic conjugation of the benzoic acid with glucuronic acid occurred, it was very rapid and possibly was accomplished in a single pass of this material through the liver. No localization in tissues other than the kidney was noted. During the initial 10 minutes following the administration of ^{11}C-labeled sodium

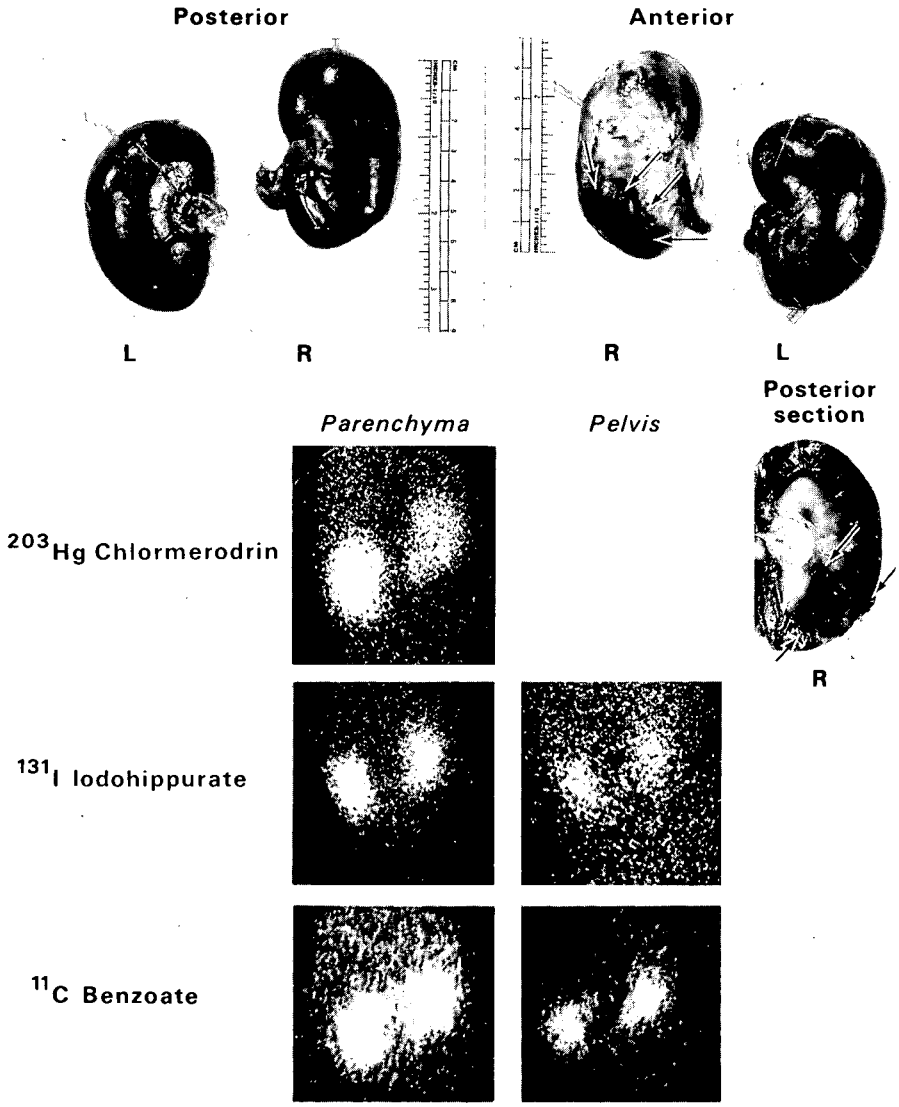

Fig. 2. Photographs, scintiphotos and positron camera pictures of dog kidneys: lesion anterior inferior aspect right kidney. Three days prior to study an electrocautery lesion was produced in the anterior inferior aspect of the right kidney leaving the posterior inferior aspect of the kidney intact. The lesion is shown in the photographs of the kidneys removed subsequent to the in vivo study during post-mortem examination. The sodium ^{11}C-benzoate study was performed 9-10 minutes (parenchyma) and 12-18 minutes (pelvis) after I. V. injection of 500 μCi. The ^{131}I Iodohippurate study was performed 1-5 minutes (parenchyma) and 12-18 minutes (pelvis) after I. V. injection of 100 μCi. The ^{203}Hg chlormerodrin study was performed 20 minutes after I. V. injection of 120 μCi. Each of the scintiphotos or positron camera pictures represent accumulations of 20,000 to 25,000 total counts in the camera field. XBB 691-567

benzoate, positron camera tomograms of the kidneys revealed what appeared to be renal parenchymal visualization, similar to that seen following administration of ^{203}Hg-chlormerodrin. Between 10 and 40 minutes following administration of the ^{11}C-labeled sodium benzoate, positron camera pictures appeared to primarily visualize the renal pelvis area, similar to that seen following the administration of ^{131}I-iodohippurate. Generally, by 40 minutes most of the radioactivity was cleared from the body by the kidneys and was found in the bladder.

Figure 2 demonstrates the results obtained in a dog in whom a lesion was created in the lower pole of the right kidney by use of electrocautery 3 days prior to the administration of sodium ^{11}C-benzoate. As can be noted in Fig. 2, the lesion was anterior and inferior in the lower pole of the right kidney. The lesion, which measured 3/4 in. in its longest dimension, was produced in such a manner that a layer of functioning renal cortex remained along the posterior-inferior border of the right kidney. The ^{203}Hg renal scintillation photo shown in Fig. 2 was obtained approximately 20 min after administration of 120 μCi of ^{203}Hg-chlormerodrin. It can be seen on this scintiphoto that although there appears to be less uptake of ^{203}Hg-chlormerodrin in the right kidney than in the left the general outline of the right kidney is similar to that on the left and is generally within normal limits. A lesion cannot be defined in the lower pole of the right kidney. The scintiphotos of the kidney during the parenchymal and pelvic phases of ^{131}I-iodohippurate excretion by the kidney shown in Fig. 2 were obtained subsequent to administration of 100 μCi of ^{131}I-iodohippurate to the same dog. It is clear that neither during the parenchymal nor the pelvic phase of ^{131}I-iodohippurate excretion was the lesion in the lower pole of the right kidney identified. The positron camera tomograms of the renal parenchyma and pelvis were obtained subsequent to administration of approximately 500 μCi of ^{11}C-benzoate to this same dog. It is clear in the parenchymal phase picture that there is a well-defined defect in the lower pole of the right kidney corresponding to the lesion shown in the photographs in the upper portion of Fig. 2. It can also be noted that the morphology of the renal pelvis is much better defined during the pelvic phase of excretion of the ^{11}C compounds than of the ^{131}I-iodohippurate.

DISCUSSION

This paper reports the first use of ^{11}C incorporated into an organic compound for organ visualization in vivo and the first demonstration of possible usefulness in renal visualization. The short physical half-life of ^{11}C results in delivery of only a small radiation dose to the body tissues in contact with this isotope. In the case of sodium ^{11}C-benzoate its rapid excretion by the kidney further reduces the radiation dose received by the body because of the short biological clearance time. The positron emission of ^{11}C allows for better resolution than that obtained with ^{131}I in iodohippurate or ^{203}Hg in chlormerodrin. The positron emission also allows for tomographic evaluation of the organ of concentration. In the present example of an electrocautery-induced renal lesion in a dog kidney, we note that tomograms of the kidney using sodium ^{11}C-benzoate resulted in clear delineation of the renal lesion, though this was not the case with the use of ^{203}Hg-chlormerodrin or ^{131}I-iodohippurate. In addition, the ^{11}C positron tomograms provided much better morphologic detail of the renal pelvis than that obtained by using a large dose of ^{131}I-iodohippurate.

These results in dogs may differ appreciably from those which may be obtained in humans. In dogs 75% of administered benzoic acid is conjugated with glucuronic acid. Virtually all of the conjugation with glycine to form hippuric acid occurs in the kidneys (8). In man most of the conjugation of benzoic acid is with glycine to form hippuric acid and occurs predominantly in the liver (8). If such hepatic hippuric acid synthesis in man is sufficiently slow ^{11}C-benzoate may be useful for hepatic parenchymal scanning as well as in renal visualization when this material is administered to man.

SUMMARY

^{11}C is a positron-emitting radioisotope with a $t_{1/2}$ of 20.4 min. This short $t_{1/2}$ allows for administration of large quantities of ^{11}C-labeled compounds with minimal radiation dose to the patient, and the positron emission provides for great discrimination in determining its localization in the body. To utilize these virtues, we are developing methods for rapid syntheses of medically useful ^{11}C-labeled compounds. In the present communication we report the use of sodium ^{11}C-benzoate in renal visualization. Deuteron bombardment of a B_2O_3 target $^{10}B(d, n)^{11}C$ yields ^{11}CO and $^{11}CO_2$ liberated from the target by recoil. The ^{11}CO is oxidized to $^{11}CO_2$ in the gas phase and is reacted with phenylmagnesium bromide to form, after acid hydrolysis and extraction with $NaHCO_3$, sodium ^{11}C-benzoate. Yield is 60–80% of ^{11}C produced and trapped by the Grignard reagent, and preparation time is 10–20 minutes. When injected IV in dogs the ^{11}C is rapidly excreted by the kidneys. Positron camera pictures of the kidneys, using this material, demonstrate a sufficiently long parenchymal filling phase (during first 10 min after injection) to allow for tomographic visualization of renal parenchyma, which appears to have advantages for lesion detection over ^{203}Hg-chlormerodrin. Positron camera tomograms taken during the filling phase of the renal pelvis also appear to show greater detail than obtained with ^{131}I-iodohippurate.

ACKNOWLEDGMENTS

The authors acknowledge the efforts of Dr. L. Theard and Dr. D. Herring of the Gulf General Atomics Corp., San Diego, California, for stimulating our interest in this project and Dr. W. G. Myers of the Ohio State University, Columbus, Ohio, for his encouragement and suggestions concerning cyclotron production of ^{11}C. We also wish to acknowledge the technical assistance of G. Armaly, B. Shipley, D. Peterson, R. M. Larimer, H. Harrington, E. F. Dowling, and D. D. Dean of the Lawrence Radiation Laboratory, Berkeley, California.

REFERENCES

1. Myers, W. G.; and W. W. Hunter, Jr.: Radiocarbon-11 for scanning. J. Nucl. Med. 8: 305 (1967).
2. Myers, W. G.; and W. W. Hunter, Jr.: Carbon-11 in bone and lung scanning. IAEA Symposium on Medical Radioisotope Scintigraphy, August 6-15, 1968, Salzburg, Austria. Designated SM-108/155.
3. Glass, H. I.; J. Jacoby; B. Westerman; J. C. Clark; R. N. Arnot; and H. G. Dixon: Placental localization by inhalation of radioactive carbon monoxide. J. Nucl. Med. 9: 468 (1968).
4. Henry, R. J.: Clinical Chemistry, Principles and Techniques. Hoeber Medical Division, Harper and Row, New York, 1964. P. 542.
5. Murray, A.; and D. L. Williams: Organic Syntheses with Isotopes. Part I: Compounds of Isotopic Carbon. Interscience Publishers, Inc., New York, 1958. P. 86.
6. Kamen, M. D.: Short-lived radioactive carbon (^{11}C), Ch. 8, in Radioactive Tracers in Biology, Second Edition. Academic Press, New York, 1951. P. 224-243.
7. Anger, H. O.: Gamma-ray and positron scintillation camera. Nucleonics 21 [10]: 56-59 (1963).
8. Hawk, P. B.; B. L. Oser; and W. H. Summerson: Practical Physiological Chemistry, 13th ed. McGraw-Hill Book Co., Inc., New York, 1954. P. 441, 804.

Synthesis of ^{11}C-Carboxylic Acids and Their Use in Organ Visualization

Meldrum B. Winstead, H. Saul Winchell, Rashid A. Fawwaz and Gery C. Armaly

^{11}C is a positron-emitting radioisotope with a $t_{1/2}$ of 20.4 minutes. This short $t_{1/2}$ allows for administration of large quantities of ^{11}C-labeled compounds with minimal radiation dose, and its positron emission provides for great discrimination in determining its localization in the body. To utilize these virtues, we are developing methods for rapid syntheses of medically useful ^{11}C-labeled compounds. In this paper we report the synthesis and use of ^{11}C aliphatic, aromatic, and heterocyclic carboxylic acids. Deuteron bombardment of a fused B_2O_3 target, $^{10}B(d, n)^{11}C$, yields ^{11}CO and $^{11}CO_2$ liberated from the target by recoil. B_2O_3 was obtained from 20th Century Electronics Ltd., New Addington, Surrey, England, 90% enriched in the ^{10}B isotope. A 20-MeV deuteron beam from the 88-inch cyclotron at the Lawrence Radiation Laboratory was defocused to cover an area approximately 1 in. in diameter at the point at which it hit the target. Beam currents used varied from 5–25 μA. Nitrogen gas containing 0.5% each of carrier gases CO and CO_2 was used to sweep out the mixture of ^{11}CO and $^{11}CO_2$ gases. The ^{11}CO is oxidized to $^{11}CO_2$ in the gas phase by passing the gas stream over CuO at 700°C. The $^{11}CO_2$ is then reacted with approximately 10 mmoles of the appropriate Grignard reagent or organolithium compound to form, after acid hydrolysis and extraction with $NaHCO_3$, the ^{11}C-labeled sodium carboxylate. Yields are generally in the range of 60–80% of ^{11}C produced, and preparation time is approximately 30 minutes. Millicurie quantities of ^{11}C-carboxylic acids have been prepared, and we expect production of curie quantities in the near future. ^{11}C-labeled carboxylic acids are being made and evaluated at the rate of approximately one every 1–2 weeks. Thus far, those carboxylic acids containing a benzene or heterocyclic ring are primarily conjugated in the liver and kidneys and excreted in the kidneys, allowing for renal visualization. The rate of renal excretion was in the order: 1-napthoic acid > benzoic acid > p-chlorobenzoic acid > phenylacetic acid and 3, 4-dimethoxybenzoic acid > 2-thiophenecarboxylic acid. A significant amount of 1-naphthoic acid underwent slow hepatic conjugation and excretion in the bile, allowing for liver and gall-bladder visualization. Tomograms of renal lesions using ^{11}C-benzoic acid in conjunction with the positron camera appeared superior to scintophotos obtained with ^{203}Hg-chlormerodrin and ^{131}I-iodohippurate from the scintillation camera. 1-Naphthoic acid, p-chlorobenzoic acid, and 2-thiophenecarboxylic acid were excluded from the brain and did not concentrate in salivary glands or mucosa of the nasal

Table 1. ^{11}C-carboxylic acids and their temporal distribution in the dog.

Product		Distribution properties
1-Naphthoic acid[a]	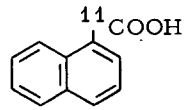	Renal excretion +++++ Bile excretion +
Benzoic acid[b]	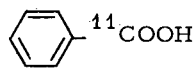	Renal excretion ++++
p-Chlorobenzoic acid[b]	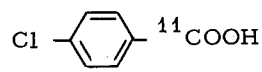	Renal excretion +++
Phenylacetic acid[b]	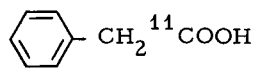	Renal excretion ++
3, 4-Dimethoxybenzoic acid[c]	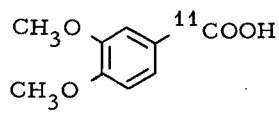	Renal excretion ++
2-Thiophenecarboxylic acid[d]	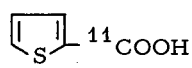	Renal excretion +
Butyric acid[b]	$CH_3CH_2CH_2{}^{11}COOH$	Liver and extracellular fluid (slow clearance)
Pentanoic acid[b]	$CH_3CH_2CH_2CH_2{}^{11}COOH$	Liver and extracellular fluid followed by slow excretion in urine and bile.
Octanoic acid[b]	$CH_3(CH_2)_6{}^{11}COOH$	Liver and extracellular fluid (slow clearance)

a. 1-Naphthoic acid was prepared by carbonating 1-naphthyl lithium, which was prepared from 1-bromonaphthalene and n-butyl lithium by metal-halogen exchange (H. Gilman and F. W. Moore, J. Am. Chem. Soc. 62, 1843 (1940).

b. The ^{11}C-carboxylic acid was prepared by carbonating the appropriate Grignard reagent, which was obtained from either Arapahoe Chemicals, Boulder, Colorado, or Alfa Inorganics, Inc., Beverly, Massachusetts.

c. 3, 4-Dimethoxybenzoic acid was prepared by carbonating 3, 4-dimethoxyphenyl lithium, which was prepared from 4-bromoveratrole and n-butyl lithium by metal-halogen exchange reaction. (M. Calvin, C. Heidelberger, J. C. Reid, B. M. Tolbert, and P. F. Yankwich: Isotopic Carbon, John Wiley and Sons, Inc., New York, 1949. P. 183-184.)

d. 2-Thiophenecarboxylic acid was prepared by carbonating 2-thienylmagnesium bromide, which was prepared from 2-bromothiophene and magnesium turnings in ether solution. (D. A. Shirley: Preparation of Organic Intermediates, John Wiley and Sons, Inc., New York, 1951. P. 282.)

sinuses, suggesting their potential usefulness in brain tumor visualization. ^{11}C-aliphatic acids (butyric, pentanoic, and octanoic acids) were in general slowly metabolized and did not show discrete organ localization. A portion of the ^{11}C-pentanoic acid was excreted in the bile, allowing for gall bladder visualization. These studies demonstrate the usefulness of ^{11}C-labeled compounds for study of in vivo distribution kinetics as well as for organ and tumor visualization.

Table 1 lists the ^{11}C-carboxylic acids prepared thus far and their temporal distribution in the dog.

ACKNOWLEDGMENTS

The authors thank Dianne Peterson, Harry Harrington, Ruth Mary Larimer, J. B. Shrum, Jr., E. F. Dowling, Frank Upham, and Dewey Dean of the Lawrence Radiation Laboratory, Berkeley, California, for their contributions to this study.

Radiation Dosimetry Using Miniature Silicon Diodes

Mudundi R. Raju

Use of miniature silicon diodes (MC 170, MC 459, MC 488B, etc., Microsemiconductor Corporation, 11250 Playa Court, Culver City, California), manufactured for electronic circuit applications, as dosimeters for heavy charged particles has been reported (1, 2). The diodes are operated in short-circuit mode because of relative freedom from temperature effects and no need of bias supply. In addition, the response is proportional to the dose rate over a very wide range of dose rates. The depth-dose distribution of 50-MeV protons and 910-MeV α particles measured with these diodes shows no saturation effects at the Bragg peak position. The depth-dose distribution of ^{60}Co γ rays and 8-MeV electrons as measured by these diodes agrees well with results from the ionization chamber. The sensitivity of these diodes is limited to about 10 rads/min because of their small size and their leakage current. However, they can be used at much lower dose rate if the leakage current of the diodes is balanced.

Trump and Pinkerton[3] also have demonstrated use of the diodes for possible application in an automatic isodose meter, and their results show excellent agreement with ion chambers for the depth-dose distribution of ^{60}Co γ rays and 6- and 20-MeV electrons.

This note provides some information of interest in the use of these diodes as radiation dosimeters.

The input impedance of the current-measuring device should be much lower than that of the diode for measuring short-circuit current. The impedance of the diodes is about 10^8 ohms (1). The input impedance of the electrometer decreases with feedback, and is inversely proportional to the gain of the electrometer. The electrometer used in this investigation is a high-gain (2500) dc amplifier with feedback.

RADIATION DAMAGE The sensitivity of these diodes does not change when they are exposed to a total dose of (a) 2 megarads of 50-kVP X rays at a dose rate of 2500 R/min, (b) 0.2 megarad of 250-kVP X rays at a dose rate of 1500 R/min, or (c) 0.5 megarad of ^{60}Co γ rays at a dose rate of 3000 R/min. However, when they are exposed to beams of either heavy

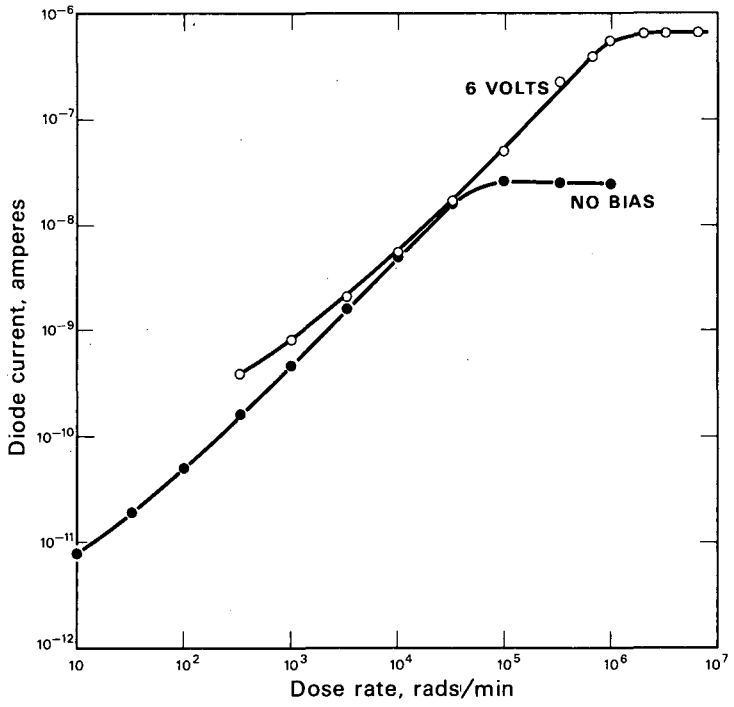

Fig. 1. Current output as a function of dose rate. DBL 6812-5543

charged particles or high-energy electrons, the sensitivity is reduced by a factor of about 2 for a dose of a megarad or so. Hence the diode can be used as a dosimeter for conventional radiation such as 250-kVP X rays and ^{137}Cs and ^{60}Co γ rays without a significant problem caused by radiation damage. For use with intense beams of high-energy electrons and heavy charged particles, however, it can be exposed to a high dose, of the order of a megarad, in order to saturate radiation damage effects. It can thereafter be used as a dosimeter for these radiations, since further small exposure does not significantly change its sensitivity.

DOSE-RATE EFFECTS The response had been found to be independent of dose rate up to an investigated dose rate of 5000 R/min (2). The dose-rate region is extended beyond 1 megarad/min by using 8-MeV electrons from a linac. The diode is first preexposed to a dose of 10 megarads, in order to saturate the damage effects. Its current output as a function of dose rate is shown in Fig. 1. Saturation effects are seen at 30 000 rad/min. A bias of a few volts is adequate for charge collection up to a dose rate of 1 megarad/min. Further increase in voltage does not seem to help any further. The saturation at 1 megarad/min is probably due to radiation damage. The increase in current at lower dose rates when external bias is applied is due to the increase in leakage current. At higher dose rates, at which the leakage current is negligible compared with radiation-induced current, the response of the biased diode follows that of an unbiased one.

TEMPERATURE EFFECTS The diode is exposed to a constant dose rate and its current is measured when the temperature is varied over a range of 5 to 60°C. The average temperature coefficient is found to be +0.4% per 1°C.

DIRECTIONAL RESPONSE The sensitivity of the diode is found to change with the angle of its orientation when exposed to 250-kVP X rays. Depending on the type of diode used, the difference in sensitivity between minimum and maximum response is as much as twofold or threefold. However, when the diode is exposed to high-energy electrons or high-energy heavy charged particles, the sensitivity is found to be independent of the angle of orientation of the diode.

ENERGY RESPONSE The sensitivity of the diode is about the same for ^{60}Co γ rays, 8-MeV electrons, and high-energy X rays, and this is in agreement with the results of Trump and Pinkerton (3). For low-energy X rays, however, the sensitivity is higher because of a higher absorption coefficient for silicon. For example, the sensitivity of the diode is found to be about 2.5 times as high for 250-kVP X rays as for ^{60}Co γ rays for a given exposure.

SUMMARY

Miniature silicon diodes are useful as dosimeters. Response is independent of dose rate, and sensitivity is about the same for ^{60}Co γ rays, 8-MeV electrons, and high-energy X rays.

ACKNOWLEDGMENTS

Part of this work was done at the M. R. C. cyclotron unit at the Hammersmith Hospital, London, and supported by the Medical Research Council, England. It is indeed a pleasure to thank Dr. D. K. Bewley, Professor J. F. Fowler, and Mr. D. D. Vonberg for their encouragement. I thank Mr. Michael Levitt for his assistance during some of the experiments at Berkeley.

REFERENCES AND NOTES

1. Koehler, A. M.: Rad. Res. Suppl. 7: 53 (1967).
2. Raju, M. R.: Phys. Med. Biol. 11: 371 (1966).
3. Trump, M. A.; and A. P. Pinkerton: Phys. Med. Biol. 12: 573 (1967).

Mudundi R. Raju is guest scientist from the Southwest Center for Advanced Studies, Dallas, Texas.

Submitted as "Instrument note" to Phys. Med. Biol.

The Oxygen Effect of π^- Mesons in *Vicia faba*

Mudundi R. Raju, Nabil M. Amer, Madvanath Gnanapurani and Chaim Richman

The oxygen enhancement ratio (OER) for stopping π^- mesons by use of Vicia faba is measured. The dose rate of π^- beam is $\approx$ 30 rads/hr, and the beam has 30% electron and muon contamination. The OER values are respectively 1.35 and 1.5 when beans are exposed at room temperature and at 4°C. The OER is dependent on dose rate when bean roots are exposed at room temperature. The OER of 1.35 for π^- mesons is to be compared with the value of about 2 for conventional radiation such as ^{60}Co γ rays.

The OER when bean roots are exposed at a low temperature such as 4°C is relatively independent of dose rate, and hence the value of 1.5 may be applicable to acute dose rate of π^- mesons. Thus a significant reduction in OER is observed for stopping π^- mesons in spite of the contamination in the beam.

The dose delivered to a medium by a π^--meson beam increases very slowly with increasing depth in the beginning and gives rise to a sharp maximum near the end of the range, as do other heavy charged particles. In addition, when π^- mesons stop in a medium, they are captured by nuclei in the medium, causing the nuclei to explode into short-range and heavily ionizing fragments. Thus the dose delivered near the end of the range is higher than at the entrance. In addition, these heavily ionizing fragments may overcome some of the radioresistance of the anoxic tumor cells. Hence in principle therapeutic application of π^- mesons should be very advantageous. A few workers, including one of the authors (Richman), appreciated this possibility as early as 1952. Detailed calculations by Fowler and Perkins (1) generated heightened interest in the use of π^- mesons for radiotherapy. Their calculations clearly indicate the usefulness of these particles in radiotherapy.

Biophysical experiments have been carried out in this Laboratory for the last 5 years. The 184-inch synchrocyclotron is the most intense source of low-energy π^- mesons available today. Accelerators that will be able to produce intense beams of π mesons (10 to 100 rads per min) are under construction at Los Alamos (New Mexico), Vancouver (British Columbia), and Zürich (Switzerland).

Negative π mesons are always associated with muon and electron contamination. It is quite possible to obtain a pure beam, but at the cost of reducing the π-meson intensity considerably. We therefore used the contaminated beam in our experiments. It has 25% electrons and 10% muons.

Physical measurements indicate that the dose at the peak is about three times as great as at the entrance, with a full width at half maximum of about 5 cm (2-4).

Biological experiments indicate that the RBE at the peak is about 4 for the proliferative capacity of ascites tumor cells (5), 2.5 for polyploidy induction in ascites tumor cells (6), and 2.5 for anaphase abnormalities in Vicia faba root meristem (7).

This paper describes the measurements of oxygen enhancement ratio (OER) for stopping π^- mesons by use of Vicia faba. The OER values obtained with this system are about the same as those obtained with cultured mammalian cells. The Vicia faba system yields OER values of 2.6 and 1.5 for conventional radiations (X rays and γ rays) and 15-MeV neutrons respectively (8, 9).

The depth-dose distribution of the contaminated π^- meson beam used in this experiment is shown in Fig. 1. This distribution is measured by using a small tissue-equivalent ionization chamber filled with air (0.75 ml). The dose at the peak is 1.7 times that at the entrance. The width of this curve is unusually small for this dose ratio. This is probably due to the beam optics in this setup. The biological effect at the entrance is quite similar to that of conventional radiation (6). The region of interest is at the peak. The horizontal and vertical profiles at the peak position, as measured with a small tissue-equivalent ionization chamber, are shown in Fig. 2.

The beam is monitored by using an ion chamber, larger than the beam, placed before the absorber used to obtain the peak. The dose at the peak is measured by using a ^{60}Co-calibrated small tissue-equivalent ionization chamber (0.75 ml). The dose at the peak is measured by this small ionization chamber for a fixed amount of charge liberated in the monitor ion chamber. The total dose at the peak is then estimated from the measured total charge of the monitor during a given exposure.

The biological technique we used is quite similar to the one used by previous workers (8, 10). The seeds used are Sutton Longpod obtained from England. They are allowed to germinate for 3 days at a temperature of about 19°C in a water tank with a constant flow of water and air. Nearly 80% of the seeds sprout. The sprouted seeds are transferred to an enclosed box filled with moist vermiculite, and are kept for 3 to 4 days. The healthy bean roots are individually numbered, and their lengths are measured from a reference mark made with india ink on the hypocotyl. They are then transferred to a water tank kept at about 19°C, with a constant flow of water and aeration. After 2 to 3 days in water the roots grow to a total length of about 10 to 13 cm. The bean roots with either subnormal or abnormal growth are discarded. The number of healthy-looking bean roots with more or less similar growth is about 30 to 40% of the number of seeds used for germination.

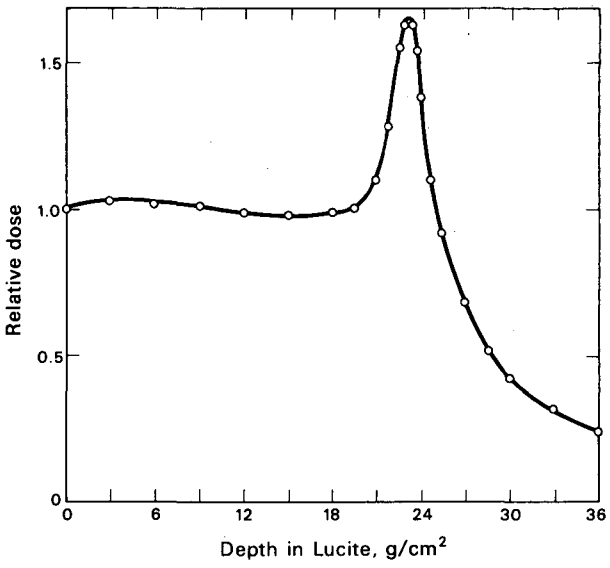

Fig. 1. Depth dose of π^- beam.
DBL 687-5324

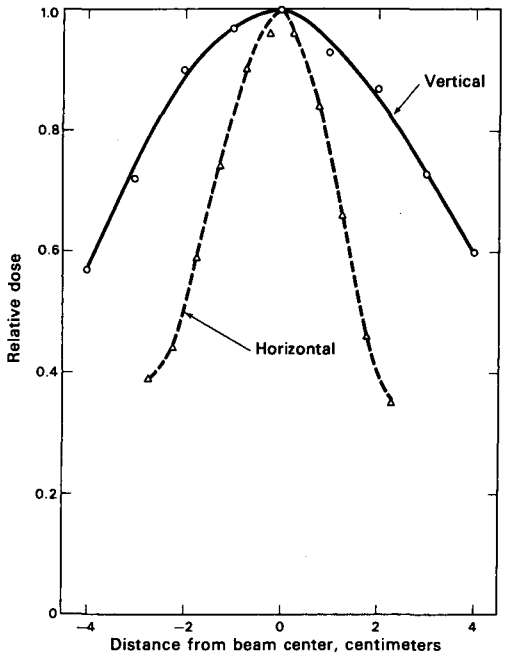

Fig. 2. Beam profiles at the peak of depth-dose distribution.
DBL 687-5325

The beans are packed in a Lucite box in such a way that most of the bean tips are in the central part of the beam and the variation in dose received by various root tips is no more than 15%. Sometimes a few tips could not be packed in the central part of the beam. Such beans are not included in the data. The box is provided with a tube in the bottom through which cold water can be circulated. Thus bean roots can be maintained at lower temperature during exposure, if necessary. The box is also provided with another tube with small holes through which either air or nitrogen is bubled to keep the beans in either an oxygenated or anoxic state. The box is also provided with a 1-mil (0.001-in.) Mylar window, and the beans are packed very close to it. Two bean boxes with their windows facing each other are placed

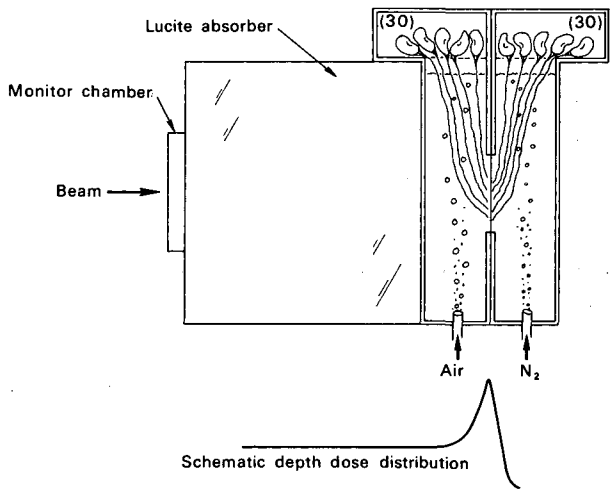

Fig. 3. Experimental setup during exposure.

DBL 6812-5558

at the peak position obtained by interposing the necessary thickness of the Lucite absorber in front of the boxes. Figure 3 shows the experimental arrangement during exposure. The beans in both the boxes are within about 5 mm of one another. Air is bubbled through one box and nitrogen is bubbled through the other. The nitrogen-bubbled box is sealed on the top. The amount of oxygen present in the nitrogen-bubbled bean box is analyzed by passing the exit gas through a Hersch cell, and it is kept lower than 25 parts per million during exposure. Our system was checked by measuring the OER for acute level of ^{60}Co γ radiation at room temperature as well as at 3°C. Our results agree with those of Hall and Cavanagh (10).

Five pairs of irradiation boxes with 30 beans in each are exposed at the peak to different doses in the range 50 to 150 rads at room temperature. The longest exposure took about 6 hr. We also have a few groups of control beans that are treated in the same way as the others but without radiation exposure. There is no detectable difference in the 10-day growth for the control beans in oxygen and in nitrogen for a 6-hour period. The length of the roots is measured and they are transferred to a water tank after the radiation exposure. The water tank is aerated and maintained at 19 ± 0.5 °C. The length of the bean roots is measured once every 24 hr for a period of 10 days. There was fungus infection on the cotyledons of some of the beans during the latter part of the 10-day period. However, such infection did not significantly affect the growth of the beans. At the end of the 10-day period about 27 roots in each group appeared to be morphologically normal, and these were used for growth measurements.

The average 10-day growth for each group of bean roots is expressed as percent fraction of the control group. The percent 10-day growth for the groups of bean roots exposed in air and in nitrogen is plotted as a function of dose and is shown in Fig. 4. Regression lines are drawn through the experimental points by the method of least squares. The 95% confidence limits were calculated for both N_2 and air regression lines. The highest OER value was ob-

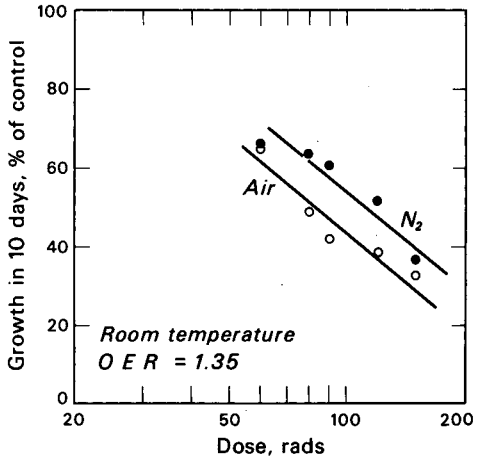

Fig. 4. The 10-day growth plotted as a function of dose at the peak of π^- beam.
DBL 6812-5554

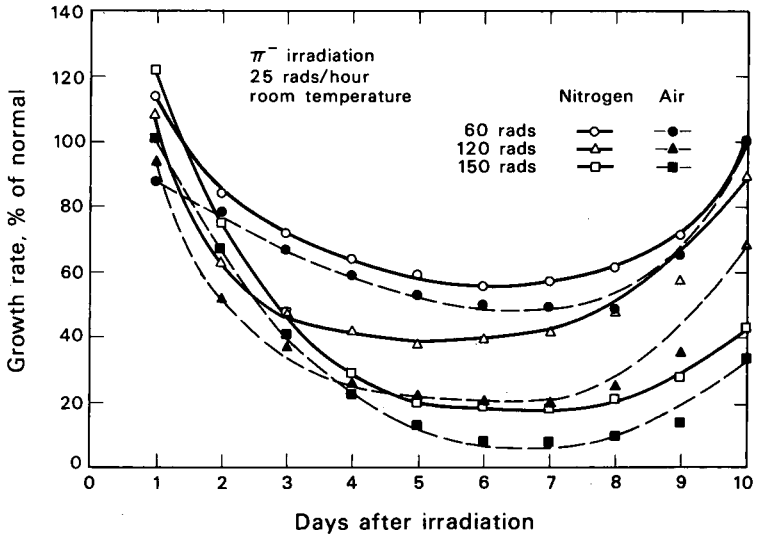

Fig. 5. Daily growth rate plotted as a function of days after exposure.
DBL 687-5340

tained by taking the ratio of doses at the maximum value for nitrogen to the minimum value for air at a given percent growth. The minimum value was obtained by taking the ratio of doses from the lowest nitrogen value to the highest for air. The OER may be calculated to be 1.35, with 95% confidence limits of 1.1 and 1.8.

The daily growth rate, expressed as percent of normal growth rate, for different groups of bean roots exposed to different doses in oxygen and nitrogen atmospheres, plotted as a function of days after exposure, is shown in Fig. 5. As can be seen from the figure, the growth rate is reduced after the radiation exposure, reaching a minimum about the 6th day, and then increases again. One can also calculate the OER by constructing a plot of minimum growth rate versus dose. Such a plot is shown in Fig. 6. The OER calculated in this fashion yields the same value of 1.35 as obtained from 10-day growth. The 95% confidence limits are 1.2 and 1.6. It may be noted from the figures that the minimum growth rate is about the same for 120 rads in air and 150 rads in nitrogen, and hence the OER is about 1.3.

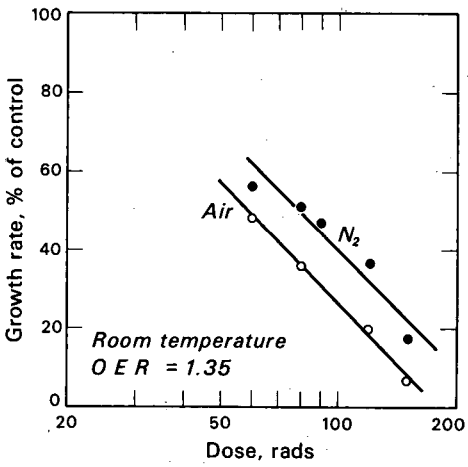

Fig. 6. Minimum growth rate plotted as a function of dose at the peak of π^- beam.
DBL 6812-5555

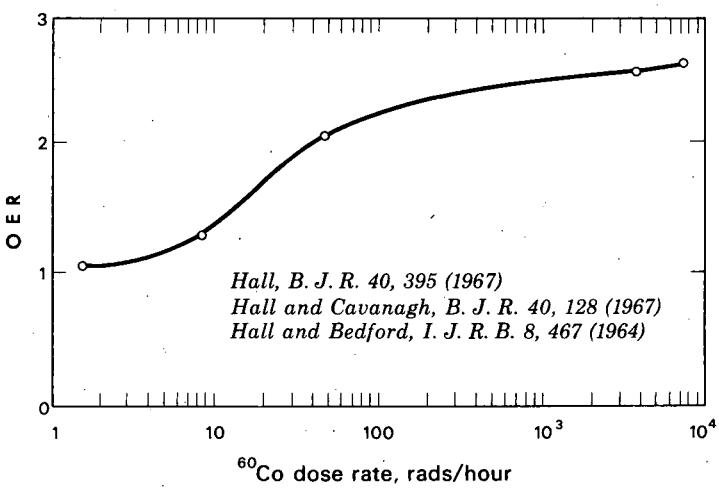

Fig. 7. Variation of OER as a function of dose rate for ^{60}Co (γ rays).
DBL 687-5327

Our preliminary results on OER, using ^{60}Co γ rays for acute and chronic exposures, agree with those of Hall and Cavanagh (10). The RBE for π^- beam at this dose rate of $\approx$0.5 rad/min, when compared with our preliminary results of ^{60}Co γ rays at a dose rate of 1 rad per min, is 3.

A plot of variation of OER with dose rate for ^{60}Co, made from the results of Hall and his collaborators (10-12), is shown in Fig. 7. The OER for ^{60}Co at a dose rate that is used in the π^- experiment is about 1.8. It may be more meaningful to compare the OER of a π^- beam with ^{60}Co at a higher dose rate, such as $\approx$90 rad/hr, taking the RBE value into consideration. The OER for $\approx$90-rad/hr ^{60}Co γ radiations is 2.2. The OER of 1.35 for the π beam has to be compared with either 1.8 or 2.2 for ^{60}Co instead of the value of 2.7 for acute irradiation.

It is of interest to extrapolate the OER measured at this available dose rate of $\approx$0.5 rad per min to the OER at acute exposure of π^- mesons. The aerated dose-response curve varies with dose rate, whereas the hypoxic dose-response curve is virtually independent of dose rate

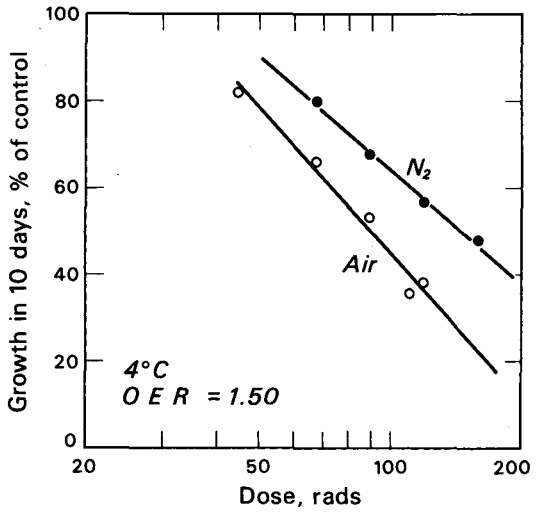

Fig. 8. The 10-day growth plotted as a function of dose at the peak of π^- beam.
DBL 6812-5556

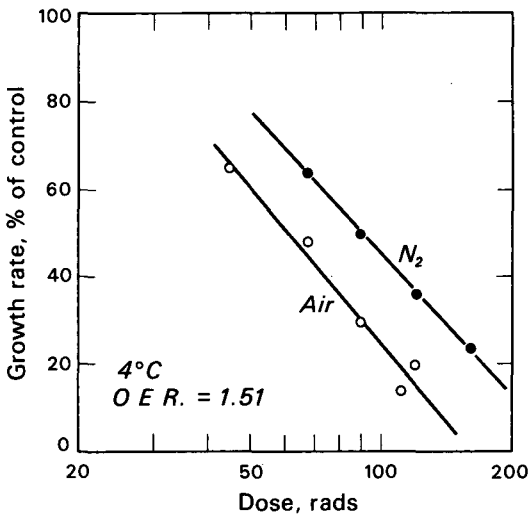

Fig. 9. Minimum growth rate plotted as a function of dose at the peak of π^- beam.
DBL 6812-5557

at room temperature. Consequently the OER is reduced for low-dose-rate exposures at room temperature. However, the results of Hall and Cavanagh (10) indicate that when the beans are exposed at a dose rate of 46 rad/hr of ^{60}Co radiation at 3°C, the dose-rate effect is small in aerated conditions, probably due to slower repair of sublethal damage at this temperature. Hence the OER measured at 3°C at a dose rate of 46 rad/hr is found to be about the same as for acute γ irradiation at room temperature. The dose rate of 20 to 30 rad/hr of π^- mesons is equivalent to about 50 rad/hr of ^{60}Co radiation if the RBE of π mesons is taken into consideration. Then the OER measured at 3°C for π^- mesons with the presently available dose rate of 20 to 30 rad/hr may be about the same as OER for acute π irradiation. With this in mind, we also repeated the experiment at lower temperature.

Because of some problems encountered with the cooling units, the temperature could be maintained at about 4°C instead of 3°C. The procedure adopted is quite similar to that of Hall and Cavanagh (10). Figure 8 shows the results of the experiment at 4°C for 10-day growth. Regression lines were fitted for the experimental points. The calculated OER is 1.5, with 95% confidence limits of 1.4 and 1.6. Figure 9 shows the results for minimum growth rate. The calculated OER is 1.51, with 95% confidence limits of 1.3 and 1.7. This measured OER value of 1.5 at this dose rate of 20 to 30 rad/hr may be applicable to the acute π^- irradiation.

Experiments on ^{60}Co γ radiation at chronic level, similar to those by Hall and Cavanagh, are in progress.

We also exposed groups of bean roots to the π^- meson beam at different doses in aerated and hypoxic conditions. Permanent slides were made at different fixation times to study chromatid aberrations. The scoring of the slides is in progress and the results will be reported later.

In conclusion, our findings show a significant reduction in OER for stopping π^- mesons in spite of contamination in the beam. The OER should be lower for a pure beam.

ACKNOWLEDGMENTS

It is a pleasure to express our thanks to Dr. John H. Lawrence and Dr. C. A. Tobias for their great interest and encouragement.

We want to thank Dr. Stanley B. Curtis for his help during the setting up of the experiment and Mr. U. Madhvanath for his help in the growth measurements.

The Cyclotron crew under the direction of Mr. James Vale was most helpful, not only in the operation of the machine but also with many problems of setting up the experiment.

This work was done with the support of the U. S. Atomic Energy Commission, the American Cancer Society, the Office of U. S. Naval Research, and the National Aeronautics and Space Administration.

REFERENCES AND NOTES

1. Fowler, P. H.; and D. H. Perkins: Nature 189: 524 (1961).
2. Richman, C.; H. Aceto; M. R. Raju; and B. Schwartz: Am. J. Roentg. Rad. Therapy Nucl. Med. 96: 777 (1966).
3. Raju, M. R.; C. Richman; and S. B. Curtis: in Proceedings of the 1st International Symposium on the Biological Interpretation of Dose from Accelerator Produced Radiation, held at Lawrence Radiation Laboratory, Berkeley, California, 1967. Conf.-670305. P. 349.
4. Curtis, S. B.; and M. R. Raju: Rad. Res. 34: 239 (1968).
5. Feola, J. M.; C. Richman; M. R. Raju; S. B. Curtis; and J. H. Lawrence: Rad. Res. 34: 70 (1968).
6. Loughman, W. D.; J. M. Feola; M. R. Raju; and H. S. Winchell: Rad. Res. 34: 56 (1968).
7. Richman, S. P.; C. Richman; M. R. Raju; and B. Schwartz: Rad. Res. Suppl. 7: 182 (1967).
8. Read, J.: Brit. J. Radiol. 25: 89 (1952).
9. Neary, G. J.; and J. R. K. Savage: Nature 204: 197 (1964).
10. Hall, E. J.; and J. Cavanagh: Brit. J. Radiol. 40: 128 (1967).
11. Hall, E. J.: Brit. J. Radiol. 40: 395 (1967).
12. Hall, E. J.; and J. S. Bedford: Intern. J. Rad. Biol. 8: 467 (1964).

The authors are associated with the Southwest Center for Advanced Studies, Dallas, Texas.

This paper is Lawrence Radiation Laboratory Report UCRL-18644, and has been submitted to Radiation Research.

A Method to Determine the Acute Radiation Response of Human Cells to π Mesons

H. John Burki, Gerrit W. Barendsen, Mudundi R. Raju, Nabil M. Amer and Stanley B. Curtis

It is now widely known that π mesons possess rather unique properties that may be useful in the future for radiation therapy (1, 2). We have recently used human cells in vitro (T-1 cells) to determine the relative biological effectiveness and oxygen-enhancement ratio for π mesons (3). These experiments were done under unusual radiobiological constraints, since the dose rate available was low (between 10 and 20 rads/hr) and the beam itself was not a pure beam of π mesons (25% electrons and 10% muons). Thus, recovery was expected to occur from the low-LET components of this mixed beam, while recovery from the high-LET components would not be expected to take place. In addition, cells were exposed at room temperature, so that the growth rate during radiation was reduced, thus inducing a parasynchronous distribution in the culture according to cell age. These difficulties complicate an interpretation of the biological effects of π mesons in terms of conventional survival curves.

We reasoned that if we could freeze cells, and thus suspend biological function, we could simulate the survival curve of human cells to an acute exposure of π mesons if the only important parameter was the integral dose delivered to the cells. Thus, with the dose rate that was currently available we might predict some of the results of a π-meson beam with a much higher dose rate.

MATERIALS AND METHODS

A heteroploid cell line of human kidney origin (4) was used in these experiments. The media and other characteristics of this cell line have been described extensively (5,6). The percent survival after treatments was determined as in previous experiments (5, 6).

The cells were frozen slowly (7, 8) in a 3% dimethylsulfoxide media solution (v/v), using a Linde slow-freeze apparatus equipped with an automatic temperature-recording device.

In frozen-cell control experiments the cells were exposed at -196°C (liquid nitrogen temperature) to γ rays from a ^{137}Cs source. The dose rate was determined by using small dosimeters in a rubber container submerged in an absolute ethyl alcohol bath in the position of the

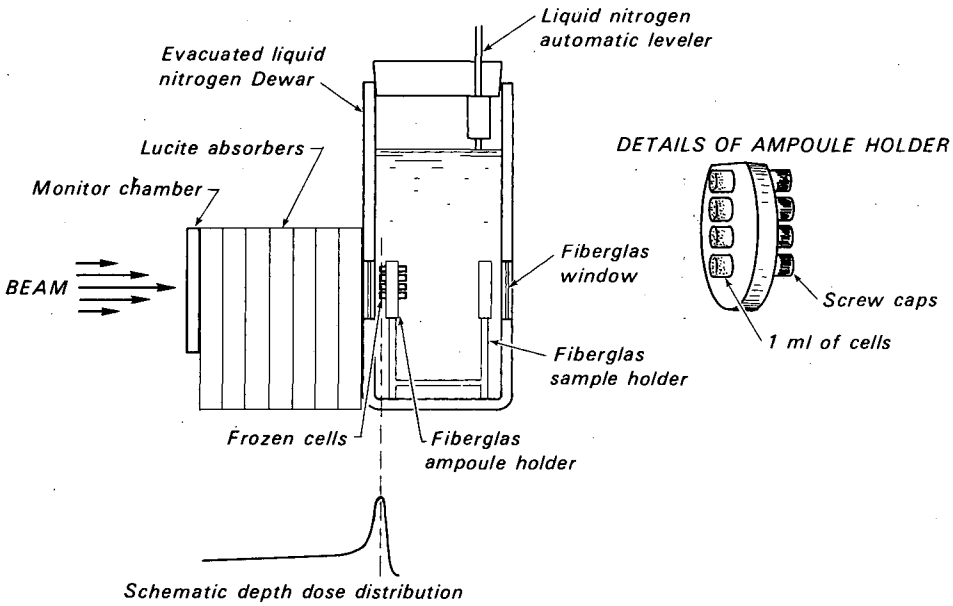

Fig. 1. DBL 694-4676

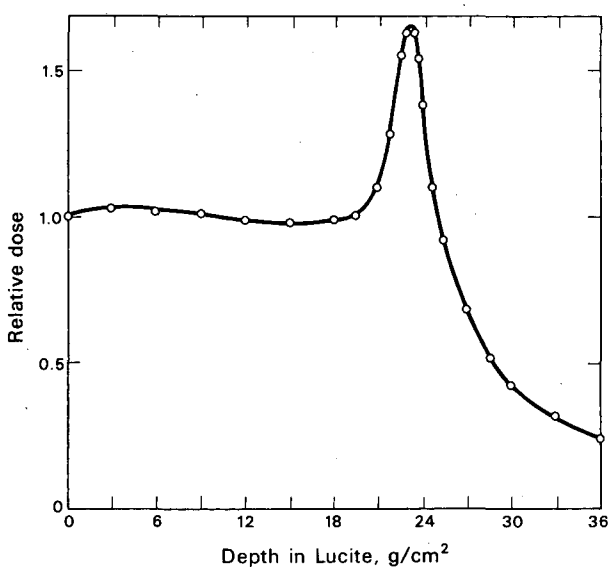

Fig. 2. DBL 687-5324

samples. Since the density of ethyl alcohol is the same as liquid nitrogen, the dose rate was measured with the correct allowance for absorption in the liquid surrounding the cells during exposure.

The experimental setup for exposure of the cells to the π-meson beam is shown in Fig. 1. The cells were exposed in small glass screw-cap ampoules. The peak in the pion depth-dose curve was adjusted to correspond to the position of the cells by using a suitable thickness of absorber. The depth-dose distribution for π mesons in Lucite is given in Fig. 2.

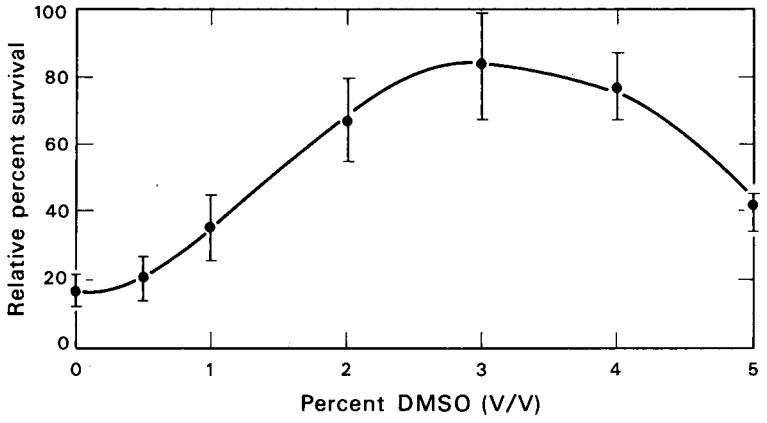

Fig. 3.
DBL 694-4675

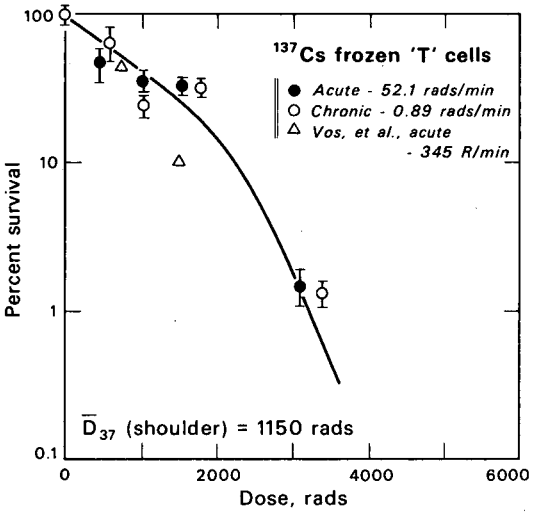

Fig. 4.
DBL 687-5342

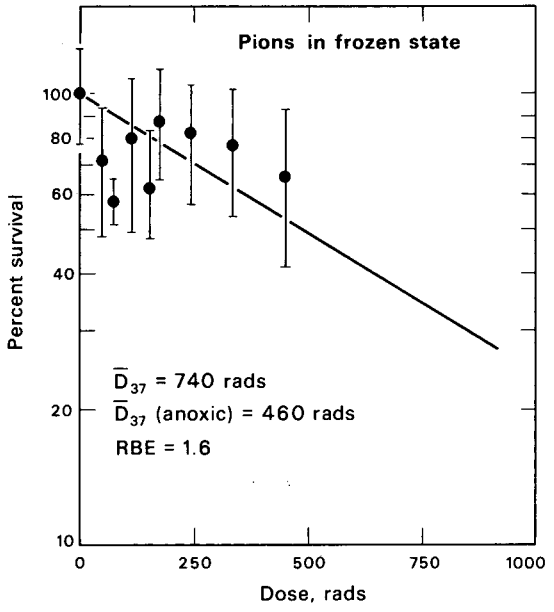

Fig. 5.
DBL 687-5341

RESULTS

The determination of the optimum freezing conditions in terms of the concentration of dimethylsulfoxide used is given in Fig. 3. It is expected that there will be little loss of viability with storage time, since this has been found with other mammalian cell lines (7). In this experiment storage time in liquid nitrogen did not appear to affect cell viability.

In preliminary experiments with L5178Y mouse leukemic cells it was found that when cells were frozen a dose-rate effect was not readily apparent (9). The results obtained with T-1 cells are shown in Fig. 4. Our results are not significantly different from the results of Vos (8). The survival curve of cells irradiated at 52 rads/min and 0.89 rad/min appear to be very similar. The D_{37} of the shoulder region of the curve is 1150 rads.

Due to limitations on the hours of exposure at the cyclotron and the low dose rate available, the maximum dose of π mesons was 450 rads. The survival of frozen cells as a function of the dose received from the π-meson beam is given in Fig. 5.

DISCUSSION

The results obtained by the technique of exposing the cells at -196°C show that quantitative results may be obtained by this method. However, the data are not yet sufficiently extensive to allow derivation of the relative biological effectiveness of the π mesons with reasonable accuracy. Nevertheless it is clear that there is no dose-rate effect in the responses of cells exposed to radiation at -196°C, and further experiments with the currently available π-meson beam may be expected to yield the survival-curve parameters of mammalian cells exposed to high dose rates. There is at present no other reliable method of obtaining such data for high doses without dose-rate effects and proliferation of cells, which interfere with interpretation of the results. It should be pointed out, however, that interpretation of the data obtained with cells exposed to radiation at -196°C also involves some uncertainties. For example, the DMSO used as freezing-protection solvent acts, also, as a protector against the effects of ionizing radiation, with a dose-modifying factor for X rays equal to 1.6. However, the equivalent factor for π mesons is not known.

Comparing data from Figs. 4 and 5, one might conclude that the RBE for π mesons is about 1.6. This value is rather low when compared with the results obtained for π mesons on cells irradiated at room temperature (3), which indicate an RBE of about 2. The value of 1.6, therefore, must certainly be considered as tentative.

Several improvements may be suggested for future studies in π mesons which frozen cells are exposed. One may freeze the cells by using a freezing solvent that is not also a radioprotective compound. Such a compound has been found by Vos (10). This compound is pyridine-N-oxide.

Another improvement is the use of higher doses so that a more complete survival curve may be determined.

SUMMARY

Human cells in culture were exposed to γ radiation in the frozen state in liquid nitrogen. The survival curve did not change, although the dose rate varied from 0.89 rad/min to 52.1 rads/min. Since, under these conditions, the effects of dose rate are eliminated, one may simulate the effects of a π-meson beam acute exposure, using the beam currently available that has a dose rate of 30 rads/hr. One preliminary experiment indicated a pion RBE of 1.6. Improved experiments of this type may allow determination of the complete parameters of the acute exposure survival curve of human cells after π-meson exposure.

ACKNOWLEDGMENTS

The authors thank Dr. C. Richman and Dr. C. A. Tobias for facilitating the group effort which the above work represents. The technical support of Mrs. Boerke as well as the special assistance of Mrs. W. Jackson is greatly appreciated.

This research was jointly supported by the U. S. Atomic Energy Commission and the National Aeronautics and Space Administration.

REFERENCES

1. Richman, S. P.; C. Richman; M. R. Raju; and B. Schwartz: Studies of Vicia faba root meristems irradiated with a π^- beam. Radiation Res. Supplement 7: 182 (1967).
2. Feola, J. M.; C. Richman; M. R. Raju; and S. B. Curtis; and J. H. Lawrence: Effect of negative pions on the proliferative capacity of ascites tumour cells (lymphoma) in vivo. Radiation Res. 34: 70 (1968).
3. Barendsen, G. W.; J. Burki; M. R. Raju; and S. B. Curtis: manuscript in preparation.
4. van der Veen, J.; L. Bots; and A. Mes: Establishment of two human cell strains from kidney and reticulosarcoma of the lung. Arch. Virus Forsch. 8: 230 (1958).
5. Todd, P. W.: Reversible and irreversible effects of ionizing radiations on the reproductive integrity of mammalian cells cultured in vitro (Thesis). UCRL-11614, 1964.
6. Barendsen, G. W.; H. Walter; J. F. Fowler; and D. K. Beweley: Effects of different ionizing radiations on human cells in tissue culture. III. Experiments with cyclotron-accelerated alpha particles and deuterons. Radiation Res. 18: 106 (1963).
7. Burki, H. J.; and S. Okada: Freezing, Storage, and Thawing of Mouse Leukemic Cells. L5178Y, In Culture, PSEBM 12y, 794 (1968).
8. Vos, O.; and M. C. A. C. Kaalen: Protection of tissue culture cells against ionizing radiation. II. The activity of hypoxia, dimethyl sulphoxide, dimethyl sulphone, glycerol, and cysteamine at room temperature and at -196°C. Intern. J. Rad. Biol. 5: 609 (1962).
9. Burki, H. J.; and N. Amer: unpublished observations on L5178Y cells.
10. Vos, O.; M. C. A. C. Kaalen; and L. Budke: Radiation protection by a number of agents preventing freezing damage. Intern. J. Rad. Biol. 9: 133 (1964).

The RBE of Negative Pions in 2-Day-Old Ascites Tumors

Jose M. Feola , Mudundi R. Raju, Chaim Richman and John H. Lawrence

Previous work by Feola et al. (1) and Loughman et al. (2) showed a relative biological effectiveness (RBE) at the Bragg peak region for negative pions ranging from 2.5 to 5.4 times as great as biological effects produced by ^{60}Co γ rays. The differences in RBE were probably due to the different parameters chosen to estimate it, namely, polyploidy induction and proliferative capacity.

The potential importance of negative pions in future cancer therapy motivated us to do as many experiments as feasible under present conditions of irradiation at the 184-inch synchrocyclotron at Berkeley. In this series of experiments we tried to obtain more information about the oxygen enhancement ratio (OER) as well as the RBE.

MATERIALS AND METHODS

In our previous experiments we used 5-day-old ascites tumors, which were irradiated for 40 hours; at the end of the experiment these tumors were then almost 7 days old. Measurements of the partial pressures of oxygen (p_{O_2}) in vivo had shown us that 5-day-old tumors are hypoxic, and, in most cases, anoxic; 2- and 3-day-old tumors instead have enough oxygen present to be considered well oxygenated. The inoculum in those experiments was 10^6 cells. Also with an inoculum of 10^7 cells, 2- and 3-day-old tumors still have enough oxygen present to be considered well oxygenated. We decided to use 2-day-old tumors at the beginning of the irradiation, with the idea of gaining some information about the OER, and also to have a new estimate of the RBE. The base line for this purpose was chosen to be ^{60}Co γ rays, at a comparable dose rate, selected according to our previous determination. In order to see the differences between survival at these low dose rates and with acute exposures, experiments were carried out with higher dose rates of ^{60}Co γ rays and ^{4}He ions.

The assay and end point were the same as previously described (1), namely, the in vivo irradiation of ascites tumors, and the test for tumor-forming ability of the cells after injection into normal mice.

The dose rate of the π^--meson beam was increased by focusing it to give 30 rads/hr over a useful cylindrical volume of 2.5 cm in diameter by 5.0 cm in height. Only one mouse could be irradiated at a time, and irradiation time limitations made it possible to obtain experimental points at only three doses. See Fig. 1.

The π^- meson beam had a contamination of 25% electrons and 10% muons. The depth-dose distribution of this contaminated beam was measured by using a small tissue-equivalent ionization chamber filled with air (0.75 ml). The dose at peak was 1.7 times that at the plateau. The cylindrical holder (Lucite, 1.5 mm thick, with holes for ventilation) was placed at the peak position after the horizontal and vertical profiles had been determined with a small tissue-equivalent ionization chamber (3). The variation in dose received by the tumors was estimated to be no more than 20%. The holder was rotated at 10 rpm during irradiation.

LAF_1 female mice (Jackson Laboratory, Bar Harbor, Maine) were injected intraperitoneally with 10^7 lymphoma cells (our designation, L-2) 2 days prior to irradiation time; they were placed in the holder and irradiated, one at a time, for 3, 4, and 6 hours. Neither food nor water was given during irradiation. Control experiments were carried out similarly, except for the ^{60}Co γ-ray exposures, for which we used different holders in order to have four animals per dose; the mice were confined in a similar enclosure, but they were not rotated.

Control and irradiated animals were sacrificed with ether, cells were withdrawn and counted with the hemocytometer, and fivefold dilutions were prepared for serial injection into LAF_1 female mice, 12 to 16 weeks old, and weighing 20 ± 3 g. Ten animals were used for each dilution, and five dilutions used for each group. The tumor "take" was evaluated at the end of 8 weeks, and the TD_{50} (the number of cells necessary to produce tumors in 50% of the mice) was estimated by Litchfield and Wilcoxon's method (4). This method and the use of the TD_{50} as an end point have been discussed most recently by Elkind and Whitmore (5), Hewitt et al. (6), and Kallman (7). The ratios of the TD_{50} for the control group to the TD_{50}'s obtained for each irradiated group gave the surviving fractions with which the survival curve was drawn. Errors were propagated according to Ku (8). Curve fitting was done by eye, and the asymmetrical 95% confidence interval obtained by Litchfield and Wilcoxon's method was divided by 4 on both sides of the TD_{50} value (9), and the resulting reduced intervals were used as an estimate of the standard deviation. The assumption was made that the asymmetry was due to the fivefold dilutions, and not to a nonnormal distribution of errors (6, 9). The mean lethal dose, D_0, the dose required to reduce survival from 1 to 0.37 in the exponential region of survival curves, was then estimated from the graphs, as well as the standard deviation. The RBE was estimated on the basis of 0.1 survival.

Survival after ^{60}Co γ-ray exposure was compared by using a dose rate of 150 rads/hr, based on a rounded value of 5.0 for the RBE; mice carrying 2-day-old tumors were then irradiated for the same length of time as with the pion beam, except for the 1000- and 1500-rad points, for which we used a dose rate of 500 rads/hr. In all our control experiments we irradiated four mice per dose, pooled the cells after sacrifice, and then proceeded with the dilutions and injections as described before.

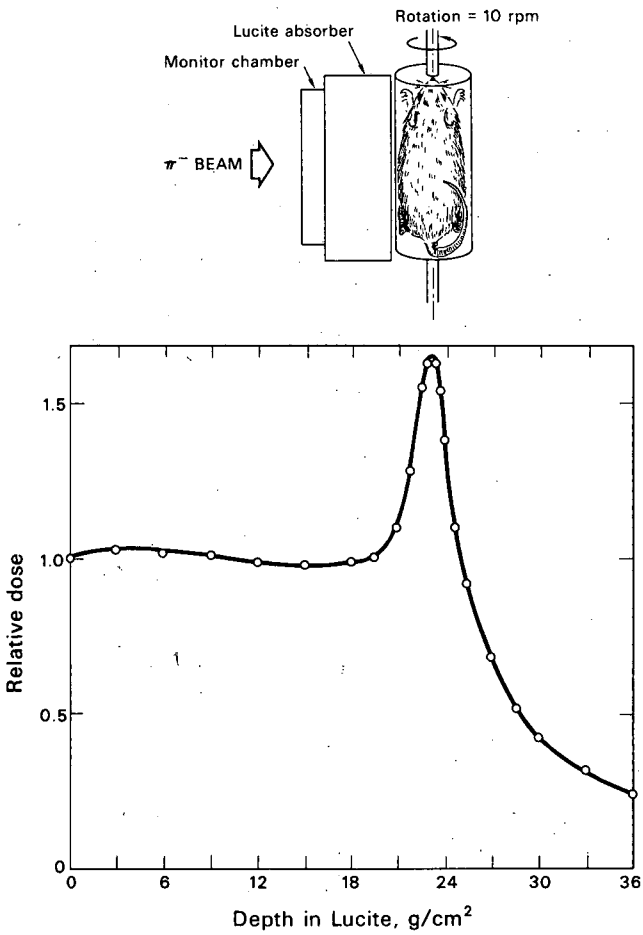

Fig. 1. Depth dose of π^- beam and schematic setup for exposures of mice carrying 2-day-old ascites tumors.
DBL 687-5324 and DBL 695-4677

Acute exposures with ^{60}Co γ rays were made at a dose rate of 45 rads/min. Roentgens were converted to rads by use of a factor 0.96 (10, Table IV. 1).

Acute exposures with 910-MeV ^4He ions were made at the 184-inch synchrocyclotron; in this case the mice were enclosed in the same holder as in the pion experiment, and irradiated one at a time. The average and standard deviation for the dose rate were 274 ± 48 rads/min.

The partial pressure of oxygen in vivo was measured with a Beckman p_{O_2} microelectrode. The microelectrode was inserted into the peritoneal cavity of mice carrying tumors of the same age as the irradiated ones, by means of an 18-gauge hollow needle. The microelectrode was calibrated with mixtures of oxygen and nitrogen, and the calibration was linear from 21% down to 0.25% oxygen, the minimum concentration we could read on the maximum-sensitivity scale of the instrument. This is in the region of interest, since a sharp rise in radiosensitivity takes place for oxygen concentrations in the range 0.2 to 0.6% (11). To measure lower concentrations of oxygen, a macroelectrode mounted on a cuvette with a constant-temperature sample and electrode holder was used. Normal mice and mice carrying from 1-day-old to 8-day-old

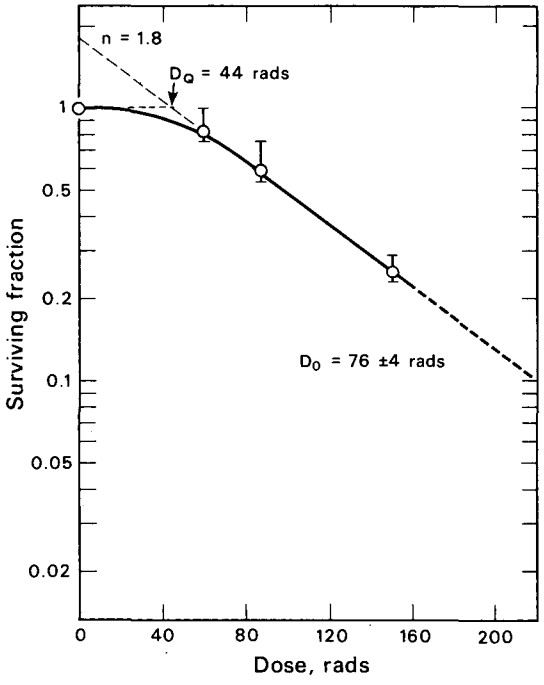

Fig. 2. Survival of lymphoma ascites tumor cells after irradiation with negative pions in the Bragg peak as shown in Fig. 1. The dose rate was 30 rads/hr.

DBL 695-4681

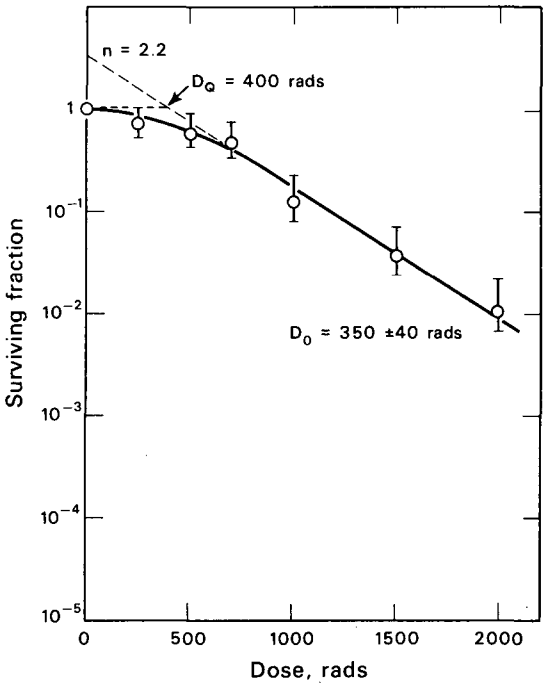

Fig. 3. Survival of lymphoma ascites tumor cells irradiated in vivo with ^{60}Co γ rays at a dose rate of 150 rads/hr. The two highest doses were obtained at a dose rate of 500 rads/hr.

DBL 695-4680

lymphoma ascites tumors have been measured; 20 mice per point were used, and all measurements graphically recorded. For the purposes of this report we give only the values obtained for 2-day-old tumors (10^7 cells inoculum) and for 6-day-old tumors (10^6 cells inoculum).

RESULTS AND DISCUSSION

Results have been summarized in Table 1, along with the results obtained in our previous report (1).

Figure 2 shows the survival curve for the negative pions at the Bragg peak. Although it may seem redundant, we have indicated the value of the extrapolation number as well as the value of the quasi-threshold dose, D_Q, in all figures. In order to reach 0.1 level of survival we have prolonged the line beyond experimental values, with the reasonable assumption that exponential survival would follow the three experimental points that fitted a straight line.

The small shoulder in this survival curve (D_Q = 44 rads) may be due to the low-LET components of the beam. The shoulder is much broader in the ^{60}Co γ-ray survival curve (Fig. 3, D_Q = 400 rads); this curve was obtained at a dose rate of 150 rads/hr, except the two highest doses, for which we used 500 rads/hr in order to keep the experiment within the same time limits as the pion experiment. The extrapolation number (n = 2.2) is not significantly different from the value obtained with π^- mesons (n = 1.8); D_Q, instead, is about 10 times as large, indicating faster recovery when irradiation is done with γ rays.

Table 1. Summary of results obtained on the survival of lymphoma ascites tumor cells after irradiation with different ionizing radiations.

Experiment No. and date	Radiation source and dose rate	0.1 Survival (rads)	RBE	Survival curve characteristics	Observations
		Two-day-old lymphoma ascites tumors			
22 6-27-68	π^- Bragg peak 30 rads/hr	220 (extended line intercept)	5.4 ± 0.6	$D_0 = 76 \pm 4$ rads $m = 1.8$ $D_Q = 44$ rads	
25-43 7-18-68 11-26-68	^{60}Co γ-rays 150-500 rads/hr	1180	$\equiv 1.0$	$D_0 = 350 \pm 40$ rads $n = 2.2$ $D_Q = 400$ rads	Dose rates chosen according to previously estimated RBE.
30 8-14-68	^{60}Co γ-rays 45 rads/min	600		$D_0 = 220 \pm 30$ rads $n = 1.5$ $D_Q = 80$ rads	Experiment done to see difference between acute irradiation and low dose rate.
24 7-15-68	^{4}He ions; 910 MeV (184-inch synchrocyclotron) 274 ± 48 rads/min	500		$D_0 = 210 \pm 40$ rads $n = 1.0$ (?)	Ibid.
		Five-day-old lymphoma ascites tumors			
17 3-18-66	π^- Bragg peak 5.0 rads/hr	150	5.4 ± 1.8	$D_0 = 65 \pm 15$ rads $n = 1$	Radiation Res. 34, 70-78 (1968) UCRL-17481, Spring 1967 pp. 145-153
35 7-7-66	^{60}Co γ-rays 5.0 and 12.5 rads/hr	806	$\equiv 1.0$	$D_0 = 350 \pm 50$ rads $n = 1$	
		Normal (no tumor): 41.2 ± 9.1 mm Hg			
p_{O_2} measurements:	2-day-old ascites L-2: 9.0 ± 3.0 mm Hg 6-day-old ascites L-2: (a) in vivo (microelectrode): $p_{O_2} < 0.25$ mm Hg; (b) samples measured in cuvette with macroelectrode: no O_2.				

Figure 4 shows the survival curve for acute irradiation with ^{60}Co γ rays, at a dose rate of 45 rads/min; the extrapolation number (n = 1.5) is not significantly different from the previous two values. D_Q is only 1/5 that for low-dose-rate γ rays, but almost twice as great as the value for π^- mesons.

Figure 5 shows the results obtained with 910-MeV ^{4}He ions. We have fitted the points to a straight line, but on the basis of this experiment it would be difficult to say whether or not the extrapolation number is 1.0. Consequently, we have written a question mark on Table 1.

Figure 6 summarizes all these experiments, and it shows the limited range of doses covered in our π^--meson experiment.

With the acute irradiations (Figs. 4 and 5) the shoulders seem to be smaller, although the fitting is not good enough to make comparisons with Berry's survival curves (12). He found that shoulders are present in the high-dose-rate curves and not in the low-dose-rate ones.

Our results indicate an RBE for this contaminated beam of about 5.4 for the tumor-forming ability of L-2 cells irradiated and assayed in vivo, regardless of the conditions of oxygenation in the ascites tumors. The RBE would be higher for the Bragg peak of a cleaner π^- beam. It is difficult to extrapolate RBE to high dose rates.

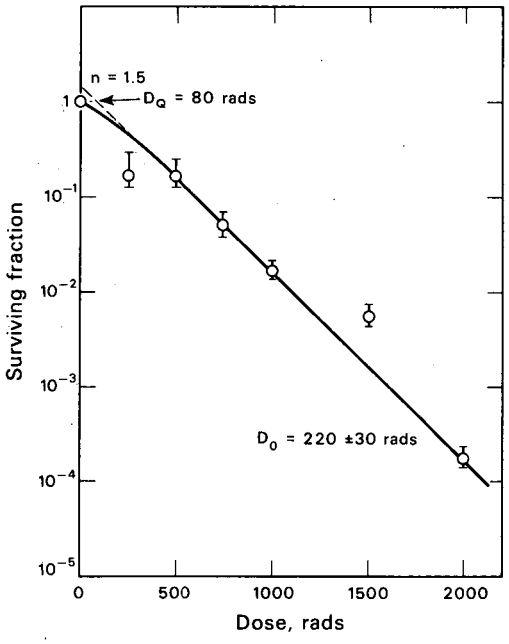

Fig. 4. Survival of lymphoma ascites tumor cells exposed in vivo with ^{60}Co γ rays at a dose rate of 45 rads/min.

DBL 694-4679

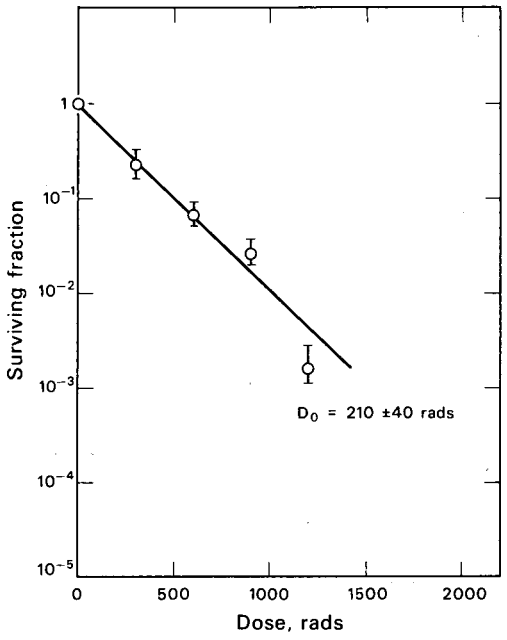

Fig. 5. Survival of lymphoma ascites tumor cells irradiated in vivo with 910-MeV ^{4}He ions at a dose rate of 275 rads/min.

DBL 694-4678

The OER cannot be estimated from survival curves obtained at different tumor ages (5, 7, 13, 14). The cells in a 2-day-old tumor are in the beginning of the log phase, and the 5-day-old tumors are entering the stationary phase. Although the concentration of oxygen seems to be the main factor responsible for the survival differences, there are other conditions--physiological and nonphysiological--that might influence survival, i.e., accumulation of toxins, partial synchronization, and concentration of cells in the ascites fluid (5, 12, 14, 15).

Low dose rates are known to reduce the OER (12). This may be one of the reasons why the mean lethal dose for our previous experiment (1) with a 5-day-old tumor (plus 40 hours of irradiation), and the present one with a 2-day-old tumor were almost the same. More data are required before we can understand the problems related to the oxygen effect, and the reasons why survival-curve parameters and OER's vary from one cell line to another (16).

SUMMARY

In a previous report (Rad. Res. 34: 70-78, 1968) we estimated the relative biological effectiveness (RBE) of 90-MeV negative pions at the Bragg peak, using the proliferative capacity of 5-day-old lymphoma ascites tumors as the end point. With ^{60}Co γ rays as baseline the RBE was 5.4 ± 1.8. In this experiment we used a 2-day-old lymphoma in order to obtain information on the survival of a well-oxygenated tumor. Partial pressure of oxygen (p_{O_2}) was measured with a microelectrode; the 5-day-old tumors were hypoxic, and the 2-day-old tumors well-oxygenated.

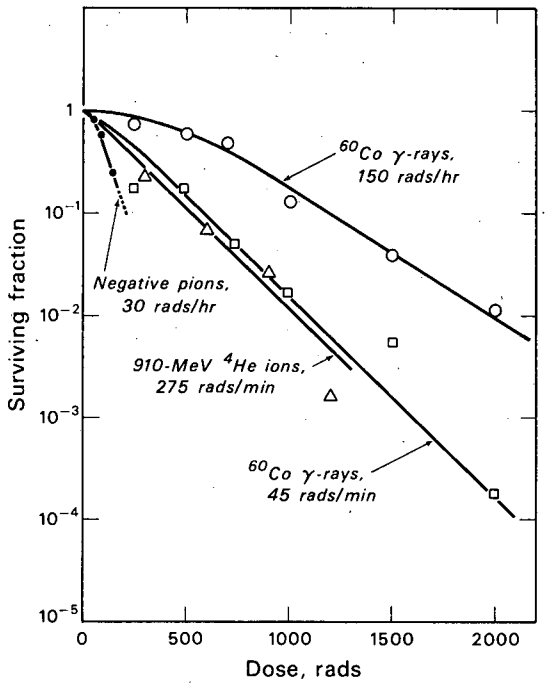

Fig. 6. Survival of 2-day-old lymphoma ascites tumors after low- and high-dose-rate irradiations with π^-, ^{60}Co γ rays, and ^{4}He ions.

DBL 695-4682

Only one mouse at a time could be irradiated at a dose rate of 30 rads/hour. Doses ranged from 60 to 150 rads. After irradiation, mice were sacrificed, cells withdrawn, counted, and serial dilutions prepared from each irradiated mouse and from nonirradiated controls. Each concentration was injected intraperitoneally into a group of 10 female LAF_1 mice; at the end of 8 weeks the TD_{50} (the number of tumor cells needed to produce 50% takes) for each group was evaluated. The ratios of the TD_{50} for the control group to the TD_{50}'s of each irradiated group gave the surviving fractions, with which the survival curve was drawn. A curve with a small shoulder was obtained: D_0 = 76 rads, and D_Q = 44 rads.

Two replicate experiments were done with ^{60}Co γ rays (150 rads/hr). The 0.1 level of survival was used to estimate the RBE, which was found to be 5.4 ± 0.6, in good agreement with our previous results.

We thank Mr. James Vale and the 184-inch cyclotron crew for their assistance in the irradiations with heavy particles.

Miss Alice Beckmann, Miss Henriette Cozza, Mr. Jerry Howard, and Mr. David Love gave their skilled technical cooperation.

REFERENCES AND NOTE

1. Feola, J. M.; C. Richman; M. R. Raju; S. B. Curtis; and J. H. Lawrence: Effect of negative pions on the proliferative capacity of ascites tumor cells (lymphoma) in vivo. Radiation Res. 34: 70-78 (1968).

2. Loughman, W. D.; J. M. Feola; M. R. Raju; and H. S. Winchell: RBE of beams in the Bragg peak regions determined with polyploidy induction in mammalian cells irradiated in vivo. Radiation Res. 34: 56-69 (1968).
3. Raju, M. R.; N. M. Amer; M. Gnanapurani; and C. Richman: The oxygen effect of π^- mesons in Vicia faba. Radiation Res. __: ... (1969).
4. Litchfield, J. T.; and F. Wilcoxon: A simplified method of evaluating dose-effect experiments. J. Pharmacol. Exptl. Therap. 96: 99-113 (1949).
5. Elkind, M. M.; and G. F. Whitmore: The Radiobiology of Cultured Mammalian Cells. Gordon and Breach, New York, 1967.
6. Hewitt, H. B.; D. P. S. Chan; and E. R. Blake: Survival curves for clonogenic cells of a murine keratinizing squamos carcinoma irradiated in vivo or under hypoxic conditions. Intern. J. Rad. Biol. 12: 535-549 (1967).
7. Kallman, R. F.: Methods for the study of radiation effects on cancer cells. In Methods in Cancer Research, H. Bush, Editor, Vol. IV, Ch. X. Academic Press, New York, 1968.
8. Ku, H. H.: Notes on the use of propagation of error formulas. J. Res. NBC-C 70C: 263-273 (1966).
9. Alper, T.; J. L. Moore; and D. K. Bewley: LET as a determinant of bacterial radiosensitivity, and its modification by anoxia and glycerol. Radiation Res. 32: 277-293 (1967).
10. National Bureau of Standards, Handbook 87, Clinical Dosimetry, 1963.
11. Deschner, E. E.; and L. H. Gray: Influence of oxygen tension on X-ray-induced chromosomal damage in Ehrlich ascites tumor cells irradiated in vitro and in vivo. Radiation Res. 11: 115-146 (1959).
12. Berry, R. J.: Hypoxic protection and recovery in tumor cells irradiated at low dose-rates and assessed in vivo. Br. J. Radiol. 41: 921-926 (1968).
13. Patt, H. M.; and R. L. Straube: Measurement and nature of ascites tumor growth. Ann. N. Y. Acad. Sci. 63: 728-737 (1956).
14. Belli, J. A.; and J. R. Andrews: Relationship between tumor growth and radiosensitivity. J. Natl. Cancer Inst. 31: 689-703 (1963).
15. Evans, T. C.; R. F. Hagemann; and D. B. Leeper: Effect of cell concentration during irradiation at low oxygen tension on survival of mouse ascites tumor cells. Radiation Res. 35: 123-131 (1968).
16. Alper, T.: The oxygen effect: pertinent or irrelevant to clinical radiotherapy. Br. J. Radiol. 41: 73 (1968).

Mudundi R. Raju and Chaim Richman are at the Southwest Center for Advanced Studies, Dallas, Texas 75230.

The Determination of Testosterone and Epitestosterone in Urine Samples by Gas Liquid Chromatography

Gerald M. Connell and John A. Linfoot

The measurement of excreted urinary steroids and their metabolites can be a useful aid in patient evaluation. As more sensitive and specific methods evolve, the determination of specific steroids will be of greater diagnostic value than the conventional gross examination of hormone levels.

Many steroids are excreted in a conjugated sulfate or glucuronide form, and therefore, it is necessary to cleave these sugar or sulfate linkages in order to measure the total excreted steroid. This cleavage can be accomplished by enzyme hydrolysis, solvolysis, or acid hydrolysis at low pH. Due to the possibility of steroid artifact formation during harsh acid hydrolysis, many methods substitute the mild enzymatic hydrolysis of urine for several days prior to steroid extraction and quantitation. These methods are reliable, but an extremely high concentration of enzyme relative to urine volume is necessary in order to insure complete hydrolysis of the steroid conjugates present in the urine sample. This significantly increases the cost per analysis, in addition to the loss of 48 to 72 hours necessary for the hydrolysis.

A recent report (1) has suggested that a mild periodic oxidation of the glucuronide conjugates of testosterone and epitestosterone present in urine was adequate to convert these steroids to their "free" unconjugated forms and thus allow their subsequent separation and quantitation by gas liquid chromatography. Because of the potential value of this new method, a preliminary examination of this technique's applicability to our clinical needs was undertaken.

METHODS

The method, as originally proposed, has been modified slightly, and is outlined below:

1. To 200 ml of urine add
   a. 80 ml 10% aqueous sodium metaperiodate,
   b. 20 ml N sodium hydroxide.

Check pH at this point and adjust to 6.8 if necessary.

2. Incubate at 37°C for 60 min.
3. After this 60-min incubation, add 25 ml 2 N sodium hydroxide and stir thoroughly.

Incubate at 37°C for an additional 30 min.
At the termination of this incubation period, all glucuronides of testosterone and epitestosterone should be oxidized to their unconjugated forms.

4. Approximately 25,000 cpm ^{3}H-1, 2-testosterone are added to each sample in order to correct for steroid losses which occur during the extraction and purification procedures.

5. The oxidized urine samples are extracted with 250 ml ether three times; the combined ether extracts are washed with 50 ml 2 N sodium hydroxide and twice with 50 ml distilled water. The ether extract is filtered through anhydrous sodium sulfate and then evaporated to dryness in a flash evaporator under reduced pressure.

6. The extract is quantitatively applied to a 2-g alumina column (10 mm i. d.) with 10 ml benzene (5 times 2 ml) and is eluted from the column with 75 ml 0.25% ethanol in benzene (v/v). The first 15 ml of eluate is discarded and the next 60 ml contains the testosterone and epitestosterone. Flow rate is approximately 1 drop per 2 to 3 sec.

7. This 60-ml fraction is dried and quantitatively applied to a thin-layer chromatographic plate coated with silica gel-G (approximately 0.250 mm thickness). The thin-layer plates are divided into lanes and each sample is applied to a separate lane. Reference standards of authentic testosterone and epitestosterone are applied to the two outside lanes, and the plate is developed in the solvent system, chloroform-ethyl acetate (80:20, v/v), until the solvent front reaches the edge of the plate. The areas of the sample lanes, corresponding in chromatographic mobility to the authentic testosterone and epitestosterone standards, are removed from the plate and eluted with ether (3 times 5 ml). This ether extract is dried under nitrogen at 37°C and then placed in a desiccator overnight.

8. The trimethylsilyl ether derivatives (TMS) of testosterone and epitestosterone are formed by the addition of 0.2 ml Regisil-TMCS and 3 drops anhydrous pyridine per sample. The samples are mixed well, tightly sealed in screw-cap reaction tubes, and allowed to react overnight at room temperature. The reaction mixture then is dried under nitrogen at 37°C.

9. The residue, which contains the TMS derivatives of testosterone and epitestosterone, are chromatographed on a second thin-layer plate in the same solvent system (chloroform-ethyl acetate, 80:20, v/v). Authentic testosterone-TMS and epitestosterone-TMS are chromatographed as reference compounds. The areas of the sample lanes, which correspond in chromatographic mobility to the reference compounds, are removed from the plate and eluted with ether (3 times 5 ml). The extracts are dried under nitrogen and then are ready for gas liquid chromatography (GLC).

To this point, the purification procedure has separated many compounds from the steroids of interest, but it was unable to separate the 17 alpha and 17 beta isomeric forms of testosterone. The selection of the proper column for GLC effectively separates these isomers and allows their quantitation.

10. The residue is diluted with 50 λ hexane, and an aliquot is removed for liquid scintillation counting in order to correct for recovery losses. Aliquots are injected into a Varian Aerograph 2100 gas chromatograph, and eluted peaks for testosterone-TMS and epitestosterone-TMS are quantitated by triangulation. Dose-response curves for standard testosterone-TMS and epitestosterone-TMS are determined before and after each chromatographic run. Separation is obtained with a 6-ft U-shaped glass column (4 mm i. d.) packed with Supercoport,

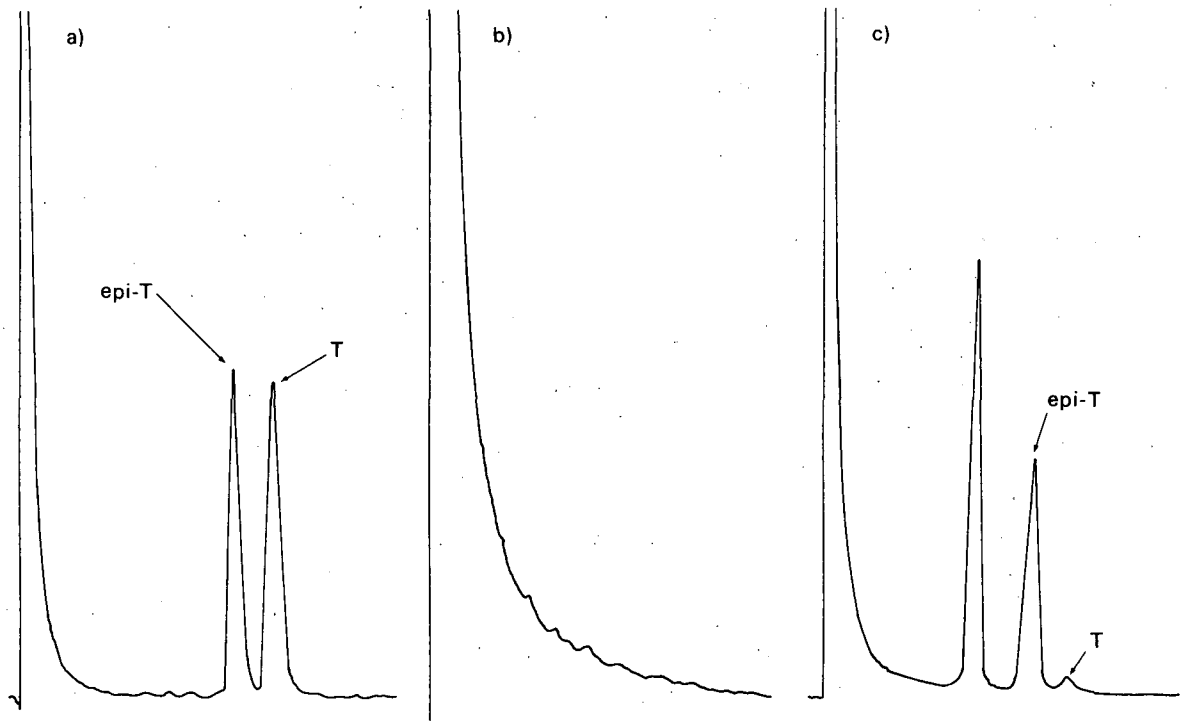

Fig. 1. GLC traces obtained under conditions outlined in step 10 of methods section. Attenuator settings for full-scale deflection (afs) are noted for each trace.
(a). 1×10^{-9} afs; 0.20 μg epitestosterone-TMS and 0.20 μg testosterone-TMS.
(b). 1×10^{-9} afs; 200-ml water blank processed through the entire procedure; 40% of sample chromatographed, and no peaks observed in the epitestosterone-TMS and testosterone-TMS areas.
(c). 32×10^{-9} afs; 200-ml urine sample, showing a large epitestosterone-TMS peak and a small testosterone-TMS peak; 20% of sample chromatographed.
DBL 695-4683

100/120 mesh, which is coated with a 1% OV-17 stationary phase. Injector temperature, 257°C; column temperature, 225°C; detector temperature, 275°C. Detection is by flame ionization, and gas flow rates are: oxygen, 120 ml/min; nitrogen, 33 ml/min; hydrogen 33 ml/min. Under these conditions testosterone-TMS and epitestosterone-TMS show retention times of 6.5 and 5.4 min respectively.

RESULTS AND DISCUSSION

Results illustrated by the GLC traces in Fig. 1 show that these two steroids can be analyzed successfully by this method proposed by McRoberts et al. (1). The OV-17 column effectively separates these isomeric forms of testosterone and allows their quantitation. This column should prove to be a better column because of the greater thermal stability of OV-17 than of the XE-60 column originally suggested. The tracing (Fig. 1a) is obtained from testosterone-TMS and epitestosterone-TMS standard solutions. Since flame-ionization detection depends upon an ionization current formed from the combustion of carbon atoms, both testosterone and epitestosterone theoretically can be quantitated from a single dose-response curve of either testosterone or epitestosterone. However, it is advisable to include both TMS derivatives for retention-time data.

Recovery for testosterone and epitestosterone were corrected by the inclusion of a tracer amount of tritiated testosterone. Because separation of these two isomers occurs only during the final quantitation step, it is thought that the labeled testosterone marker should be an adequate precaution; however, this step should be more thoroughly examined with a labeled isotope of epitestosterone in order to be absolutely confident that both compounds behave similarly throughout the entire purification procedure. Figure 1b shows a tracing obtained from 200 ml distilled water carried through the entire analysis, and indicates that no extraneous peaks are introduced which could interfere with the quantitation. Figure 1c is a tracing from a 200-ml urine sample, and illustrates the epitestosterone-TMS and testosterone-TMS peaks. The additional peak, which elutes earlier, is probably due to an excess of an unidentified 17-ketosteroid not completely removed by the purification procedure. It is well separated from the testosterone and epitestosterone peaks and therefore does not interfere with the analysis.

The data in Table 1 show results obtained from urine samples of patients who have undergone pituitary irradiation. The testosterone values observed are surprisingly low when compared with normal values reported for this method (male: 61.3 μg/24 hr testosterone and 45.8 μg/24 hr epitestosterone). The relatively high values for epitestosterone were unexpected, and may reflect an alteration in steroid metabolism. The examination of urine samples from diabetic patients (male and female) failed to show detectable quantities of testosterone, and may reflect a need to use more than a 200-ml urine sample in these patients. This response may be a true diminution of pituitary gonadal activity due to pituitary irradiation. Further examination of this point is necessary.

Table 1. Urinary testosterone and epitestosterone values.

Patient		Testosterone (μg)	Epitestosterone (μg)
H.	male acromegalic	12.4 μg/24 hr	
Ce.	male acromegalic	1.7 μg/24 hr	
Cu.	male adrenogenital	2.4 μg/6hr	396 μg/6 hr
Cu.	male adrenogenital	8.2 μg/12 hr	306 μg/12 hr

It has been reported that epitestosterone values are consistently elevated in hirsute patients; however, testosterone values were reported to be in the normal range (2). Also the rate of formation of epitestosterone from testosterone in the blood has been reported to be 30 times as great in hirsute patients as in normal men and women (3). These data suggest that examination of epitestosterone in addition to testosterone may have some clinical significance in the evaluation of certain pathological conditions.

SUMMARY

Gas liquid chromatographic analysis of testosterone and its 17 alpha isomer, epitestosterone, can be accomplished by this method with relative ease. These determinations can be a useful measurement for the evaluation of pituitary and gonadal function. In certain pathological

conditions, the contribution of the adrenal gland to the total androgen pool can be noted. In addition, some significance may emerge regarding the importance of epitestosterone--a steroid whose metabolic significance is not yet understood.

REFERENCES

1. McRoberts, J. W.; A. D. Olson; and W. L. Herrmann. Clin. Chem. 14: 565-582 (1968).
2. deNicola, A. F.; R. I. Dorfman; and E. Forchielli: Steroids 7: 351 (1966).
3. Blaquier, J.; R. I. Dorfman; and E. Forchielli: Acta Endocrinol. 54: 208 (1967).

Whole-Body Marrow Distribution Studies in Polycythemia Vera

Donald C. Van Dyke, John H. Lawrence and Hal O. Anger

One-fifth to one-third of all patients with polycythemia vera die in the "spent" phase of the disease with myeloid metaplasia (1-3). Since development of methods for obtaining pictures of the total-body marrow-distribution pattern (4-6), it has become apparent from study of a small series of patients with polycythemia vera that an increase in immature cells in the peripheral blood picture is preceded by rapid change in total-body marrow-distribution pattern. This suggested that a deterioration in total marrow-distribution pattern may herald the onset of marrow failure before other signs appear, and that marrow-distribution studies may be of prognostic value in management of polycythemia vera.

MATERIALS AND METHODS

The erythropoietic portion of the marrow is labeled radioactively with the short-lived ($t_{1/2}$ = 8 hr) positron-emitting isotope, ^{52}Fe. The distribution of activity is recorded with the positron scintillation camera (4) or with the whole-body scanner, Mark II (6). Iron-59 may be used in place of ^{52}Fe with the above-mentioned scanner, which is specially designed for high-energy γ-ray emitters, but the relatively sharp pictures of selected areas provided by the positron scintillation camera cannot be obtained with ^{59}Fe.

The reticuloendothelial portion of the marrow can be labeled with any colloid of the proper particle size (7, 8). The most satisfactory at present, because of availability, cost, and the radiation dose to the patient, is the short-lived ($t_{1/2}$ = 6 hr) technetium-sulfur colloid (9). After labeling with this colloid, the marrow, liver, and spleen can be visualized with a conventional radioisotope scanner, with the whole-body scanner, or with the γ-ray scintillation camera.

In our Laboratory the whole-body scanner and the positron scintillation camera are located in the same area, so that a quick whole-body scan can be taken first to be used as a guide in taking the smaller but more detailed positron camera pictures.

The radiation dose to the bone marrow in a 70-kg man given ^{52}Fe, ^{59}Fe, and ^{99m}Tc has been estimated to be as follows: 2.5 rads to bone marrow for a 100-μCi dose of ^{52}Fe (4), 1.0 rad for a 20-μCi dose of ^{59}Fe (10), and 0.09 rad for a 3-mCi dose of ^{99m}Tc-sulfur colloid (11).

The methods of preparation of ^{52}Fe and ^{99m}Tc-sulfur colloid have been described in the literature (9, 12).

METHOD OF MARROW LABELING When radioiron is used, pictures of the bone marrow must be taken at the time of maximum marrow uptake, after the iron has cleared the plasma and before it has passed through the marrow to the peripheral blood. For most patients this is 10–24 hours after intravenous administration of ^{52}Fe (13) or ^{59}Fe. The patient is usually injected with 100-150 μCi ^{52}Fe as ferric citrate in the afternoon, and pictures are taken the following morning.

When a colloidal preparation of sulfur labeled with ^{99m}Tc is used, most of the colloid localizes in the liver, spleen, and hemopoietic marrow within 5 minutes. Picture-taking can be begun soon after intravenous administration of the labeled colloid, and the study is completed during a single visit. In the studies presented here, 3–5 mCi of ^{99m}Tc-sulfur colloid were given.

In each study, scintiphotos of ^{52}Fe distribution are made with the positron camera, exposing 5–10 minutes per picture. At the completion of the ^{52}Fe pictures the technetium colloid is injected, and 1 hour later the same areas are photographed with the scintillation camera operating in gamma mode, using 1–5 minute exposures (14).

The 23 patients reported in this series were diagnosed as having polycythemia vera on the basis of (a) an increased circulating red cell volume exceeding 34 ml/kg body weight; (b) exclusion of disorders associated with secondary erythrocytosis; and (c) presence of associated findings such as splenomegaly, persistent thrombocytosis, or leukocytosis. Tumors associated with secondary erythrocytosis were excluded on the basis of complete medical evaluation during clinic visits and subsequent long-term followup of the patient's course. Arterial blood-oxygen saturation was performed in patients with the possibility of chronic pulmonary disease or right-to-left cardiac and vascular shunts. In most cases therapy and long-term followup were performed at the Donner Laboratory clinic. Complete records were kept of all pertinent medical information concerning procedures performed elsewhere throughout the entire course of the patient's disease.

RESULTS

Increase in the number of pro- and metamyelocytes in the peripheral blood smear is usually the first indication of the onset of marrow failure, and occurs before there is any decrease in phlebotomy or other treatment required. At this time a marrow biopsy will often show serous fat atrophy and fibrous tissue. This stage is followed by rapid onset of anemia, increased number of immature cells in the peripheral smear, and marrow failure.

Since the object of this study is to test the hypothesis that characteristic changes occur in the distribution of erythropoietic marrow before evidence of marrow failure in the peripheral blood, the patients have been classified as to whether or not they had evidence of marrow failure as judged by the findings in their peripheral blood at the time of the first whole-body marrow distribution study. The marrow distribution patterns as determined by the radioiron and radiocolloid distribution pictures have been classified on the basis of the five major types previously described (5). Examples of patients with polycythemia vera having ^{52}Fe marrow distribution patterns typical of these major categories are shown in Figs. 1-4. The patient shown in Fig. 5 had myelofibrosis without evidence of previous polycythemia. Figure 1 shows normal distribution of the erythropoietic marrow (type I) in a patient in the stable, active phase of polycythemia vera (Case 3 in the table). Figure 2 shows minimal peripheral extension of the hematopoietic marrow into femur and humerus (type II) of a patient in the stable, active phase of polycythemia vera (Case 15 in the table). Figure 3 shows peripheral extension beyond the knee and elbow (type III) in a patient in the active phase of polycythemia vera (Case 16 in the table). Figure 4 shows extension of marrow into the periphery of the extremities, loss of marrow from the lumbar spine, and extramedullary erythropoiesis in the spleen (type IV) in a patient in the active phase of polycythemia (Case 18 in the table) who developed marrow failure 9 months later. Figure 5 shows complete loss of medullary erythropoiesis, with erythropoiesis confined to the spleen (type V), in a case of myelofibrosis not known to have been preceded by polycythemia.

Table I lists studies from 19 patients in the active phase of polycythemia vera with no evidence of impending marrow failure in the peripheral blood smears, and four patients studied after the appearance of immature cells in the peripheral blood.

From the figures and the table it can be seen that patients in the active phase of polycythemia vera may have a perfectly normal distribution of erythropoietic marrow (marrow distribution type I) or, more frequently, minimal extension into proximal portions of humerus or femur or both (marrow distribution type II). Of the four patients in whom a distribution pattern of type III (abnormal expansion of marrow into the distal bones of the extremities) or degeneration to type IV was found prior to clinical evidence of failure, one developed marrow failure 9 months later (Case 18), and one 4 months later (Case 19). All patients studied after clinical evidence of marrow failure was manifest showed marrow distribution patterns of type III or higher. Direct comparisons of the distribution of erythropoietic marrow (as shown by ^{52}Fe) and reticuloendothelial marrow (as shown by ^{99m}Tc-sulfur colloid) in seven patients in the various stages of polycythemia vera demonstrated that the distribution of these two marrow functions was similar or identical in all but one.

DISCUSSION

The results from the limited number of patients studied so far indicate that although some peripheral extension of marrow characteristically occurs early in the course of the disease, the process is not a slowly progressive one, but remains stabilized during most of the active stage of the disease. Progressive peripheral extension of the marrow pattern precedes the "spent" or "burned out" stage of the disease. The assumed time course of these changes is presented graphically in Fig. 6.

Table 1. Correlation of marrow-distribution pattern with clinical stage in patients with polycythemia vera.

Clinical stage	Patient number	Type of marrow distribution	
		^{52}Fe	Tc-colloid
Active stage of the disease, requiring phlebotomy or myelosuppressive therapy	1	I	
	2	I[a]	
		I	
	3	I	I
	4	I	
	5	I	
	6	I	II
	7	II	
	8	II	
	9	II	
	10	II	
	11	II	
	12	II	
	13	II	II
	14	II[a]	
		II	
	15	II[b]	
		II	
	16	II[a]	
		III	III
	17	III[c]	
	18	IV[d]	IV
	19	IV[e]	
"Spent" stage of the disease, requiring transfusions	20	III	III
	21	IV	
	22	IV	
	23	V	

a. Two years between first and second study.

b. One year between first and second study.

c. Continued active at time of reporting, 2.5 years after study.

d. Developed marrow failure within 9 months after marrow distribution type IV found.

e. Developed marrow failure 4 months after marrow distribution type IV found.

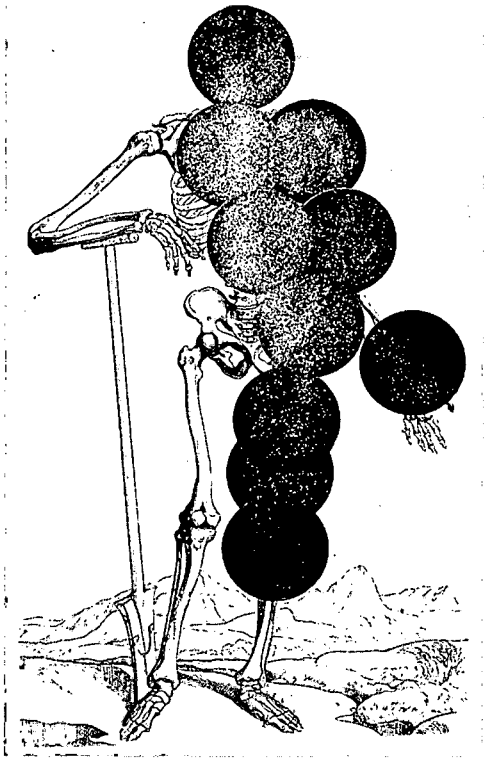

Fig. 1. Normal distribution of the erythropoietic marrow (marrow distribution type I) in a patient in the stable, active phase of polycythemia vera (Case 3 in the table). XBB 684-1925

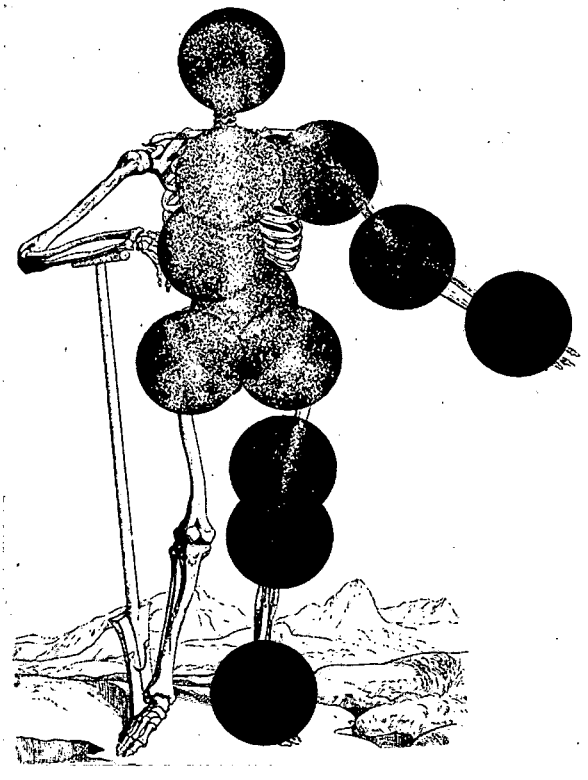

Fig. 2. Minimal peripheral extension of the hematopoietic marrow into femur and humerus (marrow distribution type II) in a patient in the active phase of polycythemia vera (Case 15 in the table). The majority of patients showed this distribution pattern. XBB 683-1334

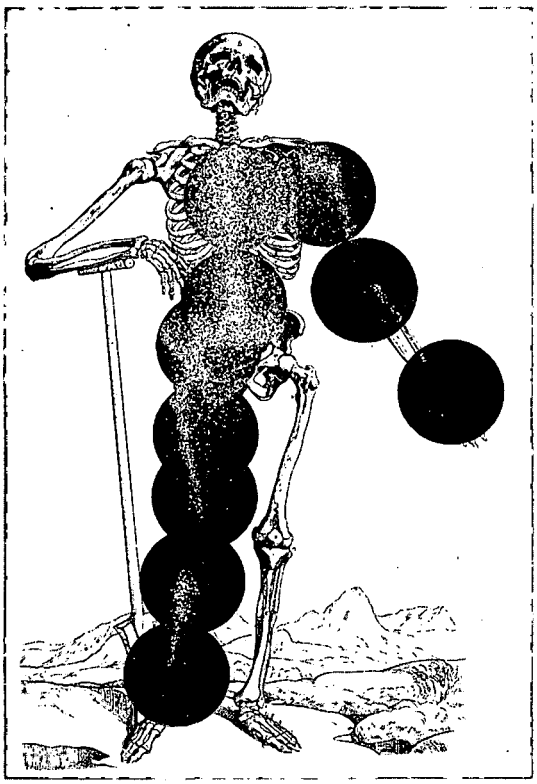

Fig. 3. Peripheral extension beyond the knee and elbow (marrow distribution type III) in a patient otherwise thought to be in the stable active phase of polycythemia vera (Case 16 in the table). This distribution pattern is interpreted as heralding the onset of marrow failure in the near future. XBB 682-616

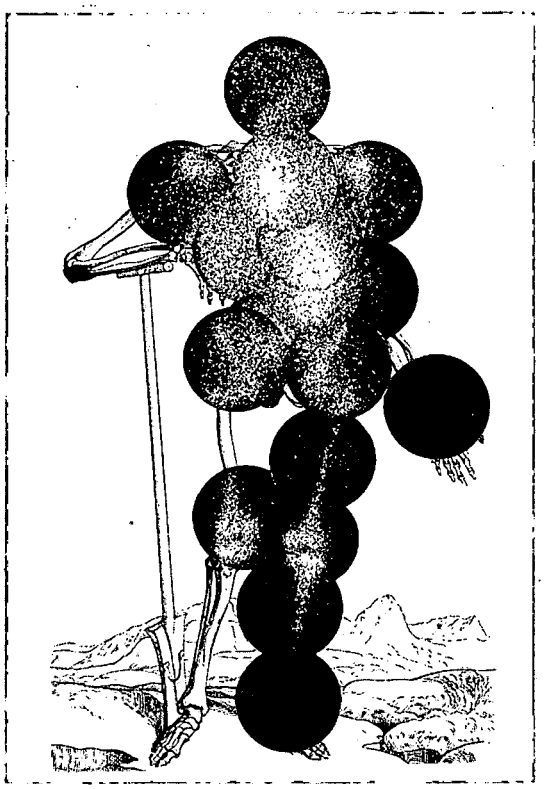

Fig. 4. Extension of marrow into the periphery of the extremities, loss of marrow from the lumbar spine, and extramedullary erythropoiesis in the spleen (marrow distribution type IV) in a patient in the active phase of polycythemia vera who developed marrow failure 9 months later (Case 18 in the table).
XBB 683-1267

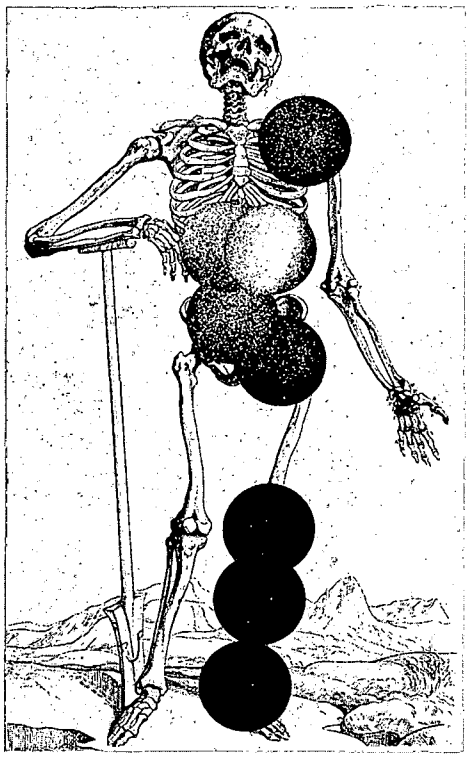

Fig. 5. Virtually complete loss of medullary erythropoiesis with erythropoiesis confined to the spleen (marrow distribution type V). XBB 684-1805

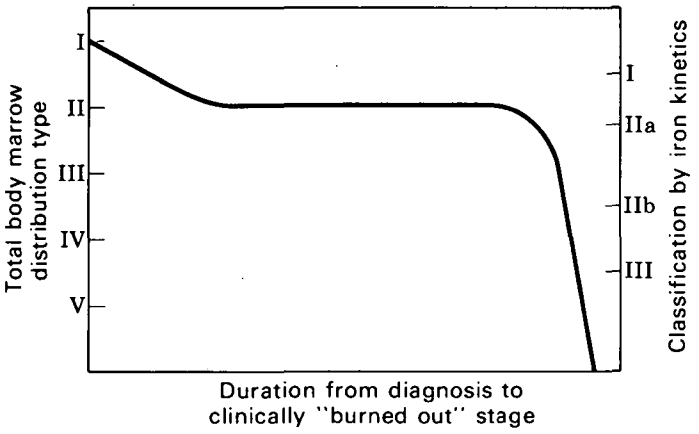

Fig. 6. Schematic representation of the change in marrow distribution pattern with time in polycythemia vera. XBL 685-810

Similar prognostic information is obtained from iron kinetics studies in patients with polycythemia vera. Pollycove et al. (15) have divided patients with polycythemia vera into four classes (Class I, Classes IIa and IIb, and Class III) on the basis of iron kinetics studies. "Patients in Classes I and IIa are in relatively earlier phases of their disease and frequently are found to develop red-cell kinetics of Class III as their disease progresses." Although simultaneous iron kinetics and marrow-distribution studies have been done on only a few patients, the results indicate that iron kinetics Classes I and IIa correspond to marrow-distribution types I and II as given here. Iron kinetics classes IIb and III correspond to marrow-distribution types III, IV, and V. This correspondence has been indicated in Fig. 6.

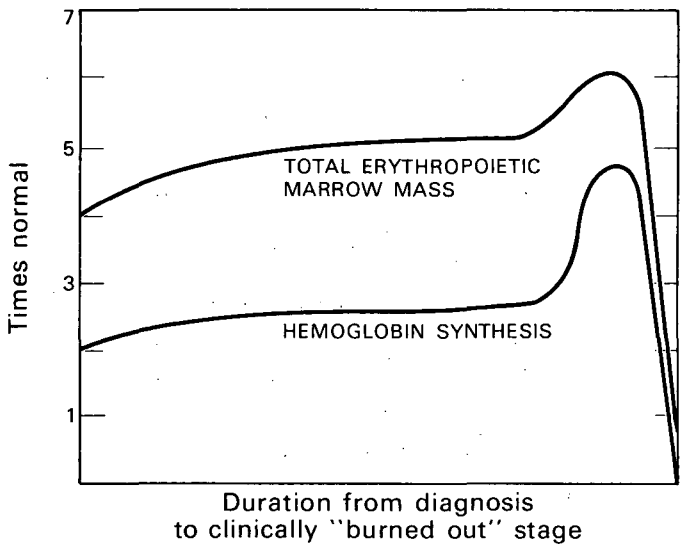

Fig. 7. Comparison of the total erythropoietic marrow mass (estimated from marrow cellularity and total-body marrow distribution) with hemoglobin synthesis values given by Pollycove et al. (15), during the evolution of polycythemia vera.
DBL 685-4747

Peripheral extension of marrow in the absence of excessive demand for increased red cell production may indicate that the usual marrow sites are occupied by other elements such as tumor or fibrous tissue. In the patient with polycythemia vera this is clearly not the case. In the untreated or inadequately treated case the marrow is markedly hypercellular from the time of earliest diagnosis to late in the evolution of the disease (16), being in the order of 80% hematopoietic tissue with 20% fat in patients in the active phase of polycythemia vera, as compared with 20% hematopoietic tissue and 80% fat in normal persons. Thus, before peripheral expansion of marrow has occurred, the untreated patient with polycythemia vera has a hematopoietic marrow mass four times normal. During the active stages of the disease the hematopoietic mass is estimated to increase from 4 to 5 or 6 times normal. Since the percentage of erythroid elements is either normal or slightly elevated, the erythropoietic marrow must also increase from 4 to 6 times normal.

Iron kinetics studies (15) have demonstrated an increase in hemoglobin synthesis from twice normal to 4.8 times normal as the disease evolves. Increased hemoglobin synthesis is offset by progressive shortening of red cell life span, which is predominantly the result of intramedullary hemolysis, in late stages of the disease. The probable relationship between total erythropoietic marrow mass and hemoglobin synthesis during evolution of the disease is shown schematically in Fig. 7. (Figures for hemoglobin synthesis are from Pollycove et al., Ref. 15.) As indicated in the figure, inefficient hemoglobin synthesis characterizes the disease from its onset, the erythropoietic marrow mass being increased twice as much as hemoglobin synthesis in the active stages of the disease.

Only in the most advanced stages of myelofibrosis does proliferation of fibrous and osseous elements proceed to the extent that it fills the marrow cavity (16). As stated by Nelson and Knisely (17), "Rarely did the volume of fibrous tissue approach that of fat normally present in

marrow, and the extramedullary hemopoiesis of 'myelofibrosis' is not simply compensatory for a reduction in the volume of cellular marrow."

Because of its 8-hr half-life and the necessity of cyclotron production, ^{52}Fe is not generally available at present. For this reason patterns for ^{99m}Tc-sulfur colloid and for ^{52}Fe were compared. In six cases of polycythemia vera in this series in which marrow distribution has been determined by both techniques, either the distributions were identical or the differences were not sufficient to indicate a different classification. In only one case (Case 6 in the table, and previously reported, Ref. 14) was the pattern distinctly different--type I by ^{52}Fe and type II by ^{99m}Tc-sulfur colloid. It has been emphasized previously (14) that in the presence of hematologic disease, the correlation between the distribution of these two marrow components has varied from identical to totally dissimilar. However, comparisons to date, in patients in various stages of polycythemia vera, indicate that both cell types are similarly affected and that the use of iron or colloid gives essentially the same total body marrow-distribution pattern in the majority of cases.

SUMMARY AND CONCLUSIONS

One-fifth to 1/3 of all patients with polycythemia die from marrow failure. Total-body marrow-distribution studies in 23 patients in various stages of polycythemia vera indicate that although some peripheral extension of marrow characteristically occurs early in the course of the disease, the process is not a slowly progressive one, but remains stable during most of the active stage of the disease. Progressive degeneration of the marrow pattern probably precedes the "burned out" stage, and provides the physician with prognostic information which may prove helpful in management of the disease. Marrow-distribution patterns in more patients done in conjunction with marrow biopsy, iron kinetics, etc., at intervals throughout the course of polycythemia vera will be needed to determine the validity of the present speculations and the value of total-body marrow-distribution studies in prognosis.

REFERENCES

1. Lawrence, J. H.: Polycythemia: Physiology, Diagnosis and Treatment Based on 303 Cases. Grune and Stratton, New York, 1955.
2. Ledlie, E. M.: Treatment of polycythemia by ^{32}P. Proc. Roy. Soc. Med. 59 [#11, Part 1]: 1095-1100 (1966).
3. Lawrence, J. H.; H. S. Winchell; and W. G. Donald: Leukemia in polycythemia vera: Relationship to splenic myeloid metaplasia and therapeutic radiation dose. In preparation.
4. Anger, H. O.; and D. C. Van Dyke: Human bone marrow distribution shown in vivo by iron-52 and the positron scintillation camera. Science 144 [June 26]: 1587-89 (1964).
5. Van Dyke, D.; and H. O. Anger: Patterns of marrow hypertrophy and atrophy in man. J. Nucl. Med. 6 [2]: 109-120 (1965).
6. Van Dyke, D.; H. O. Anger; and Y. Yano: Progress in determining bone marrow distribution in vivo. In Progress in Atomic Medicine, Vol. 2. Grune and Stratton, New York, 1968.
7. Edwards, C. L.; G. A. Andrews; B. W. Sitterson; and R. M. Knisely: Clinical bone marrow scanning with radioisotopes. Blood 23 [6]: 741-56 (1964).

8. Miale, A., Jr.; A. Gagnon; W. DeCesare; and C. Rath: Scintillation camera studies of bone marrow in blood dyscrasias. J. Nucl. Med. 7[5]: 347 (1966).
9. Harper, P. V.; K. A. Lathrop; and P. Richards: ^{99m}Tc as a radiocolloid. J. Nucl. Med. 5[5]: 382 (1964).
10. Bothwell, T. H.; and C. A. Finch: Iron Metabolism. Little, Brown & Co., Boston, 1962. P. 39.
11. Smith, E. M.: Internal dose calculation for ^{99m}Tc. J. Nucl. Med. 6[4]: 231-51 (1965).
12. Yano, Y.; and H. O. Anger: Production and chemical processing of iron-52 for medical use. Intern. J. Appl. Radiation Isotopes 16: 153-56 (1965).
13. Pollycove, M.: Ferrokinetics: Techniques. Eisenstoffwechsel: Beitrage zur Forschung und Klinik. G. T. Verlag, Stuttgart, 1959. P. 20.
14. Van Dyke, D.; C. Shkurkin; D. Price; Y. Yano; and H. O. Anger: Differences in distribution of erythropoietic and reticuloendothelial marrow in hematologic disease. Blood 30[3]: 364-74 (1967).
15. Pollycove, M.; H. S. Winchell; and J. H. Lawrence: Classification and evolution of patterns of erythropoiesis in polycythemia vera as studied by iron kinetics. Blood 28[6]: 807-29 (1966).
16. Ward, H. P.; and M. H. Block: A reevaluation of the myeloproliferative syndrome. Symposium on Myeloproliferative Disorders of Animals and Man, 1968.
17. Nelson, W.; and R. Knisely: Marrow fibrosis in myeloproliferative disorders. Symposium on Myeloproliferative Disorders of Animals and Man, 1968.

Actinide Element Studies with a Si(Li) "Wound Counter"

Howard G. Parker, Stephen R. Wright and Anne deG. Low-Beer

At Lawrence Radiation Laboratory, Berkeley, preparations for handling possible internal contamination with radioactivity require consideration of a wide variety of nuclides. Much experimental work is being done with isotopes of the elements beyond plutonium, of particular interest to the Atomic Energy Commission. Some of these are scheduled for production and use in large quantities in the near future, with a consequent potential for accidental internal contamination of humans. A number of these nuclides lack γ rays useful for in vivo measurement of their retained burdens, but have significant low-energy L X-ray emission. The classic example of this sort of nuclide is ^{239}Pu, but others are ^{244}Cm, ^{242}Cm, ^{238}Pu, and ^{253}Es. Some of the other actinides such as ^{241}Am and ^{252}Cf have useful γ rays of higher energy, but also emit significant numbers of L X rays.

Palmer et al. (1) have shown for ^{239}Pu that the strong dependence of absorption on energy in the low-energy X-ray region permits a measurement of average depth in tissue from the relative height of the different L X rays. We wished to extend this depth measurement to practical use for any actinide. Published work on it has so far been limited to ^{239}Pu and ^{241}Am (1, 2). Also, the systematic variation of L X-ray energies with atomic number, together with various associated low-energy γ rays, gives us a potential "fingerprint" for identification of each nuclide that might be retained in a wound.

These relationships led us to a systematic study of the L X rays and γ rays from available actinides, in order to do as much as possible in identification, quantitation, and depth measurement for contaminated wounds.

Experience has taught us the value of preparing our own catalog of spectra in preparation for contamination incidents. This permits us to acquire the necessary standards; gain familiarity with the equipment, the nuclides, and their spectra; and to work up the subject for a particular detector that provides adequate sensitivity for biological work, as well as resolution. The necessity for these preparations has become doubly evident for us, because difficulty of measurement and scarcity of useful handbook values are particularly notable in the low-energy region.

This paper relates some of our initial progress in working with the wound counter, and in gathering a small reference collection ("library") of actinide sources and their spectra. It covers some relevant properties of the counter, the depth measurement, and studies in absorbers commonly used as phantoms.

MATERIALS AND METHODS

A lithium-drifted silicon detector was used to study the low energy photons emitted from the actinides. The detector, preamplifier, and cryostat were purchased from the Technical Measurement Corporation of San Mateo, California. A detailed explanation of this type of system can be found in a report by Miner (3). Briefly, our system includes a 300-mm^2 detector housed in a vacuum chamber and positioned about 6.4 mm behind a 0.25-mm thin beryllium window. The depletion depth is 3 mm, and at liquid nitrogen temperatures we obtain a resolution of 1.5 keV FWHM for the 17.7-keV peak of ^{241}Am. The background in the L X-ray region of Am is 0.2 cpm per channel, and decreases to less than 0.1 cpm at 100 keV. A model 5400 Hewlett-Packard 1024-channel analyzer was used in all studies. The analyzer's stability was exceptionally good, principally due to the automatic internal gain stabilizer. The analyzer was calibrated by use of an IAEA standard of ^{241}Am. In 6 months of operation we observed only a one-channel drift out of 1024 channels. The superior resolution and stability of this system enable us to separate accurately the 13.9-, 17.7-, 20.8-, 26.9-, and 59.6-keV peaks of ^{241}Am.

Up to this time the following nuclides have been available for study: ^{239}Pu, ^{241}Am, ^{243}Am, ^{244}Cm, ^{252}Cf (associated with varying amounts of other isotopes of californium), and ^{253}Es. ^{239}Pu and ^{241}Am were separated by ion-exchange chromatography, which resulted in a high degree of purification of both nuclides. All the foregoing nuclides were prepared for counting as virtually weightless point sources by electrodeposition on stainless steel. These were counted in a standardized alpha proportional counter, and checked for radiochemical purity by alpha pulse-height analysis. Additional sources were prepared by plating measured amounts of the original material on platinum, which was then sealed between two layers of thin polyethylene. Composition of the sources varies from the particularly high-purity ^{239}Pu and ^{241}Am through different degrees of isotopic mixtures, as in ^{252}Cf. Also, some sources have been prepared of two nuclides in varying relative amounts.

The sources were used on the wound counter in various positions relative to the detector, for measurements of counter sensitivity, geometry, effect of sample size and configuration, and absorption in air, water, Lucite, fiberboard, and a "tissue-equivalent liquid" described by Clifford (4).

RESULTS

Unattenuated spectra obtained to date with the "wound counter" on our library of sources are shown in Fig. 1, which illustrates the systematic variation in energy of the L X-ray peaks with atomic number of the daughter nuclide. The additional γ-ray peaks characteristic of some of the nuclides are also evident. The Np L X rays arising from decay of ^{243}Am are theoretically the same as for ^{241}Am, and only the γ rays are different. In actuality there was a consistent shift of one channel in the X-ray peaks. The resolution obtained permits identification

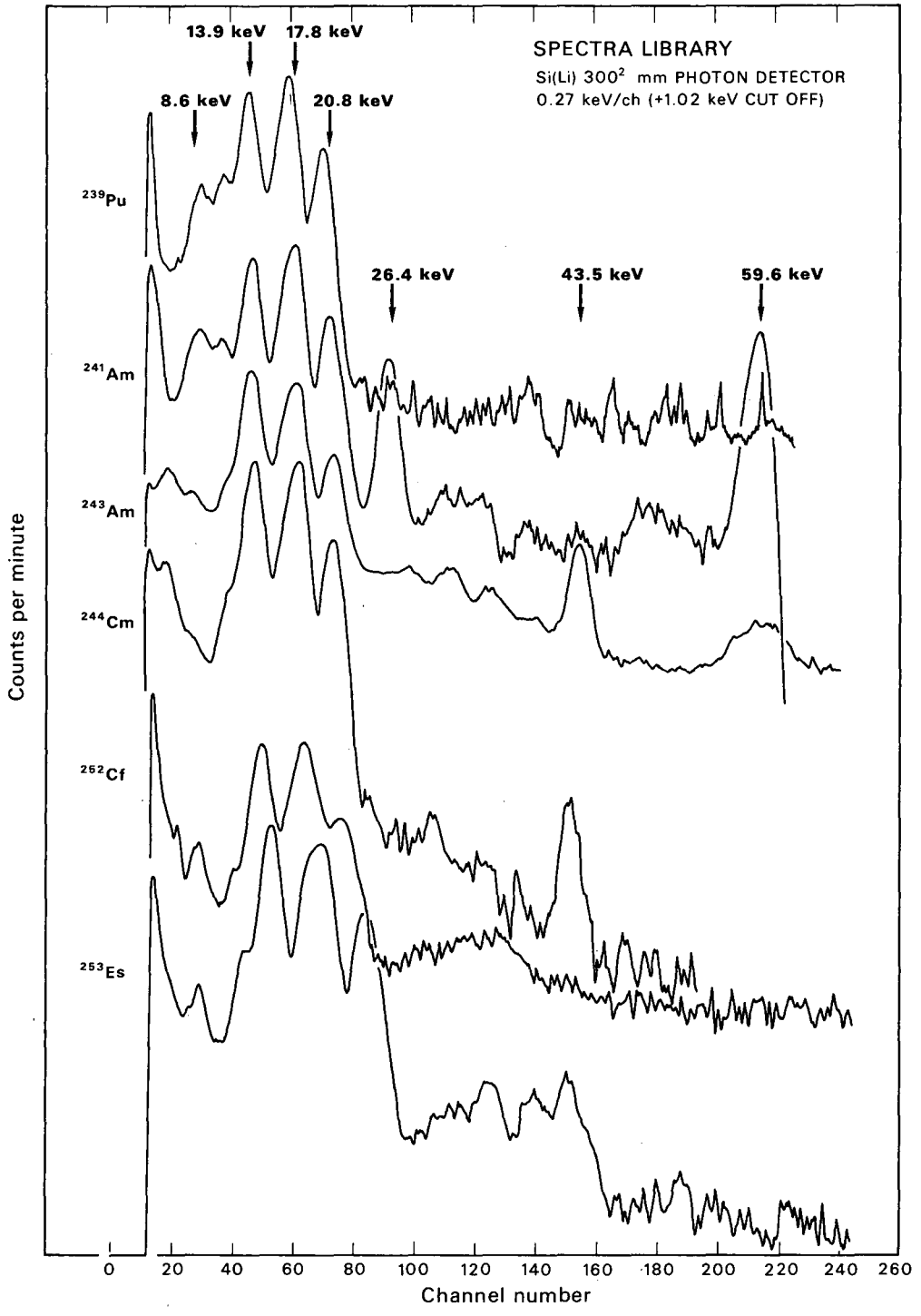

Fig. 1. X- and γ-ray spectra obtained with the Si(Li) crystal "wound counter" from the "library" of actinides. Counting rate is plotted semilogarithmically against channel number covering an energy range from approximately 1 to 70 kev at 0.27 keV per channel. The vertical scale has been adjusted to display the spectra with minimum overlap, in order of atomic number, but close enough to show the systematic changes. It does not indicate abundances of one spectrum relative to another. DBL 695-4693

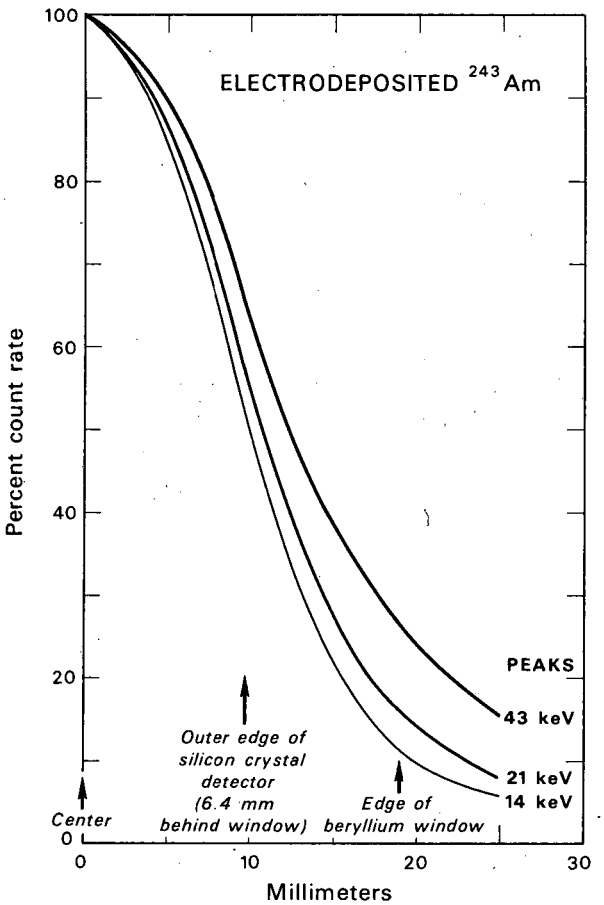

Fig. 2. Counting rate of a 4-mm-diameter electrodeposited source of ^{243}Am as a function of lateral movement across the face of the beryllium window of the wound counter in any direction away from the central axis. The rate is given as percent of the value at the center of the window. DBL 695-4697

of each nuclide only if it is known to be pure, and identification of mixtures cannot be made with confidence from the spectra alone. However, preliminary work on standard mixtures of ^{241}Am and ^{239}Pu in preparation for some double-isotope experiments have shown that quantitation of each is possible with fairly good accuracy, so long as it is known that the spectrum is due only to these two nuclides.

The curves obtained are calculated and plotted for various comparisons, using computer programs developed by us for the CDC-6600 computer and CalComp plotter with the assistance of Mathematics and Computing at LRL. Data are fed to the computer by punched paper tapes from the teletype output of our analyzer. Figure 4, showing curves at various depths of absorber, is an example of the computer-drawn curves. Automated subtraction of spectra, normalization, calculation of counts in any set of regions, etc., are making possible a more extensive study than we could otherwise manage, and we have a library of spectra that can readily be subjected to reanalysis, if necessary.

A study of counter-source geometry proved especially enlightening. One reason for our choice of a fairly sizable Si crystal, with sacrifice of some degree of resolution, was that we hoped to count samples a couple of centimeters in diameter reproducibly and with reasonable

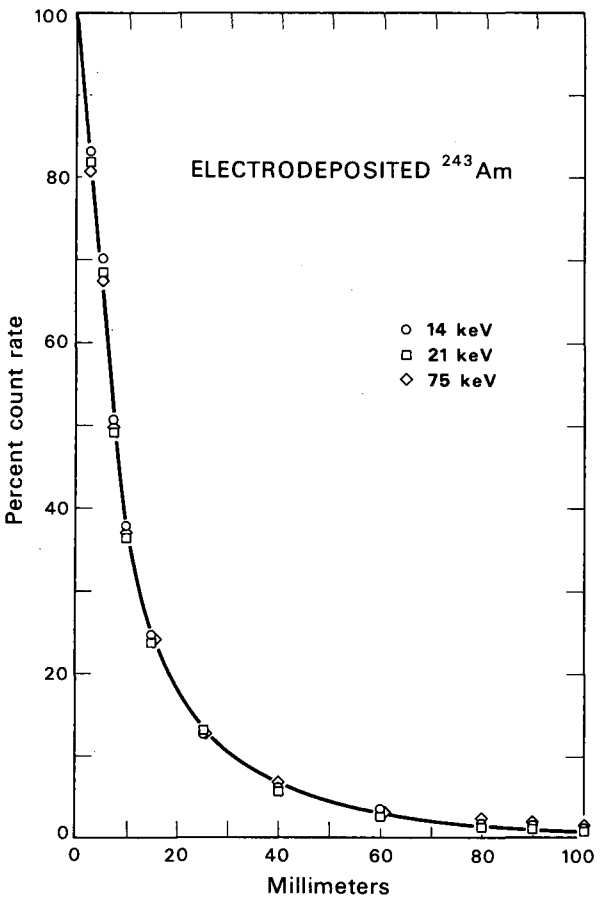

Fig. 3. Counting rate of the same ^{243}Am source as shown in Fig. 2, as a function of movement along the central axis away from the detector. The rate is given as percent of the value at the center of the window. DBL 695-4696

efficiency. Preliminary work showed the necessity for a study of geometry with a small source, since reproducibility was not good with moderate-sized sources against the window of the detector. An electrodeposited source of ^{243}Am about 4 mm in diameter was used to study the effects of lateral and perpendicular movement of the source relative to the beryllium window. Radial symmetry was good with respect to the central axis of the detector, but, as shown in Fig. 2, there is rapid decrease in counts with a few millimeters of lateral movement. The decrease varies a small but significant amount with photopeak energy. Figure 3 shows the variation of counting rate with distance away from the window along the central axis. This value was little affected by photopeak energy. Beyond about 15 mm, small sources follow an inverse-square law, but closer than that they deviate from it by having a lower count rate than it predicts (rather than higher, as might be expected from a small source and an extended detector), evidently because of the marked fall-off of counting rate as one leaves the central axis and the fact that none of our sources was sufficiently close to a point source. The result of these geometry problems is that it is difficult to reproduce counts against the face of the detector unless samples are thin and very small or very uniformly deposited. This can, of course, be improved by backing away from the detector, but with a consequent lowering in efficiency. The net result is something of a disappointment regarding quantitation of radioactivity and the

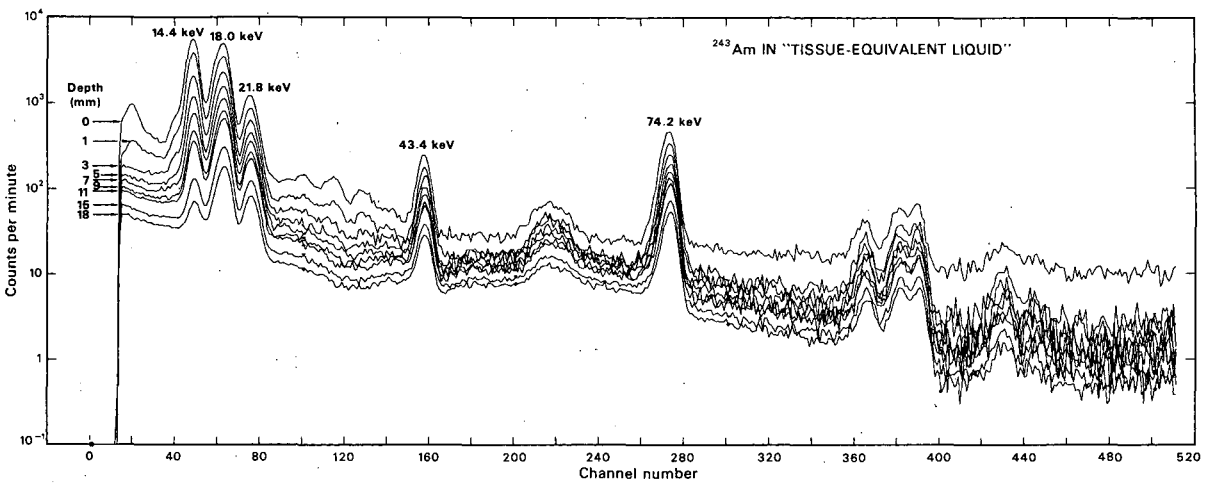

Fig. 4. Computer-drawn plots of spectra from a ^{243}Am source with various depths of tissue-equivalent liquid between it and the detector. Counts per minute is plotted semilogarithmically against channel number covering an energy range from 1 to 139 keV. The difference in absorption for the different X-ray peaks is clearly illustrated. DBL 695-4694

combination of efficiency and resolution we hoped to have, based on descriptions of this type of detector, though it does not negate its use for wound studies when resolution is needed.

A series of studies on our library of nuclides measured absorption in air, water, Lucite, fiberboard, and the tissue-equivalent liquid. Figure 4 shows typical computer-drawn spectra obtained, and Fig. 5 shows the ratios of the various X-ray peaks or photopeaks taken from them, plotted semilogarithmically against absorber depth. These curves permit us to make the measurement of average depth on any of our library of nuclides, and are giving us a basis for evaluating correction factors necessary for phantoms more convenient than the tissue-equivalent liquid, which we consider at present our best absorber equivalent to tissue. The ratio curve having the steepest slope (usually the ratio of a 14-keV X ray to a 21-keV X ray, or to a more energetic γ ray, if available) gives the most accurate depth measurement, except in low-activity samples, where another ratio may provide better statistics.

DISCUSSION

We intend to continue cataloguing nuclides of the actinide elements as they become available. ^{238}Pu is presently being prepared for study. When the opportunity is presented we shall also work with mixtures of any actinide isotopes for which there is a significant exposure hazard. Further plans include some double-isotope ^{239}Pu-^{241}Am experiments for experience in monitoring an animal injection site. They may also provide some basic information on separation of Am and Pu as they leave the site of injection, and will help us improve our L X-ray method for *in vitro* counting of ^{239}Pu in biological samples.

A comparison with thin-crystal sodium iodide detectors available to us is currently being made, and some figures of merit developed. It is evident that for some kinds of gross wound counting and localization, the wound counter is much the least sensitive, and the most subject

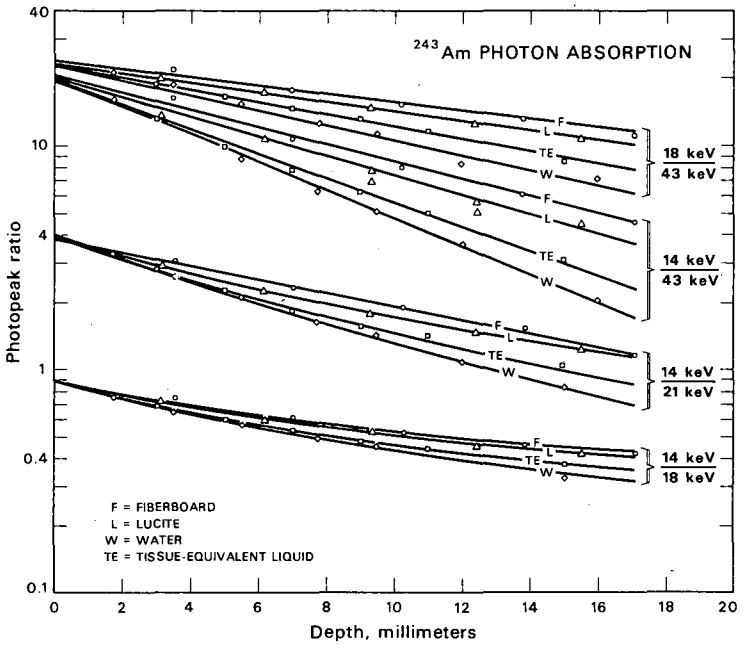

Fig. 5. Curves of X- and γ-ray peak ratios plotted semilogarithmically against depth of absorber, for fiberboard, Lucite, water, and tissue-equivalent liquid. Ratios between various pairs of peak regions (taken from data like those shown in Fig. 4) are used to prepare these curves. They facilitate measurement of average depth of the source in tissue, and the study of appropriate phantoms.

DBL 695-4695

to problems related to the geometry of distributed sources. For those reasons it is also the least satisfactory as a sample counter when the nuclide is known. Its great value is its high resolution.

We are now working to systematize our observations with the wound counter and to compare them with best available theoretical and empirical information. We hope with this effort to simplify presentation of the subject, to tabulate some useful values, and to simplify preparations for identification, quantitation, and depth measurement of any of these actinides.

SUMMARY

Preparations have been made for the use of a Si(Li) crystal "wound counter" to identify and quantitate X-ray-emitting actinide elements in human wounds, and to measure their depth in tissue. A small "library" of actinide sources and their spectra has been accumulated for the purpose. The paper gives preliminary results on some properties of the counter, computer processing of the data, the actinide X- and gamma-ray spectra obtained, the depth measurement, and some absorber studies related to the depth measurement.

REFERENCES

1. Palmer, H. E.; N. A. Wogmon; and J. A. Cooper: The determination of the depth and amount of ^{239}Pu in wounds with Si(Li) detectors. BNWL-3A 1261.
2. Bistline, R. W.; and W. H. Tyree: A comparison of low energy photon detectors for plutonium and americium wound counting. RFP-1068.
3. Miner, C. E.: A Semiconductor Detector Cryostat. UCRL-17201, Dec. 1966.
4. Clifford, C. E.: Dose distributions in phantoms exposed to 2.95-MeV neutrons. Health Phys. 15: 527 (1968).

Heavy-Particle Therapy in Cushing's Disease: A Progress Report

John A. Linfoot, Edward Manougian, Norton J. Snyder, Richard A. Carlson, Claude Y. Chong, James L. Born, Cornelius A. Tobias and John H. Lawrence

We have recently described the results of our treatment of a large number of patients with acromegaly, this work representing the first successful application of heavy particles in therapy (1). A later study, an attempt to treat Cushing's disease, is reported in this paper. In 1932 Cushing described (2) a clinical syndrome associated with hyperplasia or adenomata of the basophilic cells of the anterior pituitary gland, and sometimes associated with adrenal tumors. One of us, as an Intern and Assistant Resident Physician at about that time, saw many of these patients (3), and it was Cushing's belief that a basophilic tumor of the anterior lobe of the hypophysis was the usual cause of the syndrome. Subsequently it was also found that similar clinical pictures were seen with malignant adrenal tumors (usually unilateral) and adrenocortical hyperplasia (always bilateral). In the intervening years many investigators began believing that usually the condition was due to primary adrenal hyperfunction. More recently it has been believed, in line with Cushing's belief, that it is the result of an altered hypothalamic-pituitary-adrenal axis (i.e., small amounts of ACTH are released in spite of high circulating levels of hydrocortisone). This condition has also recently been found to result occasionally from the secretion of ACTH by malignant extrapituitary tumors (4). Between 15 and 25% of the former cases (5-7) are associated with roentgenologically detectable pituitary tumors, although the true incidence of these tumors has not been determined. Many of these tumors are not detectable until after bilateral (total) surgical removal of the adrenal glands, a procedure which, of course, corrects the hyperadrenocorticism but would not be expected to affect the altered hypothalamic or pituitary function. Although total surgical adrenalectomy (8), made possible by the availability of adrenocorticosteroid therapy, has been a successful treatment for some patients, interest has returned to the pituitary gland as the initial site for therapy (as originally suggested by Cushing) because of the existence of pituitary tumors in some cases, the occasional presence of accessory adrenal tissue in others, plus the abundant physiological data showing that altered ACTH secretion is the primary disturbance.

Unfortunately, treatment with orthovoltage X ray and more recently with high-voltage X ray (even when combined with unilateral adrenalectomy) have only irregularly been associated with adequate and sustained remissions (4, 9, 10). Surgical hypophysectomy is a formidable

procedure; it will almost invariably necessitate sacrifice of all pituitary trophic hormone function and probably should be reserved for invasive tumors. Satisfactory results have been reported following the implantation of ^{90}Y into the pituitary fossa (11). Results with such techniques are superior to those using conventional X-ray and γ-ray therapy, but these procedures also have a small but significant morbidity--particularly cerebrospinal fluid rhinorrhea. Heavy-particle therapy (12-21) is the only form of teletherapy that can accurately and safely deliver large doses of radiation to the pituitary, and this technique has been shown to be effective in the treatment of some cases of acquired bilateral adrenocortical hyperplasia (17).

Since 1959, heavy particles have been used to treat five patients with Nelson's syndrome (6) which developed after total adrenalectomy. All had the characteristic hyperpigmentation, but only three of these patients had definite enlargement of the sella turcica. The two patients who had no sellar enlargement resembled the former three cases in other respects, although the plasma ACTH values (measured by bioassay) were less elevated in these two patients. This group was treated with from 5,000 to 10,000 rads delivered in 12 days. Further pigmentation has ceased in all patients, but a gradual regression of pigmentation has been demonstrated only in the three patients with pituitary tumors. Further sellar enlargement has not developed, and no patient has required surgical decompression.

Twelve patients were treated primarily to control adrenal hypersecretion. All these patients were studied extensively to rule out the presence of adrenal tumors as well as of extrapituitary ACTH-producing tumors. Two patients had had previous adrenal surgery, but hyperadrenocorticism had recurred due to hypertrophy of a small adrenal remnant in one patient and, presumably, to presence of accessory adrenal tissue in the other. Slight to markedly elevated urinary 17-hydroxycorticosteroids (17-OHCS) were seen in all patients, but elevated 17-ketosteroids were observed in only three patients. All patients had exaggerated steroid responses during metyrapone tests (4) (this procedure separates hyperplastic from neoplastic adrenals, since the latter fail to respond). A marked fall in 17-OHCS after the dexamethasone (8 mg/d for 3 days) suppression test (4) was also found in all cases. The metyrapone test proved to be the best means of following the cases after treatment.

A typical hormonal change in one of the patients who responded favorably to treatment is shown in Fig. 1. Table 1 summarizes the steroid data for all patients. Following heavy-particle therapy (6,000 to 12,000 rads delivered in 12 days), all patients showed an early effect, as evidenced by less exaggerated responses in the metyrapone tests (see Figs. 2 and 3), and subsequent gradual fall in basal urinary steroid excretion. After longer periods of time had elapsed, less exaggerated (normal) responses to ACTH were often observed. Dexamethasone suppressibility has been studied in several patients after treatment; in some it returned to normal, while in others it remained largely unchanged, even when the basal steroid excretion had returned to normal. Although all patients showed an early effect of treatment on pituitary function, with a marked fall in steroid secretion within 3 to 6 months after treatment, four of these patients subsequently relapsed. Relapse was characterized by an increased 17-OHCS excretion and a return of the exaggerated steroid response to metyrapone. Three of these patients subsequently underwent bilateral adrenalectomies, at 6, 8, and 40 months after treat-

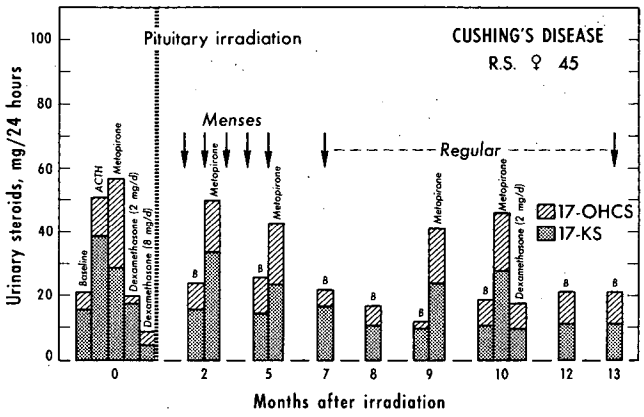

Fig. 1. Typical pre- and post-treatment steroid tests in patients with Cushing's syndrome.

MUB-3693

Table I. Summarized steroid data for all patients

Patient	Sex	Age	17 OHCS	17 KS	Metyrapone	ACTH	Dexamethasone	Circadian rhythm	
Pretreatment									
RK	F	37	↑	N	↑	↑	↓	A	
RS	F	45	↑	N	↑	↑	↓	A	
RC	M	17	↑	N	↑	↑	↓	A	
DM	F	35	↑	N	↑	↑	↓	A	↑ = Increased
JV[a]	F	56	↗	↓	→	→	→	A	↗ = Slightly Increased
JA[a]	M	24	↑	↓	↘	→	↓	A	→ = No Change
JD	F	38	↗	↗	↑	↑	↓	A	↓ = Decreased
PO	F	34	↑	↗	↑	↑	↓	A	N = Normal
PD	F	19	↑	↗	↗	↑	↓	A	A = Abnormal
RD[a]	M	46	↑	↓	↑	↑	↓	A	R = Reversed
MD	M	42	↑	↗	↑	↑	↓		
Posttreatment									
		Months post-Rx							Comment
RK	F	118	N	N	↓	↓	——	A	
RS	F	71	N/↑	N	↓/↑	↓/↑	——	R	Relapsed, 24 months
RC	M	62	N	N	↓	↓	↓	R	
DM	F	62	N/↑	N	↓/↑	↓/↑	——	R	Relapsed, 12 months
JV[a]	F	44	N	N	→	→	↓	N	
JA[a]	M	38	N	N	→	→	——	A	
JD	F	37	→	→	↓	——	——	N	
PO	F	34	N	N	↓	——	——	N	
PD	F	29	↓	↓	→	——	——	N	
RD	M	25	——	——	——	——	——	——	Relapsed, 8 months
MD	M	23	N/↑	N/↑	↓/↑	↓/↑	——	A	Relapsed, 16 months

[a] Adrenalectomy prior to heavy-particle therapy

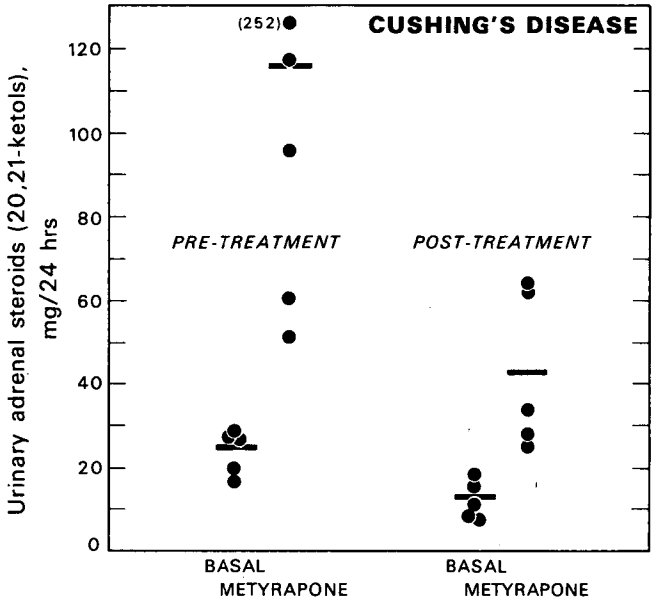

Fig. 2. Basal adrenal steroid excretion and responses to metyrapone (Metapirone®) in patients who remain in remission.

DBL 681-4555

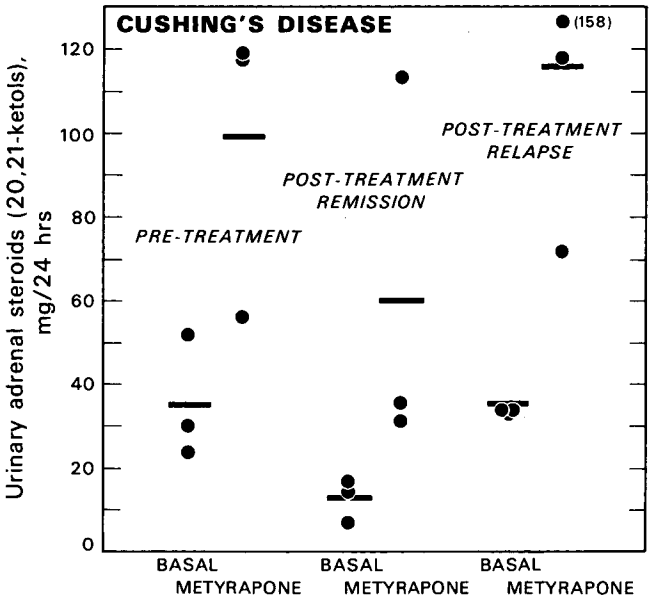

Fig. 3. Basal adrenal steroid excretion and metyrapone responses in 3 patients. The results prior to treatment, during remission, and following clinical relapse are compared.

DBL 681-4554

ment. The fourth patient, who has a severe neurological disability resulting from an attack of encephalomyelitis at 11 months of age, is currently receiving institutional care and is not thought to be able to tolerate any surgical intervention. The eight remaining patients in this group appear to be continuing to show gradual improvement. The first patient was treated almost 10 years ago, and she remains in remission.

Two of the total 17 patients treated have become mildly hypothyroid and require thyroid replacement therapy. Other trophic hormone functions appear to be intact in the remaining

patients. While these results are encouraging, further follow-up will be required before final conclusions can be reached. The first use of heavy particles for adenomata of the pituitary was in the treatment of acromegaly, where much lower doses are required to control the condition. It is clear, however, that larger doses of radiation are required for treating Cushing's syndrome than for the satisfactory control of acromegaly. The pituitary gland in cases of acromegaly due to eosinophilic adenomata is relatively more radiosensitive. Many of the early reported cases of Cushing's disease had basophilic hypophyseal adenomata (2, 3). Either these are more radioresistant or many of these patients may have pituitary basophilic hyperplasia.

REFERENCES

1. To be published in our next Semiannual Report (Spring 1969).
2. Cushing, Harvey: Bull. Johns Hopkins Hosp. 50: 137 (1932).
3. Lawrence, J. H.; and H. M. Zimmerman: Arch. Internal Med. 55: 745 (1935).
4. Liddle, G. W.; D. Island; and C. K. Meador: Recent Progr. Hormone Res. 18: 125 (1962).
5. Salassa, R. M.; T. P. Kearns; J. W. Kernohan; R. G. Sprague; and C. S. MacCarthy: J. Clin. Endocrinol. Metab. 19: 1523 (1959).
6. Nelson, D. H.; J. W. Meakin; J. B. Dealy, Jr.; D. D. Matson; and G. W. Thorn: New Engl. J. Med. 259: 161 (1958).
7. Montgomery, D. A. D.: Pituitary tumors in Cushing's syndrome. Paper presented at the Twelfth Annual Meeting of Congress of Neurological Surgeons, Inc., Houston, Texas, November 1, 1962.
8. Sprague, R. G.; R. E. Weeks; J. T. Priestly; and R. M. Salassa: in Modern Trends in Endocrinology, ed. by H. Gardiner-Hill. Paul B. Hoeber, Inc., New York, 1961.
9. Lisser, H.: J. Nervous Mental Disease 99: 727 (1944).
10. Thompson, K. W.; and L. Eisenhardt: J. Clin. Endocrinol. Metab. 3: 445 (1943).
11. Joplin, G. F.; R. Fraser; R. Steiner; J. Laws; and E. Jones: Lancet 2: 1277 (1961).
12. Lawrence, J. H.; and C. A. Tobias: Cancer Res. 16: 185-193 (1956).
13. Lawrence, J. H.: Cancer 10: 795-798 (1957).
14. Tobias, C. A.; J. H. Lawrence; J. L. Born; R. K. McCombs; J. E. Roberts; J. E. Anger; H. O. Anger; B. V. A. Low-Beer; and C. B. Huggins: Cancer Res. 18: 121-134 (1958).
15. Lawrence, J. H.; C. A. Tobias; J. L. Born; C. C. Wang; and J. H. Linfoot: J. Neurosurgery 19: 717-722 (1962).
16. Lawrence, J. H.; C. A. Tobias; and J. L. Born: Trans. Am. Clin. Climatol. Assoc. 73: 176-185 (1962).
17. Linfoot, J. A.; J. H. Lawrence; J. L. Born; and C. A. Tobias: New England J. Med. 269: 597-601 (1963).
18. D'Angio, G. J.; and J. H. Lawrence: Nucleonics 21[11]: 56-61 (1963).
19. Lawrence, J. H.: Acta Isotopica 4: 327-345 (1964).
20. Lawrence, J. H.: Radiation Res. Supp. 7: 360-368 (1967).
21. Garcia, J. F.; J. A. Linfoot; E. Manougian; J. L. Born; and J. H. Lawrence: J. Clin. Endocrinol. and Metab. 27: 1395-1402 (1967).

Staff Publications

Aceto, H.; R. Springsteen; W. Gee; H. S. Winchell; and C. A. Tobias: Erythropoietic response in dogs given sublethal whole-body proton irradiation followed by hypoxic hypoxia. UCRL-18320, July 1968.

Amer, N.; and C. A. Tobias: A possible explanation for the effects of magnetic fields upon biological systems. Radiation Res. 31: A644 (1968).

Born, J. L.; J. A. Linfoot; H. H. Stauffer; E. Manougian; C. A. Tobias; J. Lyman; C. Chong; and J. H. Lawrence: Long-term follow-up on 80 patients with heavy-particle pituitary-suppressive therapy between 1958 and 1962. Diabetics 17: 318 (1968).

Brownson, R. H.; D. C. Price; and G. P. Welch: Acute radionecrosis of proliferating cells in the hippocampus of young rats. J. Neuropath. Exptl. Neurol. 27: 164 (1968).

Buckhold, Brenda; and John V. Slater: Effect of temperature and X-irradiation on pupae of the flour beetle, Tribolium confusum. Radiation Res. 37: 567-576 (1969).

Chaudhuri, Tuhin K.; and Richard P. Spencer: Dual labeling of erythrocytes: properties and splenic handling of ^{75}Se- and ^{59}Fe-labeled cells. J. Nucl. Med. 10[3]: 122-126 (1969).

Engeset, A.; and J. C. Schooley: Morphological changes following irradiation of a segment of the rat thymus. Proc. Soc. Exptl. Biol. Med. 128: 26-31 (1968).

Engeset, A.; and J. C. Schooley: Thoracic duct lymphocyte output in rats after local thymus irradiation. Scand. J. Clin. Lab. Invest. 22, suppl. 106: 119-23 (1968).

Everson, R. A.; and E. L. Dobson: ACTH kinetics. Fed. Proc. 27: 434 (1968).

Forrester, J. C.; T. K. Hunt; T. L. Hayes; and R. F. W. Pease: Scanning electron microscopy of healing wounds. Nature 221: 373-374 (1969).

Forte, G. M.; A. V. Nichols; and R. M. Glaeser: Electron microscopy of human serum lipoproteins using negative staining. Chem. Phys. Lipids 2: 396-408 (1968).

Frederickson, D. S.; R. I. Levy; and F. T. Lindgren: A comparison of heritable abnormal lipoprotein patterns as defined by two different techniques. J. Clin. Invest. 47: 2446-2457 (1968).

Freeman, Norman K.: Applications of infrared absorption spectroscopy in the analysis of lipids. J. Am. Oil Chemists' Soc. 45: 798-809 (1968).

Garcia, Joseph F.; and Irving I. Geschwind: Investigation of growth hormone secretion in selected mammalian species. In Proceedings of International Symposium on Growth Hormone, Milan, 1967. Excerpta Medica Foundation, Amsterdam, 1968. P. 267-291.

Glaeser, R. M.; G. Thomas; R. Christensen; and W. G. Brammer: Application of electron diffraction to problems in biological electron microscopy. In Proceedings of Electron Microscopy Society of America, 26th Annual Meeting, New Orleans, Sept. 16-19, 1968, ed. by Claude J. Arcenaux. Claitor's Publishing Division, Baton Rouge, 1968. P. 398-399.

Glaeser, R. M.; J. E. Richmond; and P. W. Todd: Histotypic self-organization by trypsin-dissociated and EDTA-dissociated chick embryo cells. Exptl. Cell. Res. 52: 71-85 (1968).

Goldsmith, John R.; and Stephen A. Landaw: Carbon monoxide and human health. Science 162: 1352-1359 (1968).

Hayes, T. L.: Applications of scanning microscopy in biomedical research. In Proceedings of Electron Microscopy Society of America, 26th Annual Meeting, Sept. 16-19, 1968, ed. by Claude J. Arcenaux. Claitor's Publishing Division, Baton Rouge, 1968. P. 354-355.

Hayes, T. L.; and R. F. W. Pease: The scanning electron microscope: principles and applications in biology and medicine. In Advances in Biological and Medical Physics, vol. 12, edited by John H. Lawrence, John W. Gofman, and Thomas L. Hayes. Academic Press, New York and London, 1968. P. 85-137.

Haynes, R. H.; R. M. Baker; and G. E. Jones: Genetic implications of DNA repair. In NATO Advanced Study Institute, Portmeirion, Wales, 1967, Energetics and Mechanisms in Radiation Biology, edited by Glyn O. Phillips. Academic Press, London and New York, 1968. P. 425-465.

Hippensteele, J. R.; H. G. Parker; E. L. Dobson; and J. J. Lynch: Potassium exchange from the sodium space in the dog's leg. Fed. Proc. 28: 824 (1969).

Hirono, Y.; H. H. Smith; and J. T. Lyman: Tumor induction by heavy ionizing particles and X-rays in Arabidopsis. Radiation Botany 8: 449-456 (1968).

Hoff, H. F.; and T. L. Hayes: Description of a pulsatile circulatory artery perfusion system. Pflügers Arch. Eur. Physiol. 305: 292-294 (1969).

Howard, A. N.; G. A. Gresham; and F. T. Lindgren: Lipoprotein studies on rats fed thrombogenic and atherogenic diets. J. Atherosclerosis Res. 8: 739-743 (1968).

Lindgren, F. T.; and K. M. Sanderson: The future of the campus environment. Calif. Monthly 79: 36 (1969).

Lossow, W. J.; F. T. Lindgren; J. C. Murchio; G. R. Stevens; and L. C. Jensen: Particle size and protein content of six fractions of the $S_f > 20$ plasma lipoproteins isolated by density gradient centrifugation. J. Lipid Res. 10: 68-76 (1969).

Maccabee, H. D.; M. R. Raju; and C. A. Tobias: Fluctuations of energy loss by heavy charged particles in thin absorbers. Phys. Rev. 165: 469-74 (1968).

McDonald, Larry W.; and Thomas L. Hayes: Correlation of scanning electron microscope and light microscope images of individual cells in human blood and blood clots. Exptl. Mol. Pathol. 10: 186-198 (1969).

McDonald, L. W.; and T. L. Hayes: Scanning microscopy of human blood and marrow smears. In Proceedings of Electron Microscopy Society of America, 26th Annual Meeting, New Orleans, Sept. 16-19, 1968, edited by Claude J. Arcenaux. Claitor's Publishing Division, Baton Rouge, 1968. P. 166-167.

Mortimer, Robert K.; and Richard A. Gilmore: Suppressors and suppressible mutations in yeast. In Advances in Biological and Medical Physics, vol. 12, edited by John H. Lawrence, John W. Gofman, and Thomas L. Hayes. Academic Press, New York and London, 1968. P. 319-331.

Nichols, A. V.; E. L. Coggiola; L. C. Jensen; and E. H. Yokoyama: Physical-chemical changes in serum lipoproteins during incubation of human serum. Biochim. Biophys. Acta 168: 87-94 (1968).

Noble, R. P.; F. T. Hatch; J. A. Mazrimas; F. T. Lindgren; L. C. Jensen; and G. L. Adamson: Comparison of lipoprotein analysis by agarose gel and paper electrophoresis with analytical ultracentrifugation. Lipids 4: 55 (1969).

Pease, R. F. W.; and T. L. Hayes: Electron microscopy of sprouting seeds. In Proceedings of Electron Microscopy Society of America, 26th Annual Meeting, New Orleans, Sept. 16-19, 1968, edited by Claude J. Arcenaux. Claitor's Publishing Division, Baton Rouge, 1968. P. 88-89.

Powers, E. L.; J. T. Lyman; and C. A. Tobias: Some effects of accelerated charged particles on bacterial spores. Intern. J. Radiation Biol. 14: 313-330 (1968).

Raju, M. R.; J. T. Lyman; T. Brustad; and C. A. Tobias: Heavy charged-particle beams. UCRL-16962 Rev., March 1968.

Richards, W. Robert; and Lola S. Kelly: In vivo studies on radiation sensitization of ascites tumors by iodoacetamide. Fed. Proc. 28: 264 (1969).

Richmond, J. E.; R. M. Glaeser; and P. Todd: Protein synthesis and aggregation of embryonic cells. Exptl. Cell Res. 52: 43-58 (1968).

Roy, G.; and C. A. Tobias: A solid-state approach to the theory of the squid axon. Biophys. J., WE6 (Feb.), 1968 - abstract.

Slater, J. V.; B. Buckhold; and C. A. Tobias: Effect on a flour beetle of irradiation during space flight. Bioscience 18: 595-597 (1968).

Slater, J. V.; B. Buckhold; and C. A. Tobias: Synergism of x-irradiation and space flight factors in flour beetle, Tribolium confusum. Radiation Res. 35: A501 (1968).

Spencer, Richard P.; and Tuhin K. Chaudhuri: Quantitative estimates of changes in splenic size during life. Yale J. Biol. Med. 41[4]: 333-339 (Feb. 1969).

Spencer, Richard P.; Tapan K. Chaudhuri; Tuhin K. Chaudhuri; and Teodoro Herskovic: A continuously monitored recirculating perfusion system for measuring intestinal absorption. Am. J. Digestive Diseases, January 1969, New Series, 14[1]: 61-66 (1969).

Spencer, W. H.; J. Alvarado; and T. L. Hayes: Scanning electron microscopy of human ocular tissues: trabecular meshwork. Invest. Ophthalmology 7[6]: 651-662 (1968).

Steinkamp, R. C.; T. W. Sargent; E. Isaac; N. L. Cohen; E. M. Hutson; and N. D. Kunkel: Whole-body cesium-137 and its relation to body composition and diet. Radiol. Health Data Rep. 9: 619 (1968).

Stern, C.; and C. Tokunaga: Autonomous pleiotropy in drosophila. Proc. Natl. Acad. Sci. U. S. 60: 1252-1259 (1968).

Tobias, C. A., et al.: Status of research in the biophysical sciences. Biophys. J. 8: 734-72 (1968).

Tobias, Cornelius A.; and A. R. Gopal-Ayengar: Some biophysical approaches to the effects of radiation and their repair, Introduction. In Advances in Biological and Medical Physics, vol. 12, edited by John H. Lawrence, John W. Gofman, and Thomas L. Hayes. Academic Press, New York and London, 1968. P. 215-218.

Tokunaga, Chiyoko: Nonautonomy in differentiation of pattern-determining genes in Drosophila. II. Transplantation of eyeless-dominant leg disks. Develop. Biol. 18: 401-413 (1968).

Van Dyke, D.; H. Anger; E. Duffie, Jr.; S. Higashino; and J. Wilson: Cardiac catheterization using a radioactive catheter and the scintillation camera. Radiology 91: 749-752 (1968).

Welch, G. P.; Some effects of chronic irradiation on a steady-state yeast population. Radiation Res. 36: 274-286 (1968).

Yano, Yukio; and Hal O. Anger: Visualization of heart and kidneys in animals with ultrashort-lived ^{82}Rb and the positron scintillation camera. J. Nucl. Med. 9: 412-415 (1968).

Author Index

Amer, N. M.	92, 100
Anger, H. A.	118
Armaly, G. C.	73, 80
Barendsen, G. W.	100
Born, J. L.	135
Burki, H. J.	100
Carlson, R. A.	135
Chong, C. Y.	135
Connell, G. M.	113
Curtis, S. B.	100
Fawwaz, R. A.	64, 73, 80, 83
Feola, J. M.	105
Freeman, N. K.	25
Frye, F.	64
Gnanapurani, M.	92
Hayes, T. L.	35
Hemphill, W. P.	64, 74
Hoopes, D. A.	30
Jensen, L. C.	30
Lawrence, J. H.	64, 73, 105, 118, 135
Lindgren, F. T.	30
Linfoot, J. A.	113, 135
Low-Beer, A. deG.	128
Mamoon, A.-M.	1, 9
Manougian, E.	135
McKey, T. J.	19
Mortimer, R. K.	19
Naets, J.-P.	43
Nichols, A. V.	25
Nohr, M. L.	52
O' Lague, P. H.	9
Parker, H. G.	128
Raju, M. R.	89, 92, 100, 105
Richman, C.	92, 105
Rodarte-y-Ramon, U. S.	19
Schlapfer, W. T.	1, 9
Snyder, N. J.	135
Tauro, P.	19
Tobias, C. A.	1, 9, 135
Van Dyke, D. C.	38, 43, 52, 118
Winchell, H. S.	64, 73, 80, 83
Windsor, A. A.	30
Winstead, M. B.	73, 80, 83
Wright, S. R.	128

Personnel

Senior Staff

John H. Lawrence, Director
Hal O. Anger
Max W. Biggs
James L. Born
Ernest L. Dobson
Norman K. Freeman
Joseph F. Garcia
Thomas L. Hayes
Hardin B. Jones
Thomas H. Jukes
Frank T. Lindgren
Howard C. Mel
Robert K. Mortimer
Alexander V. Nichols
Howard G. Parker
Donald J. Rosenthal
John C. Schooley
William E. Siri
Cornelius A. Tobias
Donald C. Van Dyke
Harry Saul Winchell

Medical Investigator Staff

Max W. Biggs
James L. Born
Thomas F. Budinger
Richard A. Carlson
Claude Y. Chong
William G. Donald, Jr.
Stephen A. Landaw
John H. Lawrence
John A. Linfoot
Edward Manougian
Howard G. Parker
James Price
Donald J. Rosenthal
Henry H. Stauffer
Donald C. Van Dyke
Wen C. Wei
Harry Saul Winchell

Research Staff

Henry Aceto
Alan J. Bearden
H. John Burki
Anne S. Cleveland
Gerald Connell
Stanley B. Curtis
Patricia Durbin-Heavey
Rashid A. Fawwaz
Jose M. Feola
Gertrude M. Forte
Cornelius T. Gaffey
Robert M. Glaeser
Thormod E. Henriksen
Jerry Howard
Lin C. Jensen
Lola S. Kelly
Jack L. King
William D. Loughman
David D. Love
John T. Lyman
James McRae
Myron Pollycove
Mudundi R. Raju
Thornton W. Sargent
Richard L. Schoenbrun
Carol J. Shkurkin
Ira L. Silver
Wallace C. Snipes
Edward H. Strisower
Chiyoko Tokunaga
Graeme P. Welch
Margaret R. White
Meldrum B. Winstead
Yukio Yano

Postdoctoral Fellows

John B. Bassel
Lakshmi Basu
Tuhin K. Chaudhuri
Michael G. Chen
John C. Cummings
Helge Dalen
Jan S. Fogh
John T. Leith
Jean M. Paulus
Donald L. Puppione
Burton H. Slanger
Hannes B. Stahelin

Technical Staff

Gerald L. Adamson
Hilda M. Alexander
Cathryne C. Allan
Gery C. Armaly
Alice Beckmann
Rosemary J. Bell
Adrienne Berkowitz
Patricia J. Blanche
Mona D. Boaz
Catharine D. Boerke
Carol S. Bohlen
Gerald L. Brooks
Dorothy A. Carpenter
Emanuela N. Catena
Elaine L. Coggiola
Mary J. Cornell
Henriette C. Cozza
Laurie M. Craise
Susan J. Daniels
Theodora M. Davis
Robert E. Doyle
Doris L. Dunn
Gregory C. Eggling
Ora B. Ellington
Carolee R. Finney
Myrtle L. Foster
Roscoe Frazier
Charlie M. Fuller
Patricia A. Garbutt
Queen E. Gipson
Lois R. Gumz
Virginia C. Havens
Beverly D. Heinze
Jerilyn Hirshberg
Walter K. Ho
Mary Horan
Walter C. Hucul
Willie M. Jackson
Karen Jarrett
Nylan M. Jeung
Natalia Kusubov
Dorothy P. Leighty
James W. Lieb
Phoebe J. Lindsay
Jennie M. London
Jean R. Luce
Josephine A. Lundberg
Justine J. Lynch
Lynn J. Mahlmann
Larry E. Marbley
Johnie A. Maxion
Lafayette McIntosh, Jr.
Tommy J. McKey
Velma B. McNeal
Victor J. Montoya
Jeanette S. Nakagawa
William D. Nance
Mary L. Nohr
Virginia I. Obie
Dianne L. Peterson
Anne K. Poley
Kenneth C. Quandt
Rosanne B. Raley
Ralph L. Reynolds
Willie H. Sanders
Elizabeth A. Seaholm
Barbara A. Shipley
Patricia P. Smith
Virginia M. Spamer
Robert W. Springsteen
Gary R. Stevens
Sandra K. Stoddard
Velta Suna
Frances B. Taylor
Charles Thompson, Jr.
Carolyn V. Tolman
Wayne H. Tsuji
Cole Ulrichs
Rita L. Von Hungen
Susan M. Walker
Marilyn A. Williams
Robert D. Wills
Patricia C. Wood
Stephen R. Wright
Elaine H. Yokoyama
Philip E. Yost

Graduate Students

Raymond Baker
Steven A. Beckwitt
Richard P. Bird
Martin L. Brown
Jeremy N. Bruenn
Katherine K. Cheng
Ralph C. Christensen
Elizabeth J. Clark
Stuart R. Dole
William R. Dunham
Edward L. Elkin
Douglas A. Ewald
Robert Foreman
David E. Garfin
Michael M. Graham
Mark N. Herman
Carl F. Hodel
Junardeen Hopkirk
Paul Horan
William J. Horsley
Charles R. Hurlbut
Jessie H. Hsu
James S. Hsue
Latife Ismail
Gary E. Jones
Michael W. Kaplan
Duraiswami Krishnan
James M. Lallas
Lucy S. Lam
Lawrence R. Lawlor
Jeffrey F. Lemontt
David H. Lin

Graduate Students (cont.)

Max S. Lin
Roderick D. Macgregor, Jr.
Udipi Madhvanath
Gilbert H. Magilen
Abdel-Megid Mamoon
JaRue Manning
Bambino I. Martins
Karin Moelling
Peter C. Nosler
Paul H. O' Lague
George F. Oster
James B. Pawley
Alan S. Perelson
Esther B. Perry
David A. Pistenma
Robert G. Plantz
Wai Kit Quon
Theodore Regimbal
Juan T. Rehbock
William R. Richards
Ubaldo S. Rodarte-y-Ramon
Werner T. Schlapfer
Paul T. Shafer
Stephen I. Shapiro
Linda J. Skory
Sylvia Spengler
Joel B. Swartz
Tom S. Tenforde
William J. Tuddenham
Myonggeun Yoon

Engineering and Technical Support Staff

Robert C. Aker
Elbert L. Benjamine
Delbert H. Coleman
Robert D. Creedy
Dewey D. Dean
Dorothy E. Denney
John A. Despotakis
Edward F. Dowling
James H. Edwards
John P. Flambard
John R. Gurule
Edward A. Heilstad
David A. Hoopes
Victor P. Jensen
Edward J. Lampo
Ellis H. Myers
Karen A. Peterson
Marjory H. Simpson
John M. Sweeney
Frank T. Upham
Alfred A. Windsor

Administrative and Office Staff

Igor R. Blake
Baird Whaley

Mary M. Bryan
Janice C. DeMoor
Marian F. Edelen
Fern V. Forsberg
Joan E. Fox
Betty M. Gale
Sheri-Ann Grant
Mary C. Harmon
Dorothy B. Hedquist
Jessica Inskeep
Marcia D. Jackson
Donna E. Kennedy
Maxine Mangels
Judith S. Manning
Dorothy D. Meck
Pamela A. Mott
Shirley C. Peterson
Marilyn R. Rushforth
Michael A. Sauceda
Ruth T. Showalter
Dorothy S. Sprague
Grace H. Walpole